

Progress and challenges of halide perovskite-based solar cell- a brief review

Dibyajyoti Saikia, Atanu Betal, Jayanta Bera, Satyajit Sahu *

Indian Institute of Technology Jodhpur, Department of Physics, Jodhpur, 342037, India



ABSTRACT

Halide perovskites have drawn the researcher's attention in the last decade because of their marvellous performance in photovoltaic devices. It started in 2009 with organic-inorganic perovskite sensitized solar cells, showing a power conversion efficiency (PCE) of 3.13%. Since then, continuous efforts have been made to enhance **perovskite solar cell (PSC)** performance using different halide perovskite materials and changing other parameters. Researchers have recently achieved 25.8% PCE with perovskite-based solar cells, which challenged the mainstream solar cell technologies. Here, we have reviewed the exotic electronic and optical properties of different halide perovskites and the continuous development of PSCs with varying device architectures using these materials, fabrication techniques, and various carrier transport layers. The main problem in the commercialization of perovskites-based photovoltaic devices is poor stability in the ambient. This review also includes the challenges such as the stability of perovskite materials, device fabrications, toxicity, and performance improvement, which provides the understanding towards achieving the high PCE. Encapsulation is one of the best ways to improve the stability of the halide perovskites. A perspective to enhance the efficiency and stability of the PSC is also given at the end.

1. Introduction

Due to the growing population and industrialization, our society faces challenges in looking for clean and renewable energy sources [1–4]. Global energy demand is rising year after year, and it is expected to double by 2050 [5]. One potential way to meet this demand is to convert solar energy into electricity [6]. Many research works have been done to utilize solar energy and mitigate the problem. The conversion and storage of solar energy in an efficient, cost-effective, and eco-friendly way is always a major problem in photovoltaic technologies. In recent years, PSCs have gained significant importance in photovoltaic research due to their high performance. Since the pioneering work by Kojima et al. [7], the certified record PCE of PSCs according to NREL (Natural Renewable Energy Laboratory) now exceeds 25% [8], as depicted in Fig. 1. Based on the record-certified PCE, it could be concluded that PSCs (25.7%) already surpassed some of the mainstream solar cell technologies, like CIGS (23.4%) and thin-film (21.2%) and multi-crystalline Si (23.3%) solar cells (SCs). They are almost comparable to single crystal (non-concentrator) Si (26.1%) and Si heterostructure (26.7%) cells.

In 2009, Kojima and co-workers utilized $\text{CH}_3\text{NH}_3\text{PbBr}_3$ as a sensitizer in Dye-Sensitized Solar Cells (DSSCs) and reported 3.13% PCE by replacing Br with iodine; they realized 3.81% PCE [7]. Subsequently, 6.5% PCE was achieved by optimizing the preparation of $\text{CH}_3\text{NH}_3\text{PbI}_3$ and TiO_2 nanoparticles (NPs) [9]. However, these cells are volatile because of the use of liquid electrolytes. Thus, substituting the

problematic liquid electrolyte with a solid contact is required for higher stability. By mid-2012, Kim et al. achieved 9.7% PCE on perovskite sensitized all solid-state mesoscopic solar cells (MSSC) by using spiro-OMeTAD as a hole transporting material (HTM) [10]. The utilization of spiro-OMeTAD not only improved the stability but also efficiency. In 2013, Heo et al. fabricated PSCs with FTO/mp-TiO₂/ $\text{CH}_3\text{NH}_3\text{PbI}_3$ /PTAA/Au structure and achieved a PCE of 12%. Furthermore, the same architecture devices having spiro-OMeTAD as HTM exhibited only 8.4% PCE [11]. Subsequently, planar heterojunction (PHJ) PSCs with $\text{CH}_3\text{NH}_3\text{PbI}_{3-x}\text{Cl}_x$ were fabricated, demonstrating improved stability and carrier transportation relative to its pure iodide counterpart, and achieved a PCE of 15.4% [12]. They also revealed that perovskite absorbers operate at the highest PCEs in simple device configurations without the necessity of complicated nanostructures. By doping TiO_2 ETL with Yttrium (Y) and modifying the ITO with polyethylenimine ethoxylated (PEIE) to reduce the work function, Zhou et al. obtained an average efficiency of 16.6% with a maximum PCE of 19.3% [13]. In 2015, Seok and co-workers fabricated PSCs with FTO/barrier layer (bl)- TiO_2 /mp-TiO₂/FAPbI₃/PTAA/Au structure, achieved an PCE of 20.2% [14]. Tao et al. fabricated low-temperature (LT) processed $\text{CH}_3\text{NH}_3\text{PbI}_3$ -based PSCs with TiO_2 /60-PCBM as ETL that delivered 17.6% stabilized efficiency [15]. Saliba et al. prepared Cs containing triple cation PSCs and obtained the best PCE of 21.1% [16]. By incorporating rubidium (Rb) cation into the mixed cation perovskite material, they achieved the best PCE of 21.6% [17]. By preparing perovskite films utilizing PMMA as a template for controlling nucleation

* Corresponding author.

E-mail address: satyajit@iitj.ac.in (S. Sahu).

and crystal growth, Bi et al. fabricated PSCs that exhibited the best efficiency of 21.6%, with a certified efficiency of 21.02% [18]. Ergen et al. prepared a graded band gap PSC with the architecture GaN/CH₃NH₃S-NiI₃/monolayer-hBN/CH₃NH₃PbI_{3-x}Br_x/spiro-OMeTAD and graphene aerogel/Au. The cells delivered 18.4% averaged PCE and the highest of 21.7% [19].

It was demonstrated that adding excess iodide ions to the organic solution, which is utilized to prepare perovskite films by an intermolecular exchange process, reduces the deep-level defect states. The certified efficiency reached 22.1% in small area SCs and 19.7% in 1 cm² SCs [20]. A contact-passivation approach utilizing Cl-capped TiO₂ colloidal nanocrystal (NC) film was reported to reduce interface recombination and improve interface connection. These PSCs exhibited a certified PCE of 20.1%, with a best of 20.9% [21]. By preparing Lanthanum (La)-doped BaSnO₃ (LBSO) electrodes using a colloidal route, Shin and co-workers fabricated CH₃NH₃PbI₃-based PSCs. PSCs with LBSO exhibited 21.2% stabilized PCE, while mp-TiO₂ based SCs delivered only 19.7% [22]. By mid-2018, Luo et al. fabricated inverted PSCs based on a simple solution-processed secondary growth (SSG) method and achieved 20.91% stabilized PCE, with a best of 21.51% [23]. To minimize interfacial losses at the contacts, Wolff et al. demonstrated reproducible dopant-free 1 cm² PSCs by employing ultrathin interlayers between the perovskite and charge transport layers (CTLs) which surpassed 20% PCE (19.83% certified) [24]. Feng et al. prepared MAPbI₃ films with methanol as an additive, using a one-step deposition method. PSCs with methanol exhibited a higher PCE than those without methanol (19.51% vs 16.53%) [25]. The high efficiency is attributed to the enhanced absorption and coverage of MAPbI₃ film due to the use of methanol. In 2019, a PCE of 23.3% (certified PCE 22.7%) was reported on PSCs with poly (3-hexylthiophene) (P3HT), fabricated using a double-layered halide architecture (DHA) [26]. By passivating surface defects of perovskite films using phenethylammonium iodide (PEAI), planar PSCs with 23.32% certified PCE (quasi-steady-state) were achieved [27]. Zhao et al. prepared large-grained CsPbBr₃ perovskite films through precise control of crystallization temperature of PbI₂ film, and upon further interfacial modification by nitrogen-doped quantum dots, prepared HTM-free all inorganic PSCs. They achieved the best PCE

of 10.71% and an ultrahigh V_{OC} of 1.622 V [28]. In 2020, an efficiency of 18.06% (17.8% certified) was reported on two-dimensional Ruddlesden-Popper phase (2DRP) perovskites using 2-(methylthio)ethylamine hydrochloride (MTEACl) alkylammonium [29]. Subsequently, Jeong et al. fabricated PSCs with efficiency up to 24.82% (24.64% certified) with a voltage loss of 0.3 V [30]. Min et al. recently developed a coherent featured interlayer by coupling Cl-bonded SnO₂ with a Cl-containing perovskite precursor between SnO₂ ETL and perovskite absorber layer and fabricated PSCs of 25.8% PCE. The high PCE is attributed to the atomically coherent characteristics of the interlayer that enhance charge extraction and transport from the absorber and suppress interfacial defects [31].

While laboratory-scale PSCs have shown significant progress (see Fig. 2), several barriers need to be overcome in further developing PSCs.

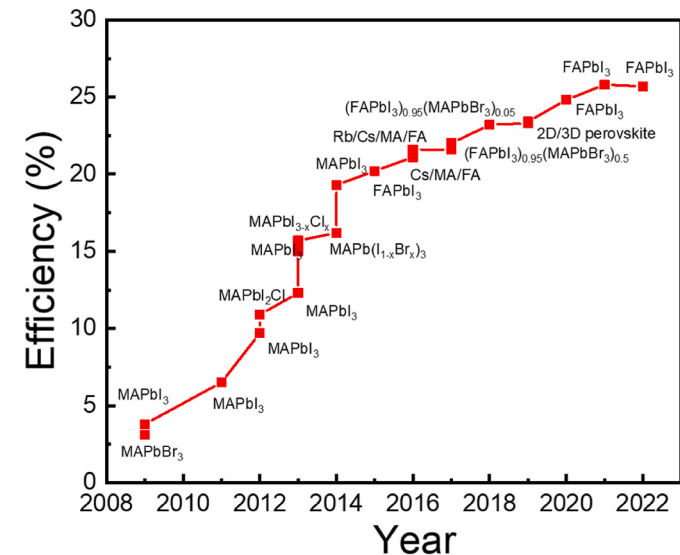


Fig. 2. PCE evolution of PSCs from 2009 to 2022.

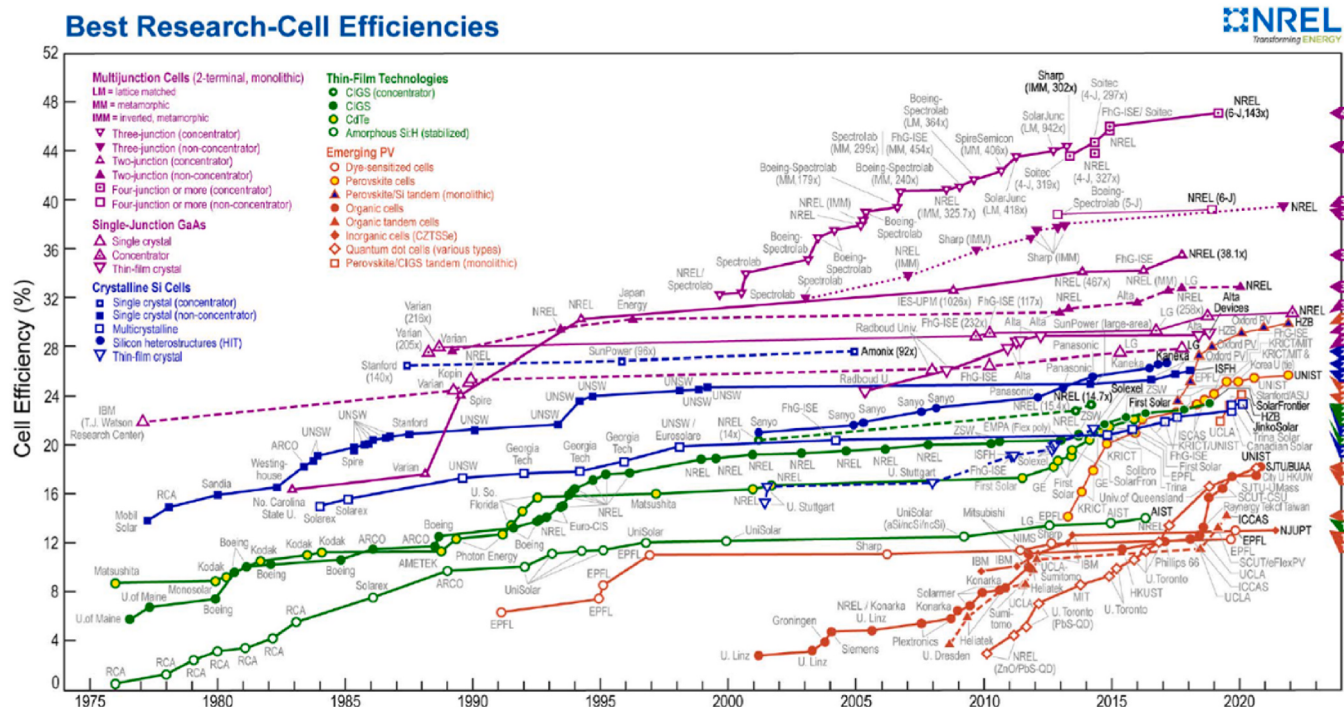


Fig. 1. PCE chart of various photovoltaic technologies taken from the website of NREL, Golden, CO, USA.

The two fundamental issues, namely, device performance instability [32] and current-voltage (J-V) hysteresis [33] currently blocking the improvement pathway. Hence, it is essential to recognize the degradation process of perovskites and other device elements like HTM and ETM. In addition, Pb toxicity could be another concern during the manufacturing, use and recycling of perovskite [4]. Although many reports on lead-free PSCs were published in the literature [34–36], the device's performance is still not promising.

2. Perovskite structure

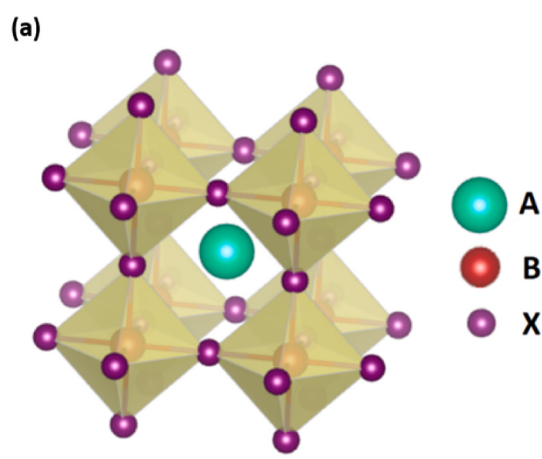
2.1. Crystal structure

Perovskite is usually referred to as a type of ceramic oxides described by the formula ABX_3 , consisting of corner-sharing BX_6 octahedra [37]. Here X is an anion and A and B are cations of varying sizes, A is larger than B. Hundreds of distinct materials follow this structure, with multiple characteristics, like insulating, semiconducting, conductive, superconductive, antiferromagnetic, piezoelectric, and thermoelectric. Perovskite materials are important due to the cubic lattice-nested octahedral layered structures and the unusual optical, thermal, and electromagnetic characteristics. Fig. 3a illustrates the perovskite crystal structure. The crystallographic stability and possible structure of perovskites could be figured out from the Goldsmith tolerance factor (GTF) t and an octahedral factor μ [38,39]. Here t is described as the ratio of the length A–X to the length B–X in an idealized solid sphere model

$$t = \frac{R_A + R_X}{\sqrt{2}(R_B + R_X)},$$

with R_A , R_B and R_X being the ionic radii of the respective ions and $\mu = \frac{R_B}{R_X}$. For a perfect cubic perovskite structure, t must be equal to 1.0 [40]. Nonetheless, octahedral distortion occurs when $t < 1$, influencing electronic properties [40]. For halide perovskites, the GTF and octahedral factor need to be in the range $0.81 < t < 1.11$ [38,40] and $0.44 < \mu < 0.90$ [38,39]. Fig. 3b illustrates some halide perovskites calculated and estimated t and μ factors.

If the A-site cation becomes too large, the 3D ABX_3 structure is changed to a low-dimensional crystalline structure, like a 2D layered structure [42]. In particular, low dimensional perovskites are more versatile because they enable the inclusion of bigger molecules with customized functions [43]. However, compared to common 3D perovskites, other structures typically yield low efficiency and thus are rarely applied in photovoltaics. This is probably due to their wide band gap, large exciton binding energy, and low conductivity in some crystallographic orientations [44].



Perovskites exhibited various phases based on temperature variations. For instance, in the case of MAPbI_3 , at a temperature below 100 K, the perovskite showed a stabilized orthorhombic (γ) phase. As the temperature increases to 160 K, a transition from orthorhombic to tetragonal (β) phase occurs, with a stable cubic (α) phase being formed at ~ 330 K [45]. Fig. 4 illustrates all those three crystal structures. Similarly, CsPbCl_3 and CsPbBr_3 are tetragonally or monoclinically distorted at room temperature. However, both CsPbCl_3 and CsPbBr_3 exhibit a transition to pure cubic perovskite structure at 320 K and 403 K, respectively [46]. In addition, light soaking may also cause reversible phase separation of perovskites [47].

2.2. Electronic structure

Density functional theory (DFT) calculations have already estimated the electronic structure of many perovskite materials. Even after accounting for spin-orbit coupling and other interactions such as van der Waals interaction, the calculated band gap for most perovskites was matched with the obtained band gap from absorption spectra [49]. The calculated band gap values also depend on the exchange-correlation functionals employed in the DFT calculations. Recently, Zhong et al. investigated the electronic properties of $\text{CH}_3\text{NH}_3\text{PbI}_3$ polymorphs using first-principles calculations with GGA-PBE and HSE06 functionals; the band structures are illustrated in Fig. 5 (b) [50].

To investigate the electronic properties of perovskites, the density of states (DOS) was evaluated. By calculating the DOS of CsPbI_3 , it was found that conduction band minimum (CBM) and valence band minimum (VBM) are dominated by the contributions of Pb and I atoms. Using Crystal Orbital Hamiltonian Population (COHP) analysis, it was revealed that the VBM is a Pb(s)/I(p) anti-bonding state, while the CBM is a Pb(p)/I(s) anti-bonding state, as illustrated in Fig. 6 [51]. Almost all of the AMX_3 structured materials have shown this trend.

Fig. 7 depicts a comparison of the DOS and absorption spectra of MAPbI_3 and GaAs, demonstrating that the p-p transition is stronger than the p-s transition in GaAs [52]. The distinct variation in DOS near the CBM resulted in a difference in joint density of states (JDOS), resulting in increased light absorption. As a result, PSCs can achieve high PCEs with very thin absorbers. Fig. 7 (d) shows that Pb-based SCs exhibit much higher PCEs than other SCs for any given thickness.

3. Evolution of device architectures

The device performance of PSCs depends on their structure, which will be decided by the materials selection, deposition techniques, and the compatibility between various elements in the device. PSC generally comprises a perovskite light-absorbing material sandwiched between

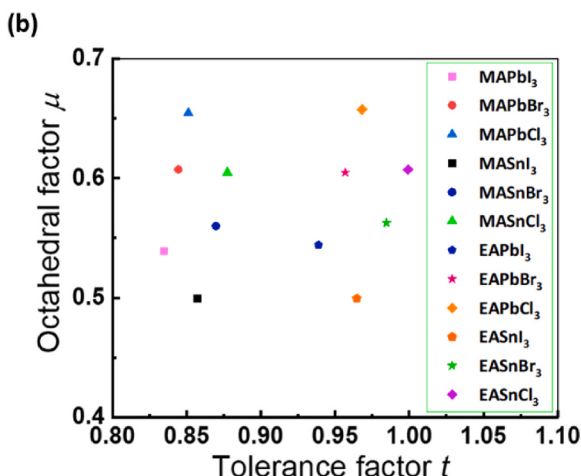


Fig. 3. (a) Cubic perovskite crystal structure (b) Estimated t and μ factors of 12 halide perovskites [41].

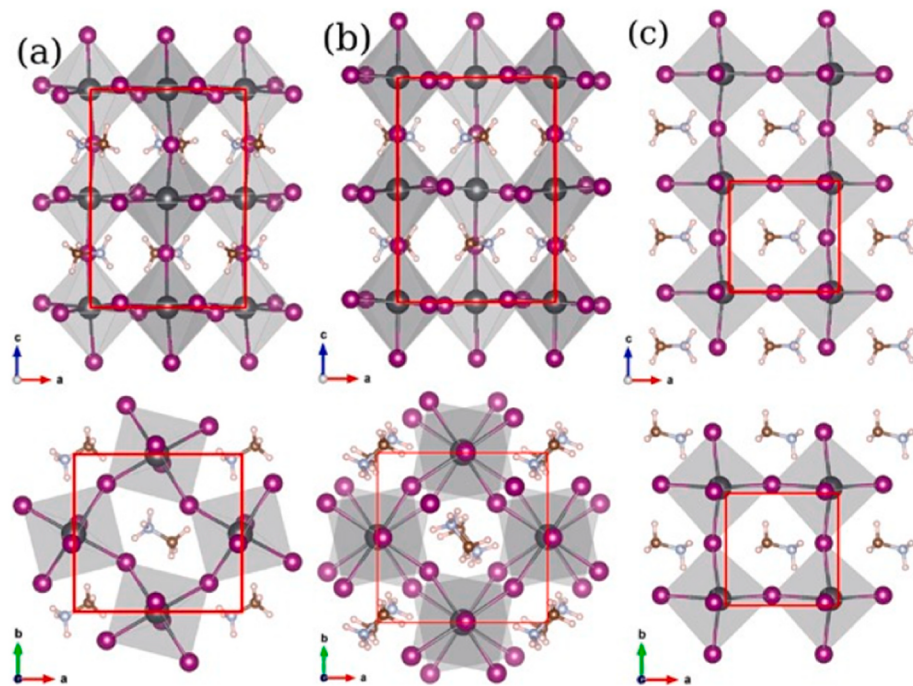


Fig. 4. Different phases of MAPbI_3 perovskite structure (a) orthorhombic, (b) tetragonal and (c) cubic. Top row: a-c-plane and bottom row: a-b-plane [48].

two electrodes. Interfacial buffer layers, including ETM and HTM, are usually applied between the perovskite absorber films and the electrodes to promote charge transportation. PSCs can be categorized as mesoporous and planar architecture based on whether the cell includes mesoporous oxide material. Furthermore, PSCs can be classified into two different configurations based on the electric current direction, including conventional (n-i-p) and inverted (p-i-n) architectures. Fig. 8 illustrates the different architectures of PSCs.

3.1. Liquid-electrolyte perovskite sensitized solar cells

These SCs are composed of a TCO substrate, nanoporous TiO_2 , a perovskite sensitizer, an electrolyte, and a metal electrode (Fig. 8a). An organic electrolyte solution that contains lithium halide and the respective halogen was used to create the HTM, which provided the positive contact. Devices with $\text{CH}_3\text{NH}_3\text{PbI}_3$ exhibited a larger short-circuit current density (J_{sc}) value than $\text{CH}_3\text{NH}_3\text{PbBr}_3$ -based devices due to a narrow bandgap and broad spectrum of the iodide absorber. Subsequently, a quantum-dot sensitized solar cell with similar structures was fabricated by utilizing an approximately 2.5 nm $\text{CH}_3\text{NH}_3\text{PbI}_3$ nanocrystal. Using TiO_2 surface treatment before deposition, a 6.5% PCE was achieved in 2011 [9]. Furthermore, perovskite sensitizer demonstrated better absorption compared to standard N719 dye sensitizers. However, these cells are highly unstable due to the instability that arises from the HTM because of the liquid medium. As a result, no further research was continued on liquid-electrolyte perovskite sensitized cells.

3.2. Mesoscopic perovskite solar cells (MSPSCs)

The mesoporous structure evolved from typical DSSCs. In PSCs, mesoporous (mp) materials enable the perovskite material to bind with the mp metal oxide structure to increase the light-absorbing area of the photoactive layer, hence improving the device performance. The mesoporous structure evolved from typical DSSCs. A typical MSPSC comprises a TCO layer (e.g., FTO, ITO), an ETL, an mp metal oxide scaffold, the perovskite material, an HTL and a counter electrode (Fig. 8b). Most state-of-the-art MSPSCs utilized compact- TiO_2 (c- TiO_2) as ETL and mp- TiO_2 (active scaffold), Al_2O_3 , ZrO_2 or SnO_2 (passive scaffold) as scaffold.

Since the first all-solid-state MSSC was fabricated by Kim and co-workers [10], MSPSCs now achieved PCEs greater than 23% [53]. A two-step sequential deposition route was demonstrated to prepare MAPbI_3 pigment inside the porous TiO_2 film and achieved 15% PCE. It was observed that the conversion took place inside the nanoporous host once MAI and PbI_2 were contacted, allowing much better control over the perovskite morphology [54]. In addition to TiO_2 NPs, TiO_2 in various shapes (e.g., nanorods, nanowires, etc.) and other n-type materials like ZnO have been employed to form the scaffold for MSPSCs, which can also perform as an effective electron collector [55]. Several groups have reported on PSCs utilizing Al_2O_3 as mesoporous material. Unlike TiO_2 , Al_2O_3 behaves only as a supporting layer in the cell and plays similar functions to that of TiO_2 in electron flow. By replacing the n-type mp- TiO_2 with Al_2O_3 , which is a wide bandgap insulator and purely acts as a scaffold, on coating MAPbI_3 perovskite upon it, Lee and co-workers reported 10.9% PCE [56]. Depositing Al_2O_3 NPs with processing temperatures not greater than 150 °C, M. Ball. and co-workers obtained 12.3% PCE on mixed halide $\text{CH}_3\text{NH}_3\text{PbI}_{3-x}\text{Cl}_x$ based PSCs [57]. For the first time, they clearly demonstrated the multi-functional roles of perovskite (light absorption, charge generation, ambipolar charge transportation) in PSCs. Like Al_2O_3 , ZrO_2 and SiO_2 can also be employed as the insulating supporting layer. By preparing MAPbI_3 PSCs using a two-step deposition route with ZrO_2 as a mesoporous layer, 10.8% PCE was achieved. For the same device structure, the ZrO_2 based cells showed larger photovoltage and longer electron lifetime than the TiO_2 based cells [58]. Hwang et al. fabricated PSCs using a scaffold layer composed of size controlled SiO_2 NPs. By introducing NPs with an optimized size of ~50 nm, they obtained a better perovskite infiltration and thus achieved 11.45% PCE and V_{OC} of 1.05 V, larger than the TiO_2 NPs-based cells [59].

Literature reports suggest that the PCE of MSPSCs is related to the scaffold layer thickness. Considering the MAPbI_3 PSCs having an mp- TiO_2 film ranging from 0.6 μm to 1.5 μm , it was revealed that J_{sc} is not strongly dependent on film thickness while V_{OC} reduces from 0.9 V to 0.85 V as the film thickness rises to 0.8 μm , it starts to decline significantly from 1.5 μm . This indicates that apart from solid-state DSSCs that needed a thicker TiO_2 scaffold to obtain adequate absorption, only a submicron thick mp- TiO_2 film is required in hybrid lead iodide PSCs for

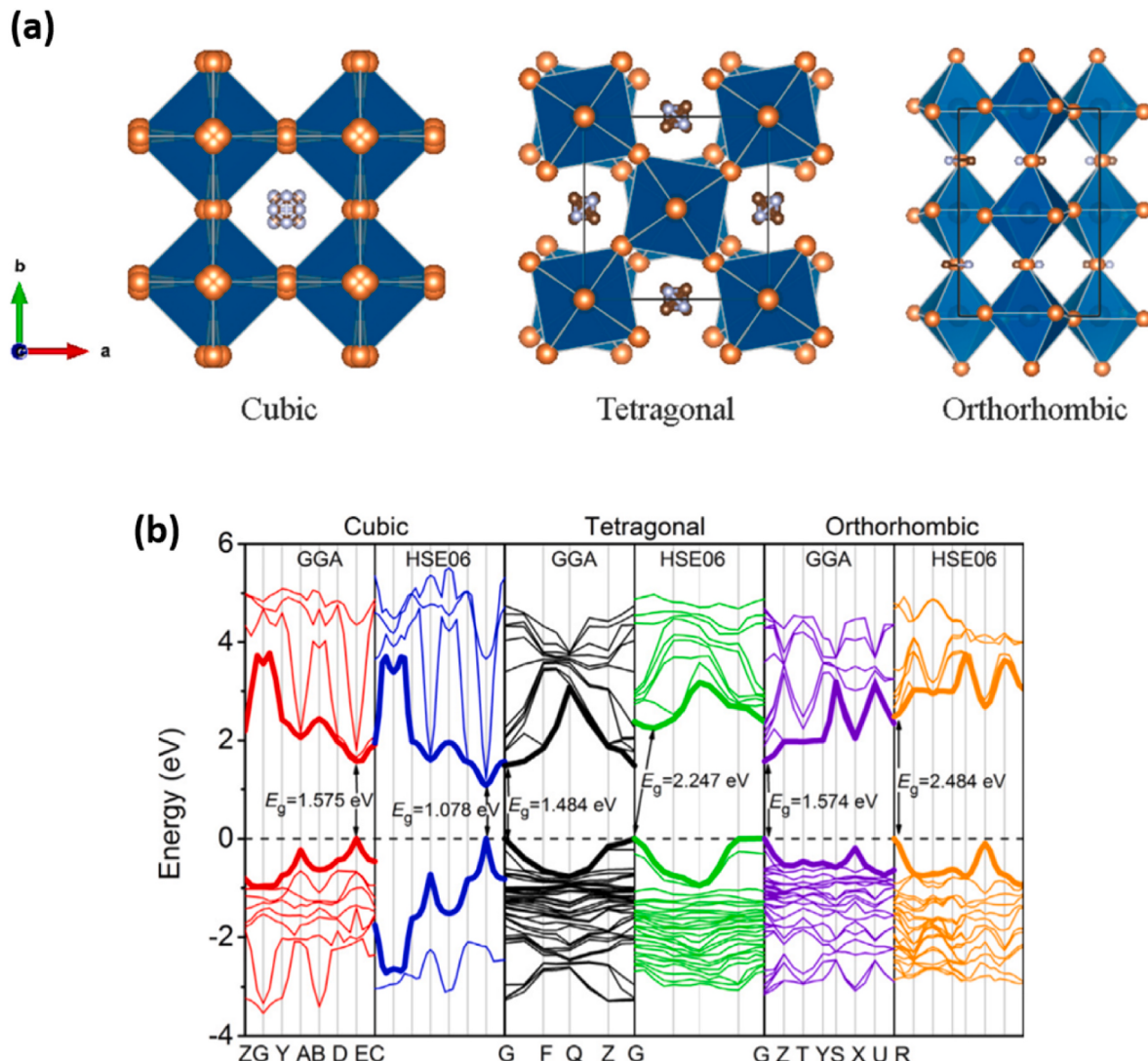


Fig. 5. (a) Top view crystal structures of MAPbI₃ polymorphs, (b) The calculated band structures of CH₃NH₃PbI₃. The colours red, blue, black, green, purple, and orange correspond to cubic (GGA-PBE), cubic (HSE06), tetragonal (GGA-PBE), and tetragonal (HSE06), orthorhombic (GGAPBE), orthorhombic (HSE06), respectively [50].

realizing better operation [10].

Active scaffolds are not restricted to n-type semiconductors. By introducing a low-temperature sputtered NiO_x thin film, Wang et al. fabricated mesoscopic NiO/MAPbI₃ PSCs and achieved a PCE of 11.6% [60]. The utilization of p-type mp film to transport and collect holes improves the diversity of PSCs. The MSPSCs fabricated with passive scaffold do not show photovoltage loss found in their active-scaffold equivalents. For instance, solar cells based on TiO₂ and Al₂O₃ scaffolds demonstrated V_{OC} of 0.8 V and 0.98 V, respectively [56]. The difference in photovoltage is because of the variation in chemical capacitances of the oxides associated with the charge storage capacity due to the presence of sub-band gap states.

In recent years device performance of MSPSCs improved significantly. Saliba et al. achieved 21.1% stabilized PCE on cesium containing triple cation PSCs by employing Li doped mp-TiO₂ layer [16]. By employing spiro[fluorene-9,9'-xanthene] (X59) as HTM instead of commonly used spiro-OMeTAD HTM, Bi et al. realized 19.8% PCE [61]. Using an ionic liquid, Yang and co-workers obtained a PCE of as high as 19.62% via the TiO₂ ETL surface optimization [62]. Surprisingly, the notorious hysteresis was eliminated in their cells, probably attributed to better ETL quality that efficiently passivated ion migration in the absorber and charge aggregation at the interfaces. A PCE of 20.8% was

obtained from PSCs that utilized mp-TiO₂ by employing α-bis-PCBM as a templating agent for perovskite films' solution processing using an antisolvent procedure [63]. The α-bis-PCBM improves perovskite crystallization and addresses the problem of slow electron collection by filling vacancies and grain boundaries in the perovskite layer. Yoo et al. employed IPA in surface treatments and developed a selective precursor dissolution (SPD) for preparing MSPSCs that exhibited 23.4% PCE with a certified stabilized efficiency of 22.6% [64]. Furthermore, they demonstrated that the strategy minimizes and stabilizes SC performance by suppressing the formation of δ-phase perovskite as well as the amorphous phase during surface treatment, which is observed in conventional procedures. Currently, mesoscopic architecture is one of the most favored architectures in PSC manufacturing.

3.3. Planar Perovskite solar cells

Although the realization of low temperature (LT) (sub-150 °C) processing methods had been reported for mesoscopic PSCs via the utilization of NPs [57,65], many published studies still utilize mp films, requiring high-temperature (HT) sintering, especially for the high performing cells. The inadequacy of mp metal-oxide scaffold results in the LT processibility of planar architecture PSCs, which provides a greater

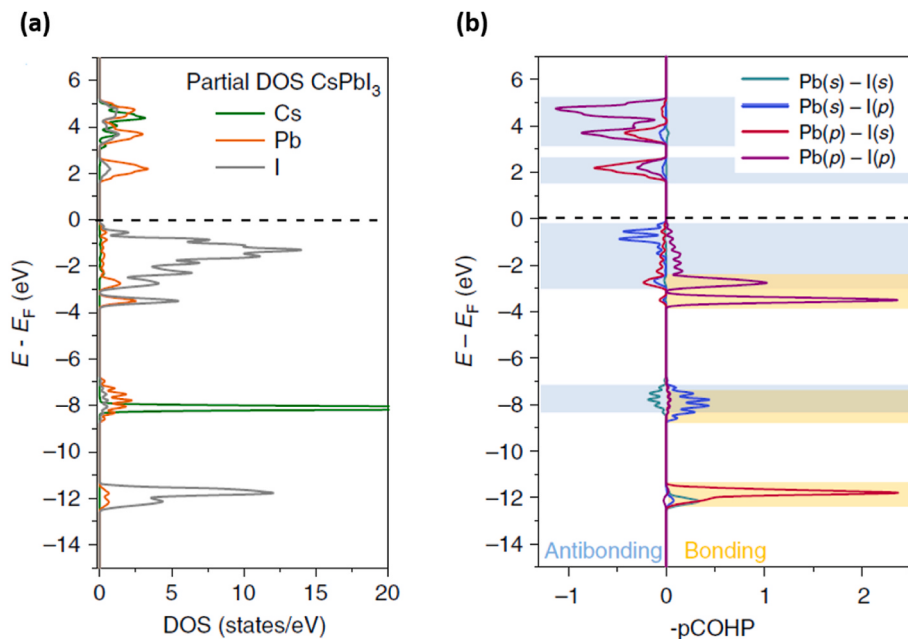


Fig. 6. Orbital contributions to the energy bands of CsPbI₃. (a) Projected DOS (b) Orbital-resolved COHP; positive (negative) sign demonstrates bonding (anti-bonding) nature [51].

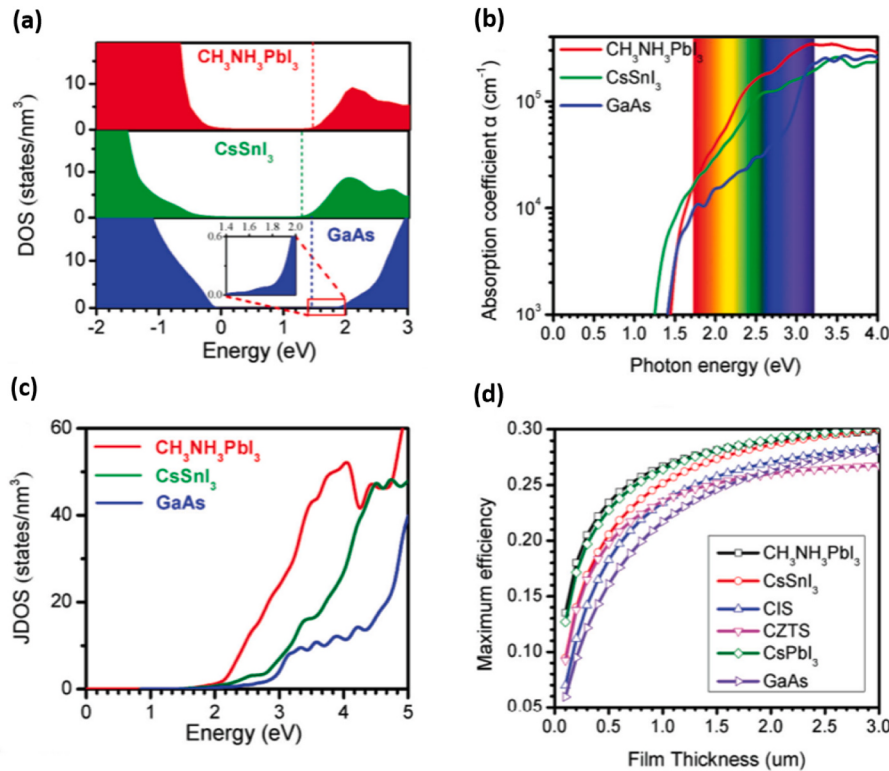


Fig. 7. (a) DOS (b) optical absorption and (c) JDOS of CH₃NH₃PbI₃, CsSnI₃ and GaAs. (d) Calculated maximum PCEs of various solar cells [52].

possibility of fabricating flexible PSCs compared to their mesoscopic counterparts. The scaffold-less planar structure offers significant flexibility in preparation methods of organometal halide perovskites (OHPs), allowing for a variety of materials to be used as CTls to pair with the corresponding perovskite. The planar architecture is an utmost case of mp architecture, where the thickness of the mp layer is zero. Planar PSCs can be defined as an n-i-p or p-i-n ones, depending on the order of different operational layers in the cell, starting from the layer to which

light is incident.

3.3.1. Conventional planar (n-i-p) PSCs

In conventional planar architecture, an n-type ETM is deposited on a TCO substrate, following the sequential deposition of the perovskite absorber layer, p-type HTM and top metal electrode (Fig. 8c). This structure strongly retains the characteristics of the standard MSPSCs, hence the term conventional. M. Ball and co-workers, for the first time,

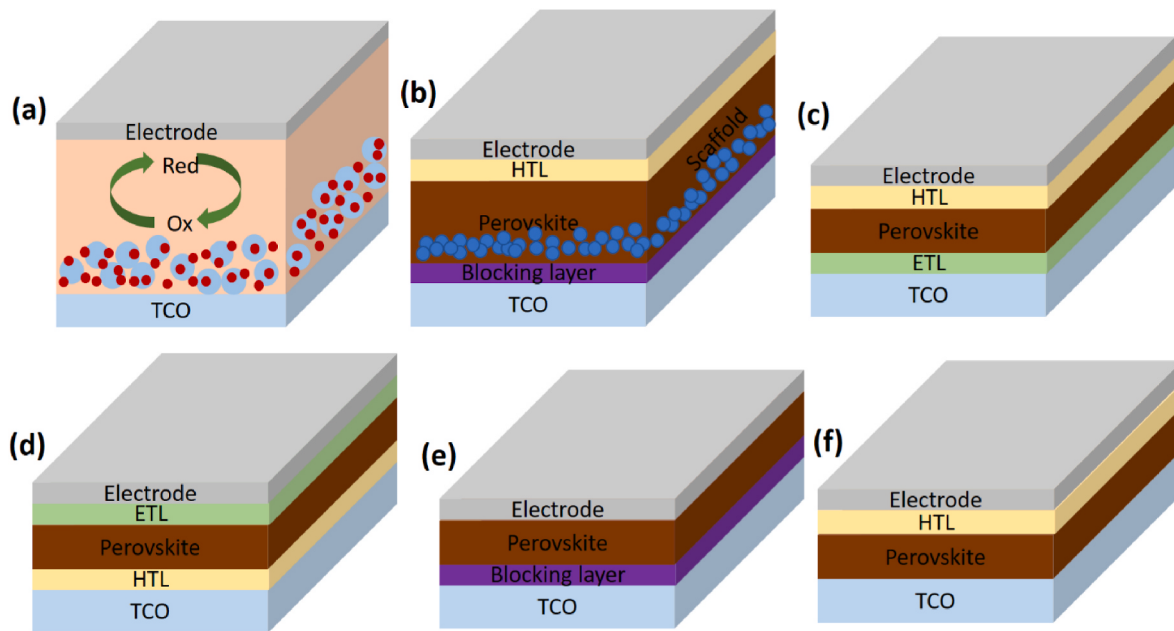


Fig. 8. Typical structures for PSCs. TCO- transparent conducting oxide, HTL-hole transport layer, ETL-electron transport layer.

reported on planar PSCs with FTO/c-TiO₂/CH₃PbI_{3-x}Cl_x/spiro-OMeTAD/Au structure [57]. Subsequently, Eperon and co-workers achieved 11.4% PCE on planar heterojunction (PHJ) solar cells by optimizing processing conditions and morphology of perovskite films. They observed that the highest J_{SC} could be achieved only with the highest perovskite coverages [66]. Liu and Kelly prepared MAPbI₃ films using a sequential deposition method that reported 15.7% efficiency using LT synthesized ZnO as ETL [67]. This LT fabrication process can lower the manufacturing cost and is suitable for polymer substrates. The performance of PHJ PSCs was further enhanced by employing novel charge transport materials utilization of interfacial layers, which improves perovskite film morphology and promotes charge extraction. Doping Yttrium (Y) on TiO₂ ETL and annealing the MAPbI₃ films under 30 ± 5% relative humidity (RH) for reducing charge recombination and facilitating charge extraction, 19.3% PCE was obtained [13]. Sandwiching Au-NPs between two layers of LT synthesized TiO_x film to improve the charge extraction efficiency, Yuan et al. obtained 16.2% PCE [68]. Although LT solution-processed TiO₂, ZnO NPs, and cesium carbonate had been reported as ETLs [13,67], the notorious hysteresis behavior prevented the correct evaluation of their potential [33]. An LT solution-processed TiO_x/60-PCBM as ETL was used to address these concerns, and the as-prepared devices with FTO/TiO_x/PCBM/MAPbI₃/spiro-MeOTAD/Au structure yielded 17.6% stabilized PCE [15]. Subsequently, a simple, solution-processed technological method was demonstrated for preparing SnO₂ films. Devices using these SnO₂ layers exhibited a high stabilized PCE close to 21% [69]. Dopant-free HTMs were also developed for PHJ PSCs. A donor-acceptor conjugated small molecule DOR3T-TBDT has been employed as dopant-free HTM, and the SCs delivered 14.9% PCE. The dopant-free molecule enhances the PCE and eases the fabrication process and potentially reduces PSCs' fabrication cost [70]. Yoon and co-workers achieved a hysteresis-free planar MAPbI₃ PSC with 19.1% PCE by employing a vacuum-processed C₆₀ ETL without a hole blocking layer (HBL). At an optimized thickness of 35 nm, the C₆₀ layer suppresses the grain boundaries of the absorber film and improves charge transport [71]. In addition, they fabricated a hysteresis-free flexible PSC on polyethylene naphthalate (PEN) substrate and obtained 16% PCE. In LT planar PSCs, efficiency and stability losses are due to imperfect interfaces and recombination of charges between the respective contact and the perovskite absorber layer [72]. To address this issue, Tan et al.

utilized Cl-capped TiO₂ films prepared at < 150 °C as ETL in MAPbI_{3-x}Cl_x-based PSCs, recorded certified PCEs of 20.1% in 0.049 cm² and 19.5% in 1.1 cm²-sized cells. The interfacial Cl atoms suppress deep trap states at the perovskite interface on TiO₂ NCs and thus significantly minimize interface recombination at the TiO₂/perovskite interface [21]. By investigating the effect of PbI₂ contents on SC performance, it was reported that devices with moderate residual PbI₂ in perovskite film delivered 21.6% PCE in 0.0737 cm² and 20.1% in 1 cm² sized cells, while too much residual PbI₂ led to severe hysteresis as well as low transit stability [73]. In most of the highly efficient PSCs, spiro-OMeTAD was used as an HTM, where LiTFSI is prevalent as a p-dopant to improve the conductivity and hole mobility. Nevertheless, Li⁺ ions are highly mobile and can migrate across the cell during operation, resulting in increased device hysteresis [74] and the potential for perovskite redox reactions [75], and moisture-induced degradation due to the hygroscopic property of Li⁺ salts [76]. To eliminate Li⁺ from the device stack, PSCs were fabricated using EH44 as HTM, which yielded 18.5% PCE [77]. Wang et al. fabricated inorganic perovskite films using a solvent-controlled growth (SCG) method and achieved PCEs of 14.21%, 16.14% and 9.81% for CsPbI₂Br, CsPb(I_{0.85}Br_{0.15})₃ and CsPbBr₃-based SCs, respectively [78]. These findings demonstrate that the SCG approach is universal, at least for better inorganic perovskite films, to obtain efficient SCs.

3.3.2. Inverted planar (*p-i-n*) PSCs

The inverted and the conventional planar architectures are differed by the relative position of CTLs. In an inverted structure, the HTM is deposited on top of the TCO substrates (Fig. 8d). In most inverted structure PSCs, the typical combination of hole and electron transporting layers are PEDOT:PSS as HTL and PC₆₁BM or PC₇₁BM as ETL. Due to the possibility of LT preparation, the requirement of dopants in the HTM and compatibility with the organic electronic fabrication process, SCs with inverted structures have advantages over conventional ones [79]. Jeng and co-workers fabricated inverted PSCs with ITO/PE-DOT:PSS/MAPbI₃/C₆₀/BCP/Al structure for the first time reported 3.9% PCE [80]. Subsequently, 9.8% and over 6.3% PCE were reported using solution-processed MAPbI_{3-x}Cl_x-based PSCs on glass substrates and flexible PET substrates, respectively [81]. By employing double fullerene layers for electron transporting, PSCs yielded 12.8% PCE. By forming a Schottky junction with the anode, the fullerene layers

significantly minimize dark current leakage and suppress traps in perovskite to improve PCE by increasing the FF to over 80%. It was also noticed for the first time that when using the one-step spin-coating technique, the optimized $\text{CH}_3\text{NH}_3\text{I}:\text{PbI}_2$ ratio of the precursor was not 1 as $\text{CH}_3\text{NH}_3\text{I}$ rich precursor yielded better morphology and efficiency [82]. Although PEDOT:PSS is employed as HTM, its acidic nature is detrimental to long-term cell performance and stability [83]. Using heavily p-doped $\text{Ni}_x\text{Mg}_{1-x}\text{O}$ and n-doped TiO_x CTls, Chen et al. fabricated p-i-n architecture PSCs that reported a PCE of 18.3% [84].

The challenge of manufacturing inverted PSCs on a TCO substrate is to achieve a smooth, pinhole-free perovskite layer to prevent leakage current via the one-step coating technique. The SCs prepared from a solution of $\text{PbCl}_2/\text{MAPbI}_3$ exhibited improved performance compared to SCs prepared from a solution of PbI_2/MAI because the later perovskite film had a rough surface and poor crystallinity, even after annealing at about 100 °C while no scaffold was employed [85]. Liang et al. demonstrated that, due to the sensitivity of crystallization to the interfacial structure, the photovoltaic output is highly reliant on the surface roughness of the substrate. They prepared $\text{MAPbI}_{3-x}\text{Cl}_x$ films using a solution-processed method with 1,8-diiodooctane as an additive for improving crystallization. ITO substrate devices had a 10.3% PCE, while PCE was 11.8% for FTO-based devices [86]. Subsequently, Luo et al. prepared perovskite films using an SSG method, which involves two steps: (a) preparation of perovskite films by solution processing and (b) secondary growth with the aid of guanidinium bromide, which yields a wide bandgap top film as well as a highly n-type perovskite film that eliminates non-radiative recombination. Devices demonstrated a 21.51% champion PCE with a 20.91% stabilized PCE [23].

In general, defects in the perovskite layer act as a recombination center and thus reduce efficiency. To passivate defects, ethylamine alcohol chlorides were added into perovskite films and thus V_{OC} and PCE of the cells rose from 0.87 V to 0.92 V and 14.52%–16.97% [87]. Lee et al. used near-infrared (NIR) annealed Co-doped NiO_x (NIR-Co:NiO_x) as HTM in p-i-n PSCs and enhanced the PCE from 15.99% to 17.77%. The enhancement in efficiency is attributed to the efficient hole extraction, less charge accumulation, and reduced V_{OC} loss resulting from the improved hole mobility, reduced interface resistance and well-matched work function [88].

3.4. Electron transport layer-free perovskite solar cells

Typical n-i-p planar PSCs always require a compact n-type metal oxide film (TiO_2 , ZnO , SnO_2) on a TCO substrate as HBL for electron selective contacts. However, high efficiencies can also be realized in the absence of such ETLs (Fig. 8e). Liu and co-workers fabricated compact layer free bilayer PSCs by depositing MAPbI_3 using a sequential deposition technique. They recorded 11.6% and 13.5% PCE by employing P3HT and spiro-OMeTAD, respectively as HTM [89]. Furthermore, this simpler architecture device shows better stability than ZnO -based planar PSC. Hu et al. introduced an interface engineering approach in which an alkali salt (Cs_2CO_3) solution was utilized to modify the TCO surface to optimize the interface energy level alignment, yielding 15.1% PCE under AM 1.5G 1000 W m⁻² [90]. For obtaining efficient ETL-free PSCs, it is necessary to avoid shunting paths between HTL and FTO, and thus preparation of uniform perovskite films with good crystallinity is required. Ke et al. reported 14.14% PCE using FTO/ $\text{MAPbI}_{3-x}\text{Cl}_x$ /spiro-OMeTAD/Au structure by applying ultra-violet ozone (UVO) treatment to the FTO substrates [91]. UVO treatment can extract the remaining organic species effectively, thereby obtaining perovskite film with improved smoothness and coverage. These efforts aim to achieve easy processing procedures and high performance on flexible substrates for future PSCs.

3.5. Hole transport material free perovskite solar cells

Recently, PSCs without HTM have demonstrated significant

potential because of their advantages of simple architecture, easy manufacturing routes, and high stability. HTL-free PSCs are fabricated by depositing metal electrodes directly on the perovskite absorber layer (Fig. 8f). Spiro-OMeTAD, which exhibits high hole conductivity and mobility and suitable HOMO energy, is used by most state-of-the-art high-efficient PSCs [15,25,73]. However, the complex and low-yielding spiro-OMeTAD synthesis process makes it challenging for further implementation of large-scale and cost-effective PSCs. In HTL-free PSCs, Perovskites are employed as light absorbers as well as hole transport channels simultaneously. Using a device simulation method, Minemoto and Murata revealed that while the work function (Φ) of metal electrodes is close to the VBM of perovskites, the removal of the HTM did not affect the built-in voltage (V_{bi}) of the cell. In comparison, while the work function is below VBM, the built-in electric field (E_{bi}) reduced rapidly, resulting in low V_{OC} and PCE. Thus, the metal electrodes' work function plays a significant role in HTL-free PSCs [92].

In 2012, Etgar and co-workers, for the first time, achieved 5.5% PCE on an HTL-free mesoscopic $\text{MAPbI}_3/\text{TiO}_2$ heterojunction SC [93]. Fabricating PSCs with FTO/ $\text{TiO}_2/\text{MAPbI}_3/\text{Au}$ structure using a sequential deposition method, Shi et al. achieved 10.49% PCE with a V_{OC} of 0.905 V [94]. Through a theoretical simulation, it was revealed that the suitable thickness of the absorber film and p-type doping was helpful for the performance of the HTL-free PSCs. It was found that the PCE of the PSCs in the absence of HTM is expected to be over 15% following the optimization of cell structure [95]. To fabricate HTL-free $\text{MAPbI}_3/\text{TiO}_2$, PSCs Shi and co-workers used a modified two-step deposition technique and obtained 10.47% PCE and a high V_{OC} of 948 mV [96]. The comparatively high V_{OC} is attributed to the lower Fermi energy of MAPbI_3 compared to spiro-OMeTAD. Furthermore, they recorded 11.1% PCE by inserting an ultrathin AlO_x insulating layer using the atomic layer deposition (ALD) technique between MAPbI_3 and Au to block electrons [97]. Mei et al. achieved 12.8% certified PCE in HTL-free fully printable MSPSC by employing a double layer of mp- TiO_2 and mp- ZrO_2 covered by a porous carbon film, in which 5-aminovaleric acid (5-AVA) cations were incorporated for the formation of (5-AVA)_x(MA)_{1-x} PbI_3 . Furthermore, in ambient conditions under full sunlight, the cell was stable for >1000 h [98]. The simple, fully printable, and durable MSPSC opens new paths for the further development of high-PCE, low-cost SCs.

4. Deposition methods of the Perovskite layer

Perovskite film morphology significantly influences the efficiency and stability of PSCs. The morphology of the perovskite film consists of basically two major precursor components, depending on the route of deposition. The precursors may be either deposited concurrently or separately. The deposition techniques of the perovskite material can be broadly divided into two categories, more widely utilized solution-processed deposition techniques and less commonly used vapor deposition techniques. Due to low-cost preparation on large-area substrates and compatibility with roll-to-roll device fabrication, solution-processed deposition methods have a preferential advantage over vacuum deposition techniques. However, vapor deposition methods are highly controllable and prepare perovskite film with better surface morphology and fewer defects. Fig. 9 shows the different deposition techniques of the perovskite absorber layer.

4.1. Solution deposition methods

The solution-processed deposition techniques of the perovskite absorbing layer can be classified as one-step method [100], and two-step method [54,101], depending on the number of steps for deposition.

The one-step deposition was commonly utilized in PSC fabrication because of its low cost and ease of operation. Usually, in the one-step deposition technique, a mixture of metal halide and organometal halide is dissolved in a typical solvent at a certain stoichiometric ratio,

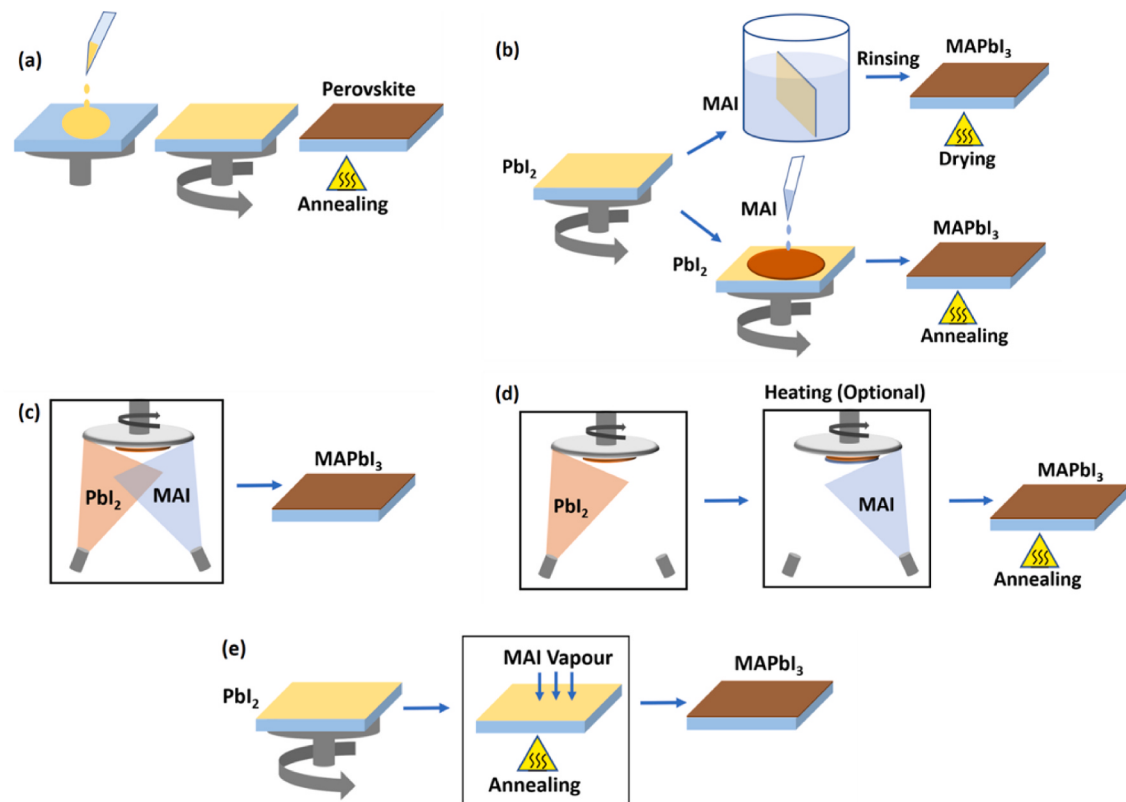


Fig. 9. Deposition routes of perovskite film: (a) solution-based one-step technique, (b) solution-based two-step technique, (c) dual-source vapor-deposition technique, (d) sequential vapor-deposition technique, and (e) vapor-assisted solution technique [99].

forming a precursor solution, which is then spin-coated directly on a substrate and annealed at an appropriate temperature to achieve the perovskite film. The one-step method for deposition is simple, but the morphology and size of synthetic crystals cannot be easily controlled. Lee et al. first demonstrated a one-step deposition method of the perovskite layer by dissolving PbCl_2 in DMF with a molar ratio of 3:1 to adjust the halide anion ratio, reported 10.9% PCE. The perovskite layer was formed after spin-coating for 30 s and post-annealed at 100 °C [56]. By fabricating large-area PSCs with a 1.02 cm² aperture area through the one-step spin coating of perovskite films, Chen and co-workers reported PCE >15% (certified PCE 15%). Hysteresis in the devices was eliminated and retained >90% of the original efficiency for 1000 h of light soaking [84]. However, PCE of planar PSCs prepared using a one-step deposition technique is typically limited because of poor film formation with pinholes stimulated by enhanced crystallization due to solvent evaporation and strong ionic interaction between metal cations and halides [80].

In two-step deposition methods, a metal halide solution is first spin-coated on a TCO substrate and then annealed to obtain the metal halide film. Next, an organometal halide is spin-coated on metal halide films and then annealed to get the perovskite films. In certain cases, in the second step, metal halide film is placed into the organic salt precursor, which creates perovskite via a chemical reaction. Thus, perovskite deposition by the two-step method needs no complete precursor preparation. Although the deposition steps are becoming more complex, the perovskite films' quality and morphology can be well controlled in either stage by changing parameters, which are more process-tunable than the one-step method. A modified two-step deposition route was reported to develop a uniform MAPbI_3 layer with better coverage and thickness of 300 nm on top of the mp- TiO_2 . The resulting perovskite film demonstrated high light-harvesting efficiency and a long carrier lifetime up to 50 ns [101]. In another work, Yang et al. first deposited a $\text{PbI}_2(\text{PbBr}_2)\text{-DMSO}$ film onto a nanocrystalline TiO_2 scaffold by spin-coating lead halide solution containing PbI_2 and PbBr_2 dissolved in

a mixture of DMF and DMSO. In the next step, FAI and MABr solution containing iodide ions dissolved in IPA was spin-coated. The resulting PSCs exhibited 22.1% certified PCE in small devices and 19.7% in 1 cm² cells [20]. Recently, a two-step-solvent engineering procedure was demonstrated for fabricating stable FASnI_3 -based PSCs. In the first step, SnI_2 was deposited using DMF as a solvent, while in the next step, the FAI layer was deposited by applying a cosolvent system containing hexafluoro-2-propanol (HFP), IPA, and chlorobenzene (CB) in a 5:5:2 ratio [102].

The sequential deposition method (SDM) allows a better-controlled perovskite crystallization [54]. Liang et al. developed a two-step SDM that uses a saturated methanol solution of PbI_2 as a precursor to spin-coat on the TiO_2 substrate. The PbI_2 -coated substrate is then dipped in a 2-propanol solution of $\text{CH}_3\text{NH}_3\text{I}$ for an appropriate time, followed by the rinsing of 2-propanol. PbI_2 reacts with MAI after drying at the appropriate temperature, resulting in perovskite film formation. Dipping time and concentration of $\text{CH}_3\text{NH}_3\text{I}$ solution are critical for the morphology and optoelectronic characteristics of the final $\text{CH}_3\text{NH}_3\text{PbI}_3$ layer [103]. In another work, Burschka and co-workers reported an SDM to prepare perovskite pigment within the porous metal oxide film. At first, PbI_2 was deposited into the TiO_2 nanopores by spin-coated a PbI_2 solution in DMF. Subsequently, perovskite film was prepared by immersing the $\text{TiO}_2/\text{PbI}_2$ composite film into $\text{CH}_3\text{NH}_3\text{I}$ solution in 2-propanol [54]. While the two components come into contact, conversion occurs inside the nanoporous host, allowing much greater control over the morphology of the perovskite. Although SDM has been widely utilized to prepare perovskite films, due to the unavailability of appropriate solvents that can dissolve both elements, and the high reaction rate of the perovskite, thin films with pinholes and incomplete surface coverage have often resulted, which reduces the quality of the film and hinders the performance of the SC [66].

4.2. Vacuum deposition methods

Vacuum deposition methods offer possible alternatives to the constraints of solution-processed deposition methods. In general, the perovskite absorber layer vacuum deposition method is carried out under high vacuum conditions. This method can be used to deposit one precursor at a time or to deposit two or more precursors simultaneously. The benefit of this process is that deposition is done in a clean environment and eliminates solvent contamination. In addition, this method is flexible to a variety of substrates, including flexible substrates and textiles, due to the low fabrication temperature. For vacuum deposition; co-deposition, one-step precursor deposition, sequential vapor deposition (SVD) [104], dual-source vapor deposition (DSVD) [105], vapor-solid reaction (VSR) [106] and vapor-assisted solution processing (VASP) [107,108] are some of the most common deposition techniques. A key benefit of vacuum deposition is the ability to deposit perovskite films at room temperature without annealing.

Liu et al. used a DSVD method to prepare $\text{MAPbI}_{3-x}\text{Cl}_x$ films. The film had extremely high uniformity on c-TiO₂ with crystalline features on the length scale of 100s of nm. Films formed by spin coating, on the other hand, form pinholes, causing leakage currents that reduce the output of the system. Furthermore, devices with vapor deposition showed enhancement in J_{SC} and V_{OC} compared to solution-processed ones due to highly uniform and fewer impurity films in vapor deposition. As a result, PSCs processed with the dual-source vapor deposition method exhibited 15.4% PCE, while solution-processed PSCs delivered 8.6% PCE only. However, compared to the vapor deposition process, solution-based sequential deposition is superior in terms of manufacturing cost and large-scale roll-to-roll compatibility [12].

Similar to the two-step solution-processed deposition method, a modified VDM, known as SVD, has been reported. In SVD, deposited layers are annealed after deposition [109] or deposited at high temperatures [104]. Hu and co-workers demonstrated a facile SVD technique for preparing high-quality MAPbI₃ film. A nanoporous PbI₂ film was first vapor-deposited, followed by MAI vapor-deposition, which reacts *in situ* with the PbI₂ film. The fresh MAPbI₃ film was further annealed for complete perovskite conversion and improved film texturing. The smooth perovskite film with ~500 nm grain size achieved 5.4% PCE in PSCs with ITO/MAPbI₃/C₆₀/Ag structure [110]. Arendse et al. demonstrated a facile two-step low-pressure vapor deposition of MAPbI₃ films in a single reactor. In the first step, continuous PbI₂ films were deposited and successfully converted to high-quality perovskite films in the second step during exposure of PbI₂ films to MAI vapor [111].

Another vapor deposition method for perovskite film deposition reported in the literature is the VSR method. The VSR methods basically involve physical vapor deposition, chemical vapor deposition, etc. At high temperatures, they can produce large grain-sized uniform thin films. Traditional VSR processes, on the other hand, must overcome a few drawbacks in order to be suitable for the mass manufacturing of uniform perovskite films. Chen et al. demonstrated a VSR method, fabricated an $8 \times 8 \text{ cm}^2$ SCs module, and obtained an average efficiency of 6% with a 1.5 cm^2 active area. By dissolving PbI₂ into DMF and water, the PbI₂ film was first spin-coated on the HTL substrate and then annealed at 70 °C in the air for 10 min. Next, in ethanol, the MAI powder was dissolved. The solution was then uniformly sprayed onto the top plate's bottom surface, which was maintained at 80 °C. Finally, perovskite films were synthesized using two parallel hot plates placed inside a vacuum desiccator. The resultant PSCs exhibited the best efficiency of 12.2% [106].

The Vapor-assisted solution-processed (VASP) technique may be interpreted as a modified two-step technique that integrates the benefits of the solution and vacuum deposition methods. This is a comparatively cost-effective technique for synthesizing better perovskite films. In order to produce organic/inorganic hybrid perovskite film, VASP was developed in which the inorganic film is prepared via the deposition of the precursor solution on the substrates and then treated with the organic

vapor desired. Ideally, the VASP method ensures stronger interaction with both precursors than with the solution. In addition, this technique effectively prevents partial perovskite dissolution, specifically during the dipping mechanism. Consequently, an improvement in perovskite film stoichiometry could be possible. Chen and co-workers first reported an LT VASP method prepared full surface coverage, small roughness, and microscale size grains perovskite films. At first, PbI₂ film was spin-coated, followed by annealing to form the perovskite films in MAI at 150 °C in the N₂ environment. PSCs based on the as-prepared films are highly reproducible and deliver 12.1% PCE [112]. For most of the VASP techniques, high vacuum conditions or inert ambient is always required, which is inconsistent with the low-cost feature of next-generation solar cells. A modified VASP route of high-quality perovskite films in the open air has been developed to address this issue, which exhibited a superior ambient tolerance even at high RH over 60%. The perovskite film crystallization has been shown to be highly dependent to vapor diffusion and reaction in interface and film recrystallization induced by the *in-situ* annealing process. The as-prepared PSCs delivered a PCE of over 18%, with a champion PCE of 18.9% [107]. The high reproducibility of high-quality films, including high purity, consistency with large areas, better control over film thickness and morphology and high PCE, are some of the most significant advantages of VASP deposited PSCs.

4.3. Other deposition methods

In addition to the typically utilized solution or vapor deposition, other deposition techniques have also been proposed. Gas-blowing during spin coating is influenced the device PCE. However, SCs with and without gas-blowing yielded poor PCE. Gas-blowing has been demonstrated to minimize the interface defects between the perovskite and PEDOT:PSS and create a flat perovskite layer [113]. However, PCEs of up to 17% were also recorded for gas blowing during spin coating, attributed to enhanced film morphology and crystallization by altering nucleation kinetics and crystal growth [114]. A three-step sequential solution-processed technique was also developed for preparing PbI₂-free MAPbI₃ films. However, all the devices using the as-prepared perovskite films yielded PCE <5%, and hence it is unworthy for high-performing cells [115].

A blade coating technique has also been frequently used for preparing perovskite films because of its simplicity, cost-effectiveness and high throughput [116]. The benefit of the blade coating technique is that the distance between the blade and the substrate and the *in situ* annealing temperature can be controlled. As compared with the spin coating deposition technique, the doctor-bladed MAPbI₃ films have a larger grain size, as well as good reliability and reproducibility in a large area [117]. Razza et al. fabricated 10 mm² PSCs with a maximum efficiency of 13.3% using a blade-coating method. Meanwhile, 4.3% PCE was reported for the 100 cm² perovskite module [118]. Recently, the fabrication of FAPbI₃ films by employing a cost-effective, high-yielding doctor-blade-coating method has been reported. By optimizing the blading temperature, crystal sizes of over 10 μm were obtained, which yielded an efficiency of 7.29% in PSCs [119].

There are also several other promising deposition techniques that result in high-performance devices. A Direct contact-intercalation method to prepare perovskite films has been reported. Upon direct contact of the PbI₂ films with the MAI layer leading to the MAPbI₃ films after intercalation reaction at 150 °C in a closed container. PSCs made up of the as-prepared films exhibited PCE as high as 16%, with an average value of 14.3% [120]. By using the solution-based hot-casting method, continuous organometallic perovskite thin films without pinholes and millimeter-scale crystalline grains were prepared. In another work, Liang et al. reported a facile spray deposition process for perovskite film preparation under the ambient environment with up to 50% RH in the absence of post-annealing treatment. The as-prepared films have micrometer size grains with complete surface coverage [121]. Very recently, high-performance PHJ PSCs using MAPbI₃ films have been

demonstrated on a bi-layered ZnO/TiO₂ ETL from aqueous Pb(NO₃)₂ using an easy, environmentally friendly, efficient and cost-effective dip-coating deposition method [122]. It could be concluded that considering its complexity, a two-step deposition technique enables independent control of each precursor in the deposition conditions and hence their reaction afterwards. Consequently, this allows greater control over the phase of perovskite film formation.

In addition, hybrid perovskite deposition methods were also demonstrated for the preparation of PSCs. The hybrid deposition method enables the formation of perovskite films having smooth surfaces, full surface coverage, uniform chemical composition, and semi-transparency. Through the precise control of CH₃NH₃PbI₃ flow, which has a high vapor pressure character, and metal halide deposition rates, 11.5% efficient PSCs have been developed [123]. In another work, perovskites were synthesized using a hybrid chemical vapor deposition (HCVD) method, and the SCs achieved 11.8% PCE [124]. Recently, Qiu et al. demonstrated a rapid HCVD method for PSCs based on a fast thermal process that significantly decreases the deposition time to less than 10 min (comparable to that of the solution deposition process) and effectively suppresses hysteresis. The fabricated 22.4 cm² perovskite module delivered 12.3% PCE, maintaining 90% of its initial efficiency over 800 h under continuous irradiation [125]. The method is particularly attractive because of its ability to precisely control gas flow rate, temperature and pressure with high reproducibility, which can be scaled up to the industrial level.

The progress in deposition methods aims to obtain high quality, lightweight, and better coverage perovskite films. The key reason for the research in deposition techniques is to make better electrical contact across different layers, reduce defect density and carrier losses during charge transportation, and realize high PCE with better stability and reproducibility.

5. Methods for improving the performance of PSCs

In general, the performance of PSCs can be improved through three methods. The first approach is to tune the chemical composition of perovskite, adjust its band gap and increase the generation charges [16, 21, 126, 127]. The second method is to increase perovskite grain size, reduce cracks and pin-holes, result in the passivation of recombination of bulk defects and electrical leakage, and increase V_{OC} [63, 73, 100, 128]. The third method is the modification of interfaces for interface and surface recombination passivation, decreasing interface contact resistance, thus increasing J_{SC} [13, 24, 27, 64, 129].

In perovskite solar cells, as device size increases, the series resistance (R_S) increases among the CTIs, perovskite layer and electrodes. Concurrently, the number of cracks and pinholes that form shunt resistance (R_{SH}) increases and the value of R_{SH} decreases. Increasing R_S and decreasing R_{SH} increases the interface losses, hindering photovoltaic device performance [130].

5.1. Chemical engineering

The band gap of perovskite materials can be regulated by exchanging the chemical element to achieve a suitable bandgap for photovoltaic performance. Using a mixed-halide perovskite MAPbI₂Cl, 10.9% PCE was reported. Unlike MAPbI₃ plumbates in SCs, this mixed-halide perovskite was significantly stable in air processing. Moreover, compared to its pure iodide equivalent, MAPbI_{3-x}Cl_x perovskite has shown better stability and carrier transport [56]. W.S. Yang and J.H. Noh fabricated PSCs with FAPbI₃ using an intermolecular process (IEP) between FAI(MABr) and DMSO with FAI(MABr) solution and pre-deposited PbI₂(DMSO) layers. The FAPbI₃ film deprived of PbI₂(DMSO) has a dense and well-developed grain structure having grains larger than the FAPbI₃ film deprived of PbI₂. Meanwhile, devices showed efficiency as high as 20.2% [14]. By partially substituting HC(NH₂)₂⁺ with Cs⁺ Lee et al. found perovskite films with better photo and moisture stability

because of the improved interaction between FA⁺ and iodide due to cubo-octahedral volume contraction. In addition, upon Cs⁺ incorporation, trap-density is decreased by one order of magnitude, and thus PCE increased from 14.9% to 16.5% [131]. By incorporating Cs into the perovskite, devices were fabricated with Cs_x(MA_{0.17}FA_{0.83})_{100-x}Pb(I_{0.83}Br_{0.17})₃ (x is in %) perovskite that exhibited a stabilized PCE of 21.1% [16]. The impact of the smaller Cs on the combination of MA/FA leads to a decrease in the effective radius of the Cs/MA/FA cation, thus shifting the GTF to a cubic lattice structure corresponding to the black phase perovskite. In another work, Li et al. prepared FA_xPEA_{1-x}PbI₃ perovskite by incorporating phenylethylammonium iodide (PEAI) into FAPbI₃ and realized a PCE of 17.7%. The enclosure of PEA⁺ ions at the boundary of the crystal grain can not only act as a molecular lock for tightening FAPbI₃ domains but also suppress surface defects to increase the stability of both phase and moisture [127]. Yang et al. incorporated extra iodide ions into the organic cation solution for preparing perovskite films through an intermolecular exchange process, which reduces deep-level defect concentration. The (FAPbI₃)_x(MAPbBr₃)_{1-x}-based SCs delivered 22.1% and 19.7% certified PCEs in small size and 1 cm² cells, respectively [20]. Jiang et al. fabricated (FAPbI₃)_{1-x}(MAPbBr₃)_x-based PSCs and achieved PCEs of 21.6% and 20.1% in 0.0737 cm² and 1 cm² cells, respectively, with a certified PCE of 20.9% in small size devices. Furthermore, they revealed that moderate residual PbI₂ could provide stable and highly efficient SCs without hysteresis, whereas too much residual PbI₂ would result in extreme hysteresis and low transit stability [73].

5.2. Improvement of preparation methods

The cracks and pinholes in the absorbing layer can create electrical leakage (formation of R_{SH}), reducing V_{OC} and FF, thus reducing device efficiency. Therefore, a better large-area perovskite film (cracks and pinholes-free) is needed to achieve highly efficient SCs. In certain devices, the grain size greatly impacts PCE, and it has been claimed that it defines the recombination of charges at grain boundaries. Using Kelvin probe force microscopy and AFM measurements in MAPbI₃ film in MAPbI₃/TiO₂/FTO/glass heterojunction, Yun et al. observed a potential barrier and higher photovoltage along the grain boundary under dark and illumination, respectively. In addition, AFM measurement showed higher J_{SC} near grain boundary, demonstrating the beneficial role of grain boundary in the efficient collection of carriers [132]. Xiao and co-workers reported 15.6% PCE by preparing large grain size perovskite films using solvent annealing technique. In solvent-annealed MAPbI₃ films, the average grain size increased to 1 μm, which is close to film thickness, while for films with thermal annealing, the maximum grain size was only about 260 nm [133]. A solvent engineering approach has also been proposed for preparing MAPb(I_{1-x}Br_x)₃ (x = 0.1–0.15) perovskite films. The use of butyrolactone and DMSO mixed solvent following toluene drop-casting resulted in highly uniform and compact perovskite films through MAPbI-PbI₂-DMSO intermediate phase, allowing preparation of significantly improved hysteresis less SCs with 16.2% certified PCE [134]. In subsequent work, Nie et al. demonstrated that in small grain PSCs, most of the recombination appeared from bulk defect (40%), while for large grain cells, bulk-recombination is only 5% of the overall recombination, demonstrating that defect-assisted recombination is the dominant recombination process in small grain cells [135]. Li et al. observed numerous pinholes and islands in the film deposited by a conventional one-step solution deposition process (CP) [10], and the perovskite did not completely coat the mp-TiO₂. In contrast, the VASP method resulted in pinhole-free with grain sizes between 400 and 1000 nm homogeneous films that completely covered the TiO₂ layer (Fig. 10. (a),(b)). Moreover, the perovskite films prepared by the VASP method exhibited much stronger absorbance and much faster photoluminescence decay than that of the film prepared by the CP method (Fig. 10. (c),(d)) [136]. For MAPbI₃ films, Chen et al. reported a deposition technique that depends on the rapid transformation of amine

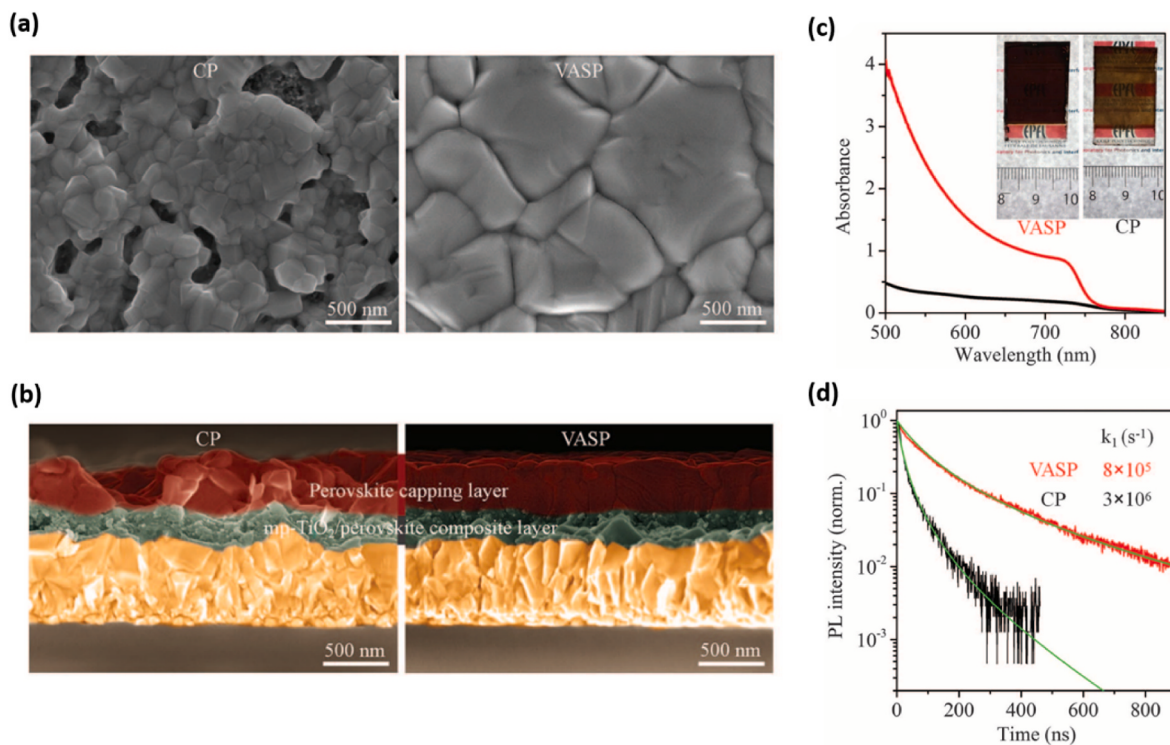


Fig. 10. (a) Surface and (b) cross-sectional SEM images of perovskite films fabricated by CP and VASP. (c) UV–Vis spectra and (d) time-resolved photoluminescence decay of perovskite films [136].

complex precursors into perovskite films, followed by pressure application. The method resulted in highly uniform, pinhole-free films, and the as-prepared cells delivered a certified PCE of 12.1%. Furthermore, the deposition technique can be carried out at LT in the air, enabling the manufacture of large-area PSCs [137].

5.3. Interface engineering

Interface engineering can improve interface contact, reduce carrier recombination and enhance carrier extraction, which is very important in order to obtain highly efficient PSCs with better stability. Interface engineering involves doping, plasma etching, self-assembled monolayers, interface buffer layers, etc. Doping CTls can enhance their electrical performance, improving carrier concentration and mobility. For instance, the conductivity of Li–Mg co-doped NiO (Li–Mg:NiO) films (2.32×10^{-3} S/cm), which is ~12 times higher than that of bare Mg_xNi_{1-x}O. Similarly, doping of TiO₂ films by Nb⁵⁺ increases the conductivity (~104 S/cm) ~100 to 1000 times [84]. To achieve rapid extraction of charge carriers, Li–Mg:NiO and Nb-doped TiO_x were used as HTL and ETL, respectively, in inverted PSCs, resulting in enhancement of FF from 0.64 to 0.827. In addition, SCs of >1 cm² active area exhibited >15% certified PCE [84]. In LT planar PSCs, contact passivation improves interface binding and reduces interface recombinations. By employing a contact passivation strategy using colloidal Cl–TiO₂ NC film as ETL, Tan et al. demonstrated an improvement in the recombination lifetime of charge carriers from 64 to 145 μs. Devices with the size of 1.1 cm² exhibited 19.5% certified PCE without hysteresis [21]. Interlayers include thin layers or monolayers of organic molecules that modify a particular interface in the device [138]. To modify the interfacial properties of PSCs, Chang et al. introduced a thiol-functionalized self-assembled monolayer (SAM), which reduced charge recombination at the interfaces, thus increasing J_{SC} (19.43–21.68 mA/cm²) and FF (0.67–0.72), achieved 15.98% PCE on 1.2 cm² ITO-free PSCs [59]. Inserting a conjugated polyelectrolyte (CPE) PFN-P2 between the absorber layer and HTL (PTAA) and an ultrathin (0.6–1 nm) LiF between

the absorber layer and ETL (C₆₀) resulted in a substantial decrease of interfacial recombination, PCE >20% (19.83% certified) was achieved [24]. Using Ta-WO_x/conjugated polymer multilayers in a simple planar architecture device, a maximum PCE of 21.2% was achieved [130].

6. Challenges in Perovskite solar cell

6.1. Stability

PSCs have certainly shown the probability of achieving extremely high PCEs compared to those achieved for thin-film SCs in the near future. However, PSCs yet confront various issues regarding their commercial viability. Stability has been recognized as one of the major issues with perovskites and, therefore, PSCs [139]. Many factors such as temperature, illumination and air (moisture and oxygen) exposure, etc., influence the stability of PSCs, and there are several reviews regarding this important issue [140–142].

6.1.1. Degradation mechanisms

The degradation of PSCs has arisen due to every single component of the cell. We discuss the degradation mechanisms of PSCs because of various functional layers, namely, the perovskite absorbing layer, charge-transport layers, and electrodes.

6.1.1.1. Degradation of PSCs due to perovskite absorber. Moisture is a critical component that causes the instability of perovskites. The most studied perovskite material in solar cell application, MAPbI₃, is susceptible to moisture, which, based on the context, can have both positive as well as negative consequences. The appearance of moisture has been reported to significantly affect the film morphology [66] and has been argued to improve device efficiency [13]. However, perovskite materials like MAPbI₃ readily react with water due to their hygroscopic nature and finally degrade into MAI and PbI₂, including intermediate by-products of monohydrate MAPbI₃·H₂O and dihydrate (MA)₄PbI₆·2H₂O during the degradation [143,144], on the other hand, at the same time, H₂O

was proposed to stimulate perovskite crystallization containing isolated $[\text{PbI}_6]^{4-}$ octahedra [143]. In the absence of illumination, the degradation of MAPbI_3 upon exposure to moisture includes hydrate formation, which may be reversible [145]. However, continuous moisture exposure and/or light exposure results in irreversible degradation of PbI_2 [146]. In addition to MAPbI_3 , FAPbI_3 also showed instability against humidity. The black perovskite phase of FAPbI_3 converts to the non-perovskite yellow phase in the presence of solvent when FA^+ decomposed to NH_3 and sym-triazine in water, yet both are stable under a dry environment [147]. On the other hand, the moisture content is crucial to forming large grain ($\sim 500 \text{ nm}$) MAPbI_3 films with good morphology and fewer pinholes [148], attributed to moisture assisted crystal growth phenomenon. A numerical model was recently proposed to elucidate the kinetic details of perovskite grain degradation and reconstruction under the influence of water molecule diffusion [149]. The numerical simulation reveals that the moisture diffusion needs to be initiated by a certain level of structural imperfection and is non-Fickian, below which degradation happens slowly. However, the diffusion is much accelerated as the perovskite structure opens by the hydrogen debonding, leaving behind isolated pockets. On the other hand, the structure recovery has to follow reverse diffusion, which is accompanied by hysteresis and instability.

In addition, perovskite materials in PSCs undergo degradation under illumination and exposure to ambient air. The light-induced perovskite degradation highly depends on the composition of hybrid perovskite and is also correlated with light intensity and ambient temperature [150]. UV light illumination along with O_2 accelerates perovskite degradation by HI decomposition in iodide-based perovskites. Although many factors (e.g., temperature, phase behaviour, pressure, UV light, moisture and crystallinity) was found to affect PSC stability [151], moisture-induced degradation is generally considered the dominant effect influencing the stability of MAPbI_3 SCs under environmental conditions. In contrast, under both light and O_2 exposure, MAPbI_3 showed fast degradation. The reaction is initiated by the deprotonation of MA^+ by a photo-generated

reactive oxygen constituent (superoxide, O_2^-) [152]. Bryant et al. reported that illumination and O_2^- induced degradation is the key reason for the poor operating stability of MAPbI_3 PSCs exposed to ambient conditions [153]. In the presence of both illumination and dry air, they observed a fast degradation of unencapsulated MAPbI_3 PSCs within minutes to a few hours. Furthermore, degradation in the presence of O_2 was perceived under electric bias-driven current flow under dark conditions. On the other hand, considerably slower degradation was found for MAPbI_3 SCs under moisture exposure only (85% RH in N_2). Chen et al. investigated the mechanism for the initial stage of light-induced degradation of encapsulated PSCs by analyzing the effects of light-induced heat, strain, electric field, and charge carriers [154]. They demonstrated that strain and electric field are not involved in the initial fast degradation of MAPbI_3 under irradiation. The generation of extra recombination sites facilitated by high temperatures and additional charge carriers is shown to eventually result in fast light-induced degradation, as shown in Fig. 11 and Fig. 12. Recently, Akbulatov et al. used a series of analytical techniques to reveal the first systematic assessment of inherent photothermal stability of a broad set of complex lead halides APbX_3 incorporating different cations ($\text{A} = \text{MA}^+, \text{FA}^+, \text{Cs}^+$) and halogen anions ($\text{X} = \text{Br}, \text{I}$). They demonstrated that heat stress and light soaking induce a severe perovskite degradation even in the absence of moisture and O_2 , as shown in Fig. 13 [155].

The thermal stability of PSCs is also raising concerns for commercial purposes. Temperature plays a major role in the organic-inorganic hybrid perovskites' phase transition and crystal structure. The thermal degradation of perovskites occurs when the temperature rises and the color of perovskite film go from dark brown to yellow [156]. A. Poglitsch and D. Weber studied the temperature-dependent structure evolution of methylammonium trihalide perovskites MAPbX_3 ($\text{X} = \text{I}, \text{Cl}, \text{Br}$) [157]. At RT, MAPbI_3 typically exhibits a tetragonal structure, while MAPbCl_3 and MAPbBr_3 exhibit a cubic structure. MAPbI_3 begins to degrade at 230°C , whereas FAPbI_3 decomposes at a temperature of 290°C [158]. MAPbI_3 films have been reported to be inherently

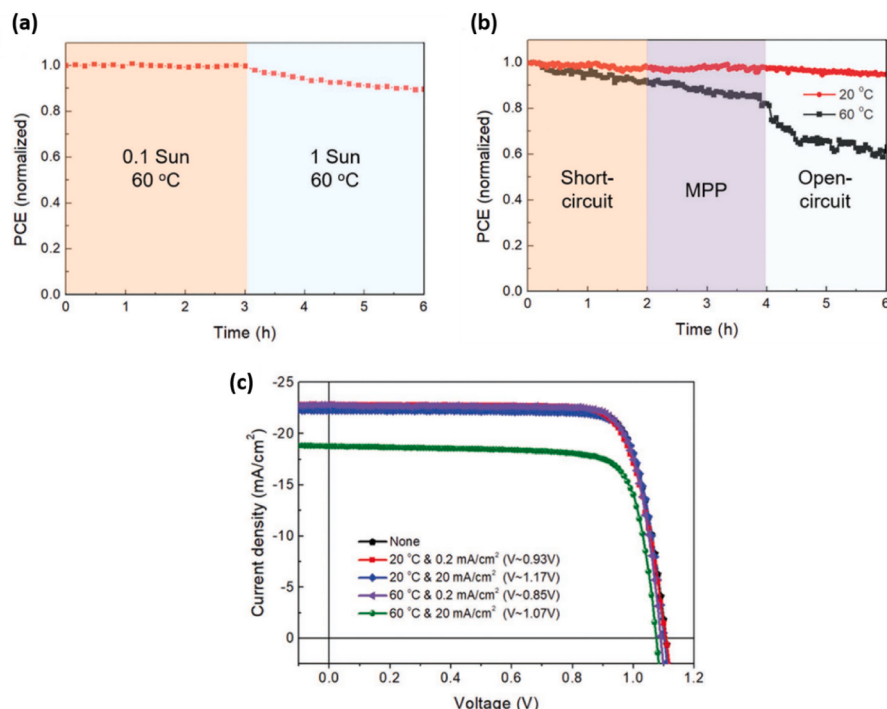


Fig. 11. Influence of excess charge carriers and temperature on the stability of MAPbI_3 SC. (a) PCE decay of encapsulated device under 0.1 and 1 sun illumination with device temperature maintained at 60°C . (b) PCE decay of encapsulated device at short-circuit, MPP, and open-circuit condition with device temperature of 60 and 20°C , respectively. (c) J-V curves of MAPbI_3 SC after charge injection under constant current density in the dark for 2 h with different operating temperatures [154].

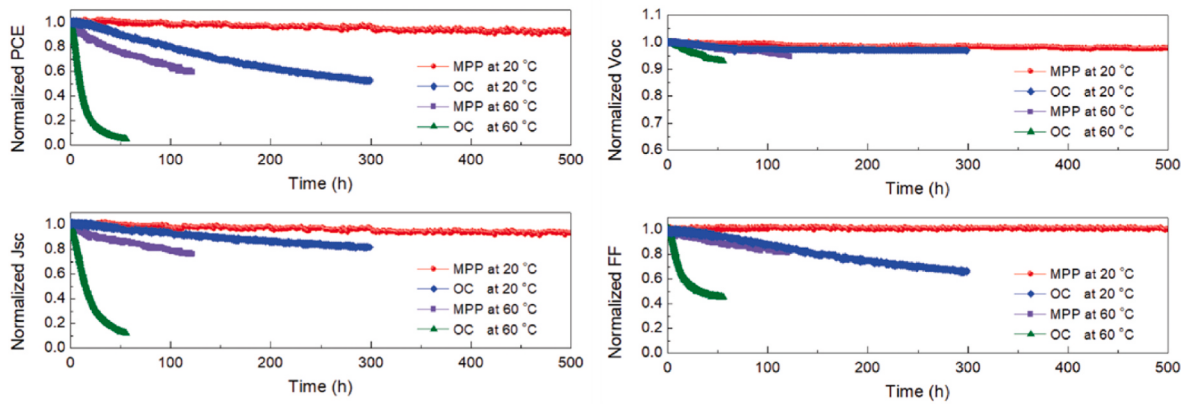


Fig. 12. Long-term stability of encapsulated MAPbI₃ SCs under 1 sun irradiation under MPP at 20 °C, OC (open-circuit) at 20 °C, MPP at 60 °C, and OC at 60 °C, respectively [154].

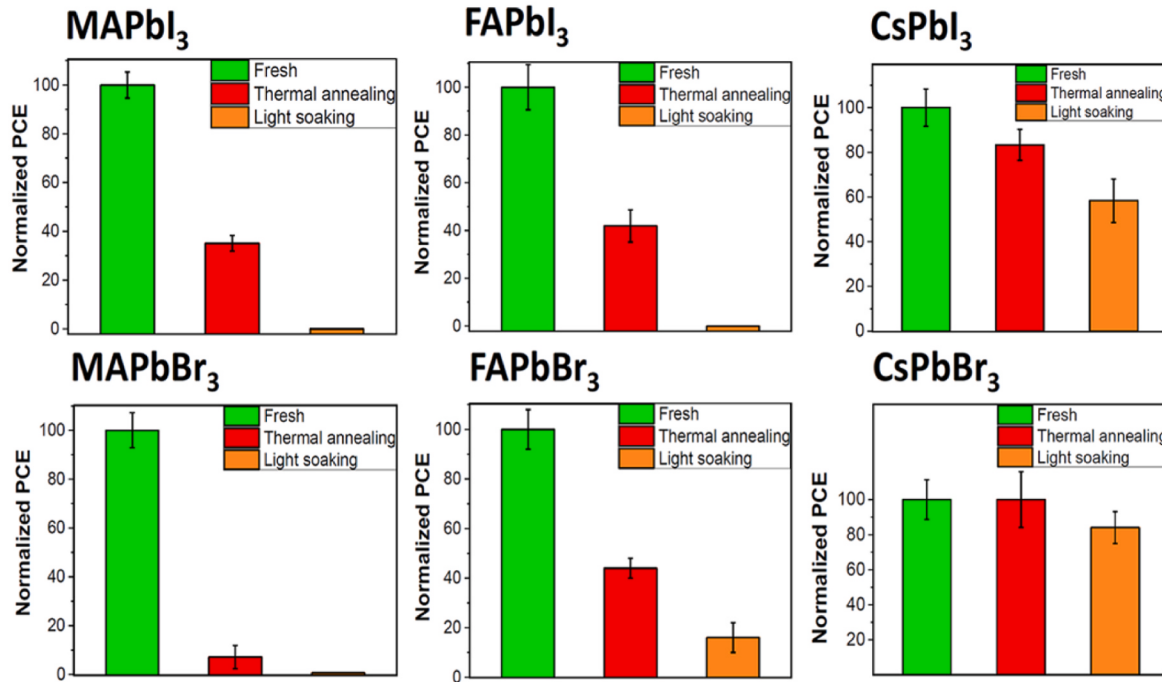


Fig. 13. Roll-off in the SC PCE (normalized) after applying thermal annealing (70 °C) or light soaking (1000 W/m², 70 °C) to the device for 300 h [155].

unstable and degrade at temperatures >85 °C even in an inert atmosphere or 100 °C [159]. Moreover, irreversible changes of MAPbI₃ take place at temperatures above 50 °C [160]. Recently, Wang et al. investigated the thermal-induced instability of CH₃NH₃PbI₃ using molecular dynamics simulations [161]. They observed that a local instability in the crystal structure is caused by a gradually rising tilt in the PbI₆ octahedra as well as the breaking of the octahedral network, which spreads further in the CH₃NH₃PbI₃ crystal. At lower temperatures, point defects enhance the accumulation and coalescence of these local lattice instabilities, facilitating an irreversible instability. The low thermal conductivity of the perovskite layer is primarily responsible for PSC thermal instability. For MAPbI₃, the thermal conductivity was calculated to be 0.34 ± 0.12 W/mK at RT. Because of the low thermal conductivity, the heat produced in the perovskite film does not spread quickly in a high-temperature environment. As a result, the excessive heat accumulation causes the degradation or phase transition of MAPbI₃ perovskite [162].

6.1.1.2. Degradation of PSCs due to charge-transport layers (CTLs). In addition to the perovskite active layer, CTLs of PSCs also degraded in the presence of illumination and ambient conditions. In most of the highly efficient PSCs, TiO₂ was utilized as an ETL. However, it has been reported that devices with TiO₂ showed instability, especially under UV-light exposure [151,163]. Ito and co-workers reported that UV-light degradation of perovskite layers in SCs is probably because of the photocatalytic characteristics of TiO₂ [163]. Leijtens et al. have demonstrated critical instability in mp-TiO₂-sensitized SCs due to light-induced decomposition of surface-absorbed oxygen. By replacing mp-TiO₂ with mp-Al₂O₃, PSCs result in stabilized J_{SC} under continuous illumination and operation in simulated sunlight for over 1,000 h [151]. However, in the presence of both illumination and dry air, perovskite film on mp-Al₂O₃ degrades through a reaction caused by superoxide ions produced due to the transfer of an electron from photoexcited perovskite to molecular oxygen. While Al₂O₃ was replaced by TiO₂, the degradation was minimized due to less formation of superoxide ions [152]. Furthermore, in the absence of other factors, applied bias causes

reversible migrations of oxygen from the TiO_2 to $\text{CH}_3\text{NH}_3\text{PbI}_3$. Moreover, PSCs using the PCBM layer as ETL undergo rapid degradation under illumination without exposure to oxygen and moisture. The PC_{61}BM layer strongly facilitates the photoinduced decomposition of MAPbI_3 perovskite films by absorbing some of the degradation products, leading to their accumulation in ETL and inducing severe corrosion of the top metal electrode [164].

In addition to ETL, HTLs of PSCs have also contributed to stability. Although spiro-OMeTAD was extensively employed as an HTM in PSCs, it has been reported that devices with spiro-OMeTAD showed inferior stability [165,166]. Using UV-vis measurements, Sanchez et al. revealed light-induced oxidation of spiro-OMeTAD, both in the ambient and inert environment. The photo-oxidation is triggered by the widely used additives of the Spiro-OMeTAD (LiTFSI and tBP) (Fig. 14. (a), (b), (c)), and by the interface contact with the ETL (TiO_2) [165]. This result indicates that spiro-OMeTAD degradation is the key process that causes the limited operation of PSCs. Carrillo et al. demonstrated that the cation radical of spiro-OMeTAD probably oxidizes I^- with I_2 formation, indicating a major degradation route at the perovskite/HTM interface [166]. Furthermore, at elevated temperatures, spiro-OMeTAD encountered severe morphological distortion, displaying large voids in it, which further declined the device's efficiency. PEDOT:PSS, a commonly used HTM in inverted PSCs, also showed poor chemical stability due to its acidic characteristics. The PEDOT:PSS displayed a phase separation, with the PEDOT-rich phase primarily accounting for interface degradation in the oxygen environment [167]. Recently, Sekimoto and co-workers studied the influence of HTL on the light-induced decomposition of mixed organic-inorganic halide PSCs, especially at the perovskite/HTL interface, by hard X-ray photoelectron spectroscopy (HAXPES) and impedance spectroscopy. They demonstrated that light-induced iodide diffusion to the perovskite/HTL interface and the electrochemical reaction to form iodine molecules are important factors for the light-induced degradation of PSCs [168]. Almost simultaneously, Boldyreva et al. studied the photochemical stability of MAPbI_3 interfaces

with five distinct CTLs: naphthalene, perylene diimides, PC_{61}BM , PC_{71}BM and spiro-OMeTAD. Both NDI and PDI greatly trigger the MAPbI_3 photodecomposition due to their specific interaction with PbI_2 formed as distinct perovskite decomposition products. On the other hand, fullerene derivatives absorb other degradation products, MAI, which also induces rapid aging of the perovskite layer. Furthermore, using TOF-SIMS measurements, they observed the gathering of the perovskite degradation products in spiro-OMeTAD and a significant degradation at the perovskite/ SnO_2 interface [169].

6.1.1.3. Degradation of PSCs due to electrodes. Metal electrodes are a key element of PSCs used to collect charge carriers. There are several reports on the instability of electrodes in PSCs published in the literature. Guerrero et al. electrically characterized a variety of PSCs incorporating various metal electrodes with the structure ITO/PEDOT:PSS/ $\text{CH}_3\text{NH}_3\text{PbI}_3$ /PCBM/metal electrode before and after degradation induced by constant irradiation. They demonstrated that decomposition of electrode and energy profile modification in the perovskite layer near the contacts are responsible for device degradation [170]. PSCs fabricated with Ag electrodes undergo rapid PCE deterioration. It was proposed that AgI is formed when the migration of MAI is enhanced by the tiny pinholes in spiro-MeOTAD. Moreover, air exposure triggers the corrosion of silver electrodes compared to dry N_2 exposure [171]. It has been reported that degradation of PSC is primarily caused by metal electrode corrosion: mobile halide ions, such as iodide, migrate to the electrodes via the absorber layer and adjacent electron extracting layer [170,172]. It is clear that the gold contact is not smooth as it contains coarse grains, and the PCBM/Au interface shows signs of delamination while the MAPbI_3 /PCBM interface is rather bright (Fig. 14 (e)), pointing to the presence of a high amount of heavy metal atoms at the interface. In contrast, the $\text{Cr}_2\text{O}_3/\text{Cr}$ surface is smooth, and the interfaces close to the cathode are difficult to differentiate (Fig. 14 (f)). Rivkin et al. investigated the operative environment stability of MAPbI_3 PSC that incorporates either an organic or inorganic HBL [173]. X-ray

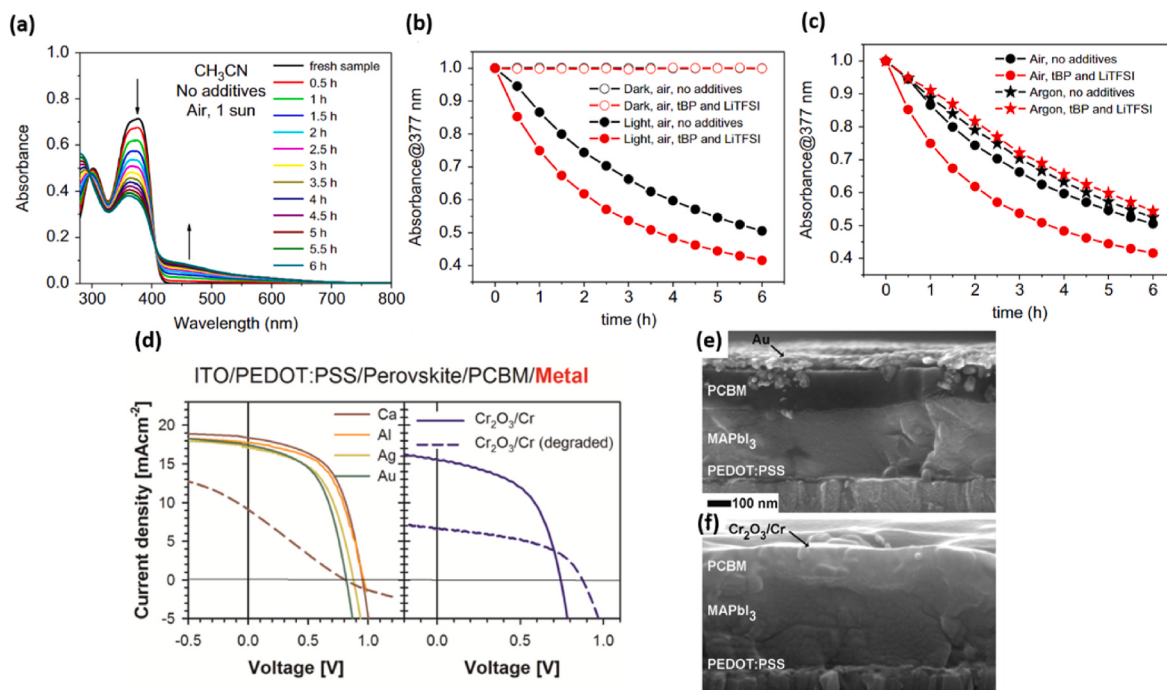


Fig. 14. (a) UV-vis absorption evolution of a Spiro solution (10^{-5} M) in acetonitrile illuminated under 1 sun in air, (b) Evolution of the absorbance in the dark (hollow) and under 1 sun (solid) with the absence (black) or presence (red) of additives in air, (c) Evolution of the absorbance under 1 sun with the absence (black) or presence (red) of additives in the air (circle) and in argon (star) [165]; (d) J-V curves of devices fabricated with different metal contacts measured at 1 sun, Metals providing S-shape curves after degradation, while $\text{Cr}_2\text{O}_3/\text{Cr}$ containing contact does not show an S shape after degradation (Degraded devices are shown as broken lines); Cross-sectional SEM images of degraded devices (e) showing an S-shape J-V curve and (f) degraded device not showing an S-shape J-V curve [170].

photoemission spectroscopy measurements of degraded SC electrodes revealed that only electrodes of cells with an organic HBL exhibit a remarkable iodine signal. Furthermore, under real operating conditions (i.e., constant illumination in different ambient conditions), both types of cells have almost the same deterioration behavior.

In addition to the above degradation mechanisms, bias-dependent degradation of PSCs has also been reported. Recently, M.V. Khenkin and co-workers reviewed on bias-dependent degradation of different photovoltaics [174]. In another work, Domanski et al. reported the effects of electric load on device degradation [175]. They observed that MPP monitoring results in the least deterioration of the cells. Aging the cells at short circuit results in rapid degradation, while open circuit tracking results in the most severe degradation.

6.2. Stability requirements to commercialize the PSCs

For the commercialization of PSCs, they must be at least stable during device operation, viz., when illuminated with a working load/bias in specific environmental circumstances when used. When a device is used in practice, its operational stability influences its behavior/lifetime, highlighting a range of operational stresses and environmental stresses that boost device aging, such as heat, humidity, mechanical load, etc. Unlike environmental factors, which can be efficiently avoided by implementing exterior protection such as encapsulation [176], operational stresses are intrinsically associated with working devices. Hence, the improvement of intrinsic robustness of PSCs against operational stresses is very important to achieve sufficient operational stability. Operational stability is determined by the lifespan of devices operating at constant 1 sun illumination with an applied bias, particularly the MPP tracking, representing PSCs' intrinsic stability.

Besides operational stresses, PSCs are sensitive to various environmental factors such as heat, humidity, mechanical load, and so on, which impede their commercialization. The most relevant testing standards issued by the International Electrochemical Commission (IEC), namely, IEC 61215, contain a series of detailed stress tests that were used to evaluate the potential lifespan of an SC under real operating conditions [177]. P. Holzhey and M. Saliba reviewed on current IEC 61215 tests, where PSCs should remain stable when subjected to a variety of conditions such as 1 sun irradiation ($100 \pm 10 \text{ mW/cm}^2$), thermal cycle (-40 to 85°C), damp heat (85°C and 85% RH), humidity freeze (-40 to 85°C , 85% RH), UV-light (15 kWh/m^2 of UV illumination between 280 and 400 nm), outdoor operations (MPP tracking at least 60 kWh/m^2 of irradiation), hot-spot ($50 \pm 10^\circ\text{C}$ under 100 mW/cm^2 illumination with the maximum power dissipation), hail impact (ice balls with a weight of 7.53 g and a speed of 82.8 km/h) and mechanical load (at least 2400 Pa), and so on [177]. Furthermore, high bias voltage that is not specified in IEC 61215 should not be overlooked as applied bias can cause ion migration as well as SC degradation [154]. Thus, the passing of IEC 61215 testing is necessary for the commercialization of PSCs.

6.3. Approaches to improve stability

The PCE and stability of PSCs depend primarily on the characteristics of perovskites, ETLs, HTLs, electrodes, cell structure, manufacturing techniques, etc. Several approaches have been studied for the improvement of device stability. However, it is worth noting that in a variety of such approaches, the films or cells were not simultaneously subjected to multiple stressors (moisture, UV irradiation, high temperature). Therefore, it is difficult to understand how important these improvements would be under more severe testing protocols than typically demonstrated ambient storage in the absence of irradiance. Perovskite material engineering is one of the techniques to enhance the stability of perovskite as well as PSCs. It was reported that the introduction of Br into the I site in MAPbI₃ resulted in much better moisture stability [178]. Furthermore, bromide has been found to succeed in suppressing

perovskite conversion into monohydrate, likely due to stronger hydrogen-bonding interactions with organic cation [179]. Mixed cation perovskites have also been proposed for the improvement of device stability [16,131,180]. For example, devices based on Cs_x(FA_{0.83}MA_{0.17})_{1-x}Pb(I_{0.83}Br_{0.17})₃ perovskites showed improved stability at $x = 5\%$ compared to $x = 0\%$ [180]. Recently, Xie et al. reported a doping approach to study the influence of individual Br and MA on the inherent operational stability of FAPbI₃ PSCs. The addition of MA into the FAPbI₃ SCs is detrimental to the long-term stability due to defect-induced degradation. However, the addition of Br is helpful for improving the stability of FAPbI₃ devices by reducing the trap density in the perovskite films [181]. This result indicates the significance of defect management in the long-term stability improvement of PSCs. Very recently, J. Cao and co-workers developed a two-step SDM, incorporating Cs⁺ and benzylammonium cation (BA⁺) in FA-based perovskite thin films. The FABACs-based PSCs demonstrated 22.5% PCE maintained more than 95% of its original efficiency under air exposure for 2 months without device encapsulation [182]. In addition, layered perovskites have been demonstrated for the improvement of stability. Usually, the layered perovskites demonstrate better stability but poor performance than 3D perovskites. Recently, Ahmad et al. developed a series of Dion-Jacobson phase 2D perovskites by incorporating diammonium cations into MAPbI₃ and demonstrated that unencapsulated devices maintain more than 95% PCE upon exposure to different stresses that include ambient air (40%–70% RH) for 4,000 h, humid heating (85°C , 85% RH) for 168 h, and constant irradiation for 3,000 h (Fig. 15) [183]. The increased device stability over the RP counterpart is due to alternate hydrogen bonding interactions between diammonium cations and inorganic slabs, which strengthens the 2D perovskite structure. In subsequent work, Liang et al. reported phase-pure quantum well (QW) thin films by introducing *n*-butylamine acetate (BAAc), a molten salt spacer, instead of the commonly used halide spacer *n*-butylamine iodide. The strong ionic coordination between BAAC and the perovskite framework has been attributed to the formation of phase QW films with microscale vertically aligned grained, followed by the formation of a gel-like intermediate phase. The as-prepared PSCs showed only <10% of initial PCE degrading under $65 \pm 10\%$ humidity for 4,680 h, under operation at 85°C for 558 h, or continuous illumination for 1,100 h [184].

Another strategy to improve perovskite film stability and devices is the optimization of preparation and characteristics of the perovskite layer. Crystallinity and coverage have been shown to affect the perovskite layer stability and hence PSCs. In addition, the stability of air storage cells depends on perovskite preparation methods, with blade-coated films being more stable than spin-coated films [185]. This is probably for the reason that film morphology, such as grain size defects in grain boundaries, influences O₂ and moisture diffusion. The stability of the perovskite film depends on grain size; films having large grains exhibited better stability [186]. For instance, solvent engineering enhances perovskite film stability in dark storage at high temperatures (85°C) and low humidity (20–30%) [187]. Very recently, a pressure-assisted solution processing (PASP) method was reported to control the nucleation and growth of perovskite layers having $\mu\text{-}$ sized grains and $\mu\text{-}$ s-range carrier lifetimes. The as-prepared devices exhibited the best PCE of 20.74% (20.33% stabilized PCE), maintaining 91% and 93% of their initial PCEs even aging 60 days and constant 1-sun irradiation for 200 h in ambient conditions without encapsulation, respectively [188].

The addition of additives in perovskite precursor solution has also been demonstrated to improve the stability as well as efficiency of PSCs. Incorporation of polyvinyl alcohol (PVA) enhances the MAPbI₃ film quality; the resulting PSCs yielded a PCE of 17.4%, maintaining over 90% of its original PCE even after 30 days in high humid conditions (90% RH) without device encapsulation [189]. Jin et al. observed the effect of zinc chloride (ZnCl₂) as an additive on MAPbI₃-based PSCs [190]. The partial substitution of PbI₂ by 3% ZnCl₂ enhances the PCE from 16.4 to 18.2% compared to the control cell. Furthermore, the cell

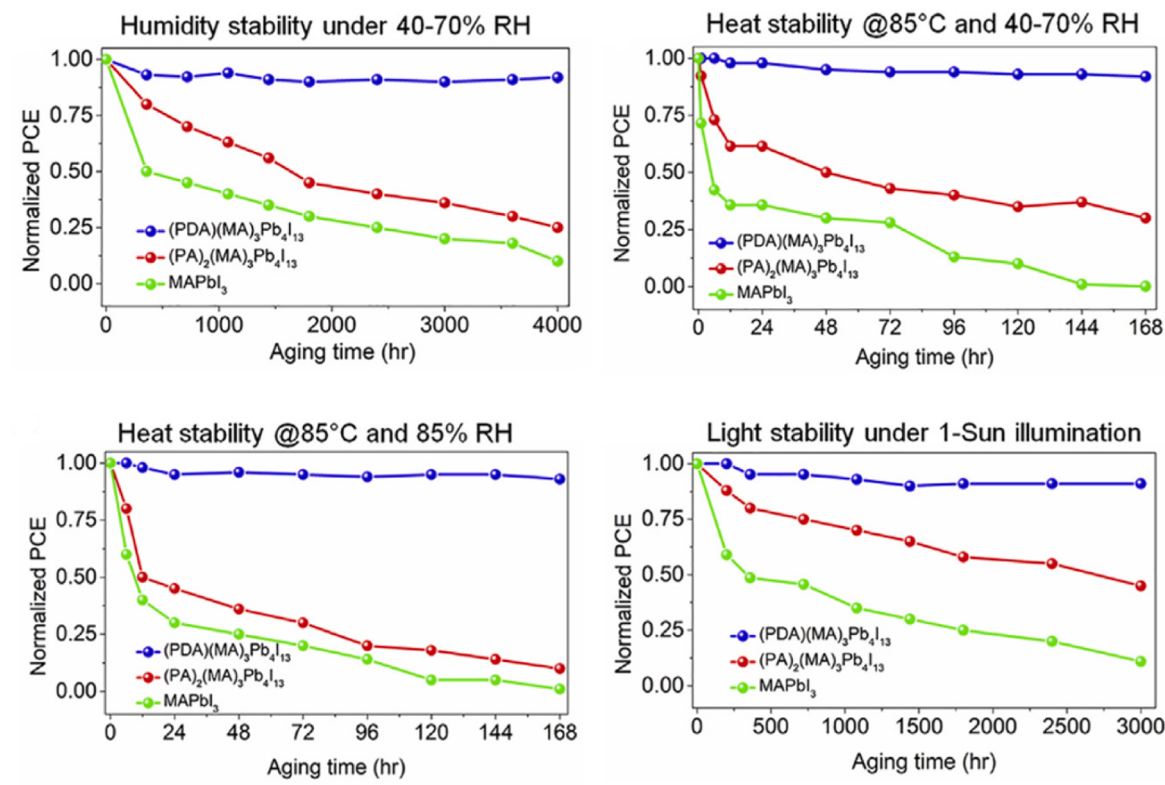


Fig. 15. Stability test of MAPbI₃, (PA)₂(MA)₃Pb₄I₁₃, and (PDA)(MA)₃Pb₄I₁₃ under different operational conditions [183].

was more stable compared to the control cell, with only 7% degradation after aging under ambient air at 25–28 °C with 30–55% humidity without encapsulation for 30 days. Very recently, Liu et al. demonstrated a facile additive strategy by introducing a bifunctional additive guanidine sulfamate (GuaSM; CH₆N₃⁺, Gua⁺; H₂N–SO₃⁻, SM⁻) into the [Cs_{0.05}(MA_{0.12}FA_{0.88})_{0.95}Pb(I_{0.88}Br_{0.12})₃] layer. At an optimal concentration of GuaSM (2 mol%), the PSC delivered a champion PCE of 21.66% that retained 90.7% of its initial performance under 25% RH at room temperature for 800 h without any encapsulation [191].

In addition to the perovskite film modifications, other approaches of stability improvement include altering the cell structure by exchanging the CTls, interface engineering, as well as changing the electrodes. It was reported that PSCs with mesoporous architecture demonstrate better stability in comparison to the planar structure [192]. In addition to the perovskite film modifications, other approaches of stability improvement include altering the cell structure by exchanging the CTls, interface engineering, as well as changing the electrodes. Interface and contact layers across the cell structure play a significant role in overall stability that, when properly adjusted, results in cells that suppress both the rapid initial decay (often called burn-in) and the progressive slower decay. By tailoring the interfaces, Christians et al. reported that even under combining stresses of illumination (together with UV illumination), O₂ and moisture, unencapsulated PSCs maintain 94% of maximum PCE in spite of 1,000 h continued operation at ambient conditions (10–20% RH) [77]. An interfacial layer was also proposed for the improvement of PSC stability. By employing ultrathin inorganic CsPbBr_{1.85}I_{1.15} perovskite QDs on PSCs, Akin et al. achieved PCEs exceeding 21%, maintaining nearly 91% of initial PCE under ambient conditions (RH ≥ 40%) up to 30 days. Moreover, the SCs maintained 94% of their original PCE under continuous light irradiation over 400 h [193]. Defect passivation is also highly desirable to obtain high-performance and stable PSCs. Dou et al. reported the manufacturing of highly reproducible, stable and high-performing SCs via interface engineering with CoO nanoplates that effectively passivate

the trap states, suppress dark recombination, and enhance moisture resistance. The devices yielded a champion PCE of 20.72% and retained 82.16% of the original device performance under ambient conditions (room temperature, 30–50% RH) for 30 days [194].

The replacement of the CTls could be improved the SC stability in two senses, one by improving the stability of CTL itself and the other by improving the stability of perovskite film by reducing the diffusion of moisture and/or other elements such as dopants into it. S. S. Mali and C. K. Hong reviewed the synthetic strategies and role of HTL and ETL towards improved air stability of planar PSCs [195]. Although ZnO is demonstrated as a promising ETM of PSCs due to its large charge carrier mobility and LT processing, ZnO-based cells generally display lower stability than TiO₂-based cells [196]. However, Chang et al. reported 20.12% efficient PSCs with ZnO ETL by low-temperature TiO_x post-treatment that retain 96% and 98% of their original efficiency under ambient storage for 144 h and N₂-filled glove box for 348 h [197]. Recently, Kim et al. fabricated PSCs by replacing mp-TiO₂ with a thin layer of polyacrylic acid-stabilized tin(IV) oxide quantum dots (paa-QD-SnO₂) and achieved 25.4% certified PCE. Under ambient conditions (25% RH, 25 °C) paa-QD-SnO₂@c-TiO₂ based PSCs retained 80% of the maximum PCE (25.7%) for 100 h, while the m-TiO₂@c-TiO₂- and QD-SnO₂@c-TiO₂ based PSCs retained only 30 and 40% of their initial efficiency, respectively, indicating that the paa-QD-SnO₂@c-TiO₂ based cell is more resistant to the moisture and O₂ than the widely used mesoporous structured PSCs [198]. Similar to ETL, HTL also affects the device stability, and various HTMs have been proposed in this regard. The replacement of widely employed HTL spiro-OMeTAD and other organic materials, along with hydrophobic polymers, has been demonstrated to enhance the PSC stability [199]. Recently, Zhao et al. developed a facile method for functionalization of HTMs to suppress perovskite surface defects and allow perovskite films with reduced surface trap state density and efficient charge transfer to HTL. They synthesized two compounds, namely, YZ18 and YZ22 (Fig. 16. (a)), and employed them as HTM in replacement of Spiro-OMeTAD in PSCs. On

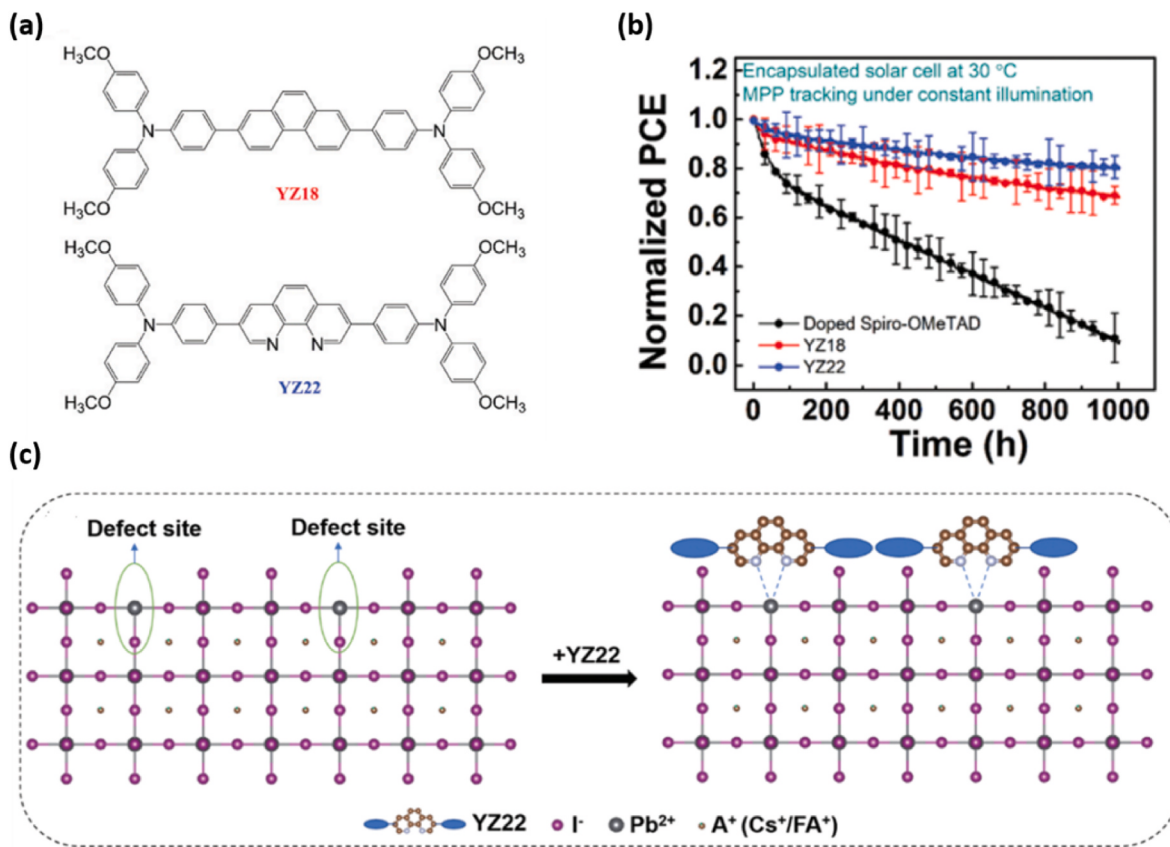


Fig. 16. (a) Molecular structures of YZ18 and YZ22, (b) normalized PCE over time for encapsulated devices with doped Spiro-OMeTAD (black), dopant-free YZ18 (red), or dopant-free YZ22 (blue) as HTL that were held at MPP at 30 °C under an equivalent of B1.1 sun illumination, (c) representation of how YZ22 passivates under-coordinated lead [200].

average, devices based on YZ22 and YZ18 maintain over 60% of their original efficiencies for 1000 h operation, whereas SCs based on doped Spiro-OMeTAD only maintain ~10% of their original efficiencies under an identical environment (Fig. 16. (b)) [200].

Finally, improvement in the stability of PSCs can be achieved by changing the typically employed electrodes Au and Ag. It was reported that mixed-cation PSCs with Cu electrodes have better stability in comparison with Al electrode-based cells. The unencapsulated devices with Cu electrode stored in the ambient condition of ≈25 °C at 20%–60% RH could maintain the performance without any PCE loss for up to 20–30 d, whereas PCE of the cells with Al electrode dropped to near zero after storing it in the air for only 2 d [201]. Subsequently, Seok et al. reported that PSCs with LBSO electrodes maintained 93% of their original PCE under complete solar illumination for 1000 h [22]. PSCs with carbon-based electrodes also demonstrated promising long-term stability [202]. Remarkable stability (>2000 h under ambient storage) of 70 cm² perovskite modules is due to the hydrophobic nature of carbon electrodes [203].

6.4. Encapsulation

The final component of SC that has an important role in overall stability and hence lifetime is device encapsulation. A large number of literature reports have demonstrated cell stability without device encapsulation. Although better stability would be obtained in a low humid environment without device encapsulation, encapsulation is essential to evaluate cell lifetime truly in real operational conditions, including a range of temperatures and moisture. Encapsulation is important to increase cell lifetime and shine a light on the inherent degradation mechanism of the absorber materials. It is done by

protective film deposition and/or sealing the cell. Protective films can be deposited utilizing various methods. Specifically, ALD is a favourable method for the conformal growth of very thin oxide films. However, the utilization of ALD to deposit films on top of the perovskite layer may be difficult because of the required substrate temperature and the utilization of oxidants (water, ozone, hydrogen peroxide) [176]. A significant stability enhancement of p-i-n SCs against liquid water and elevated temperature (100 °C) was obtained by employing an ultrathin amorphous oxide ETM using ALD [176].

Several approaches have been reported for PSC encapsulation. Fu et al. studied the encapsulation process by employing three distinct hot-melt films (polyurethane, PU; polyolefin, POE; and ethylene vinyl acetate; EVA) along with glass on printable MSPSCs. POE and EVA, the commonly used encapsulants for Si and thin film SCs, have been found not to be ideal for PSC encapsulation because of high laminated temperatures (>130 °C) or perovskite layer corrosion. On the other hand, encapsulation using PU can be performed at a comparatively low temperature of 80 °C, greatly improving the thermal stability of SCs. While this encapsulation technique is employed in large-area submodules (100 cm² substrate area) of printable PSC, they retained 97.52% of their original PCE in an outdoor environment for 2136 h [204]. Subsequently, an advanced laser-assisted glass-frit encapsulation technique is demonstrated to seal HTL-free PSCs. The hermetically sealed PSCs have passed 70 thermal cycles (−40 °C–85 °C) and 50 h humid heating (85 °C, RH of 85%) tests in accordance with IEC61646 protocols [205]. However, encapsulation has been found to influence the SC performance significantly during stability tests. Aside from sealing materials, it has been reported that the sealing mechanism itself is also critical to PSC. In fact, thermal stress, UV curing, and high pressure, commonly applied in sealing mechanisms, may harm the SCs and lead to an overall PCE loss

after encapsulation [206].

6.5. Hysteresis

Hysteresis has been commonly reported in PSCs, and it acts as a barrier to the further development of the PSCs. Numerous reports, as well as reviews published in the literature, have discussed the possible origins of hysteresis in PSCs. The proposed possible origins include trapping/de-trapping of charge carriers at deep trap sites created by defects, ferroelectric polarization of the perovskite, capacitive effects, and ion migration associated with a change in interfacial field and barriers resulting from the accumulation of ions at interfaces. It was shown that hysteresis is influenced by the measurement standards. Unger et al. reported that J-V measurement scan direction, delay time, and illumination and voltage bias constraints prior to measurement all significantly affect the hysteresis as well as PCE. At a short decay time of 10 ms, significant hysteresis was observed for both mesoporous and planar devices. The negligible hysteresis of the devices both at fast and slow scan rates is probably because of a very slow response time (Fig. 17) [207]. It was demonstrated that the rate-dependence of hysteresis is associated with a slow field-induced mechanism, which tends to neutralize the electrical field in the cell at each supplied bias voltage. It is due to the accumulation of spatial charges in close proximity to the contacts, independent of irradiation and possibly because of the ionic displacement, which is increased while the cell is aged [208]. Two types of hysteresis have been investigated: normal and inverted hysteresis. Normal hysteresis delivers a higher PCE during reverse bias scan, and

inverted hysteresis shows a lower efficiency, while in forward bias scan, both the hysteresis goes exactly the opposite way. Nemnes et al. reported normal and inverted hysteresis for the same device with FTO/TiO₂/MAPbI_{3-x}Cl_x/spiro-OMeTAD/Au architecture, strictly depending on the applied poling bias (V_{pol}). Normal hysteresis was obtained for $V_{pol} > V_{OC}$ and inverted hysteresis for $V_{pol} < 0$. For $0 < V_{pol} < V_{OC}$, the hysteresis loop has a crossing point where the forward and reverse characteristics meet [209].

Hysteresis effects are observed in both mesoscopic and planar architectures; however, planar PSCs commonly exhibit more severe hysteresis than that of MSPSCs. Furthermore, SCs based on metal-oxide CTLs typically exhibit more hysteresis than that of organic CTLs based cells [210]. Several approaches have been employed to remove this notorious hysteresis. Depositing fullerene layers on perovskites, Shao et al. efficiently suppress the charge trapping states, consequently removing the hysteresis [211]. Recently, Zhong and co-workers studied the significance of PCBM in the passivation of device hysteresis [212]. Using temperature-dependent chronoamperometric measurements and X-ray photoemission measurements, they observed that PCBM suppresses the iodine-related defects as well as the reduced activation energy of ion migration in PSCs. A universal method was demonstrated to minimize hysteresis observed in mesoscopic and planar PSCs employing TiO₂ ETLs [213]. The observed severe hysteresis can be removed upon doping the perovskites with potassium iodide (KI), attributed to the substantial reduction of low-frequency capacitance and bulk trap density. Furthermore, it was demonstrated that the atomistic origin of the PSCs is not iodide vacancy migration but due to iodide Frankel defect

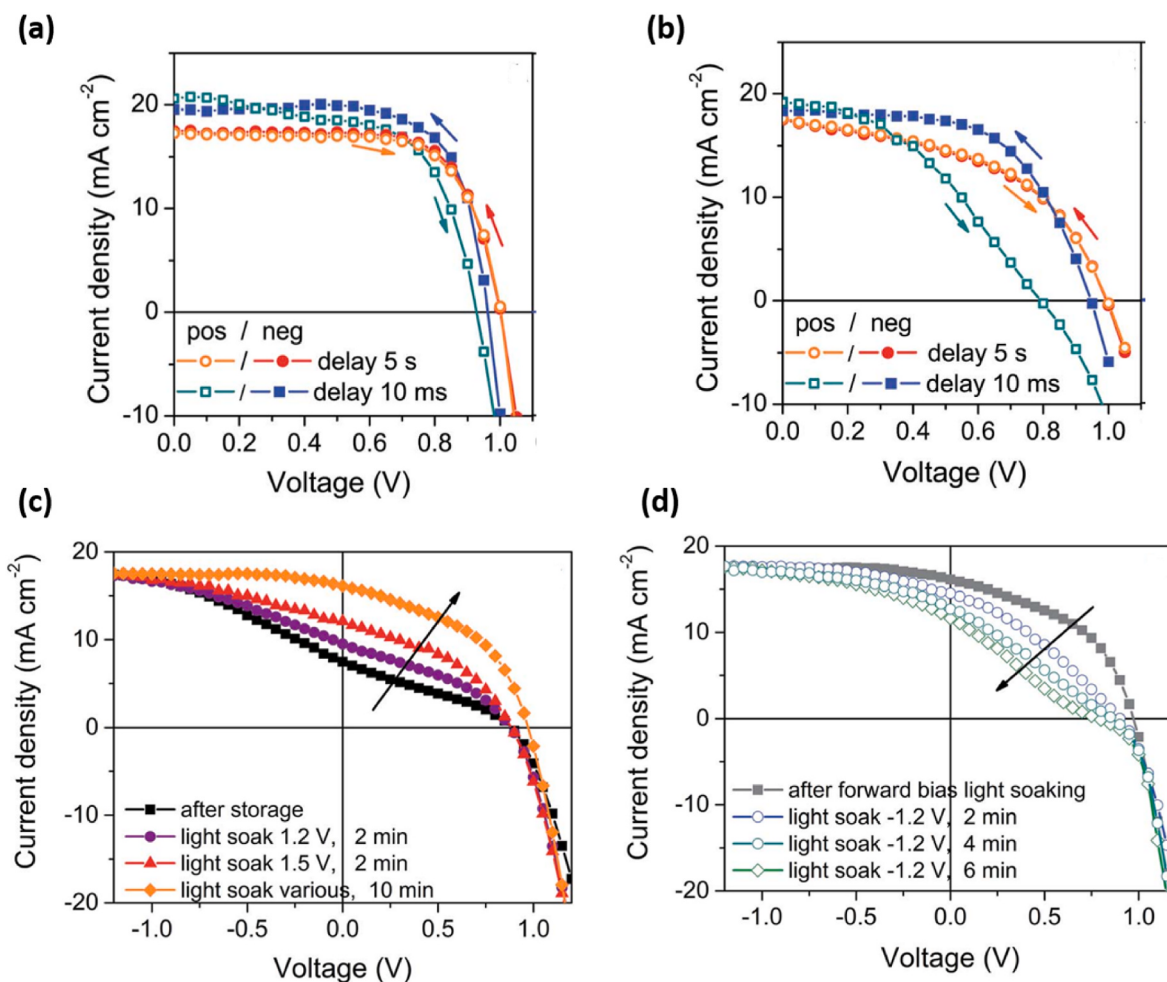


Fig. 17. J-V measurements of (a) mesoporous and (b) planar PSCs in different scan directions (pos: 0 V to forward bias, neg: forward bias to 0 V) and delay times (0.01 s for a fast scan and 5 s for a slow scan); Light soaking at (c) forward and (d) reverse bias [207].

formation [213]. In subsequent work, Kim et al. observed moderate retardation of ion migration in K^+ -doped $(FAPbI_3)_{0.875}(CsPbBr_3)_{0.125}$ using *in-situ* photoluminescence imaging. The non-hysteretic behaviour is due to the kinetic stabilization of the ionic double layer in the perovskite at the perovskite/contact interface [214]. This result reveals the physical cause of hysteresis and opens a new window for the elimination of hysteresis in PSCs.

6.6. Environmental issues—Toxicity

Environmental issues are well-recognized issues of PSCs, mainly because of large-scale fabrication waste treatment. As already discussed, PSCs are unstable in the ambient environment, and they could be decomposed into by-products that are easily leached into the environment. The presence of toxic heavy metals, especially Pb, causes the toxicity of PSC. In addition to heavy metals, toxic organic solvents used in the fabrication stage, which are miscible with water, worsen this issue [215]. These waste materials will have a negative impact on the environment, such as land/water pollution, and eventually, the contaminants may become available to human beings through leaching and transport via water, air, and soil. In addition, there could be several other mechanisms like acidification and nanotoxicity that can make perovskites potentially harmful to the environment and human health [216]. Recently, through dynamic leaching tests, it has resulted that Pb leaching concentration exceeded the hazardous waste limit (5 mg/L) [217]. Furthermore, Pb was found to be leaching out continuously in the water extraction leaching processes. These results indicated that almost all the chemicals used in the fabrication of PSCs could readily leach out when exposed to water, rain, and landfill leachate [217]. Moreover, total carbon and oxygen demand analyses indicated that discarded PSC would enhance O_2 consumption and emit CO_2 to the atmosphere [217].

To address the issues regarding Pb, significant attempts have been made to develop Pb-free PSCs and numerous reports and reviews have been published regarding the same. Sn was the first well-studied divalent cation as a replacement for Pb. However, under ambient conditions, Sn^{2+} would readily oxidized to Sn^{4+} , resulting in poor cell performance compared to Pb-based cells [218]. Other materials, including $CsGeI_3$, $MgGeI_3$, and $FAGeI_3$ [219], $A_3Bi_2I_9$ ($A = MA, Cs$) [220], etc have been proposed as alternatives of Pb and Sn-based perovskite. Nevertheless, these lead-free and tin-free PSCs exhibited a very low PCE. Recently, Zhang et al. reviewed the developments of greener fabrication methods for PSCs, particularly environmentally friendly solvents for perovskite precursors, green antisolvents, and the novel molten salt approach [221]. The Pb leakage from PSC modules with 300 nm-thick perovskite layers would increase the concentration of Pb in the first centimeter of the ground surface under the solar panel by approximately 70 ppm, which is categorized as a low level of contamination (<400 ppm) and cannot be considered a disaster [221]. For industrial applications, recycling of PSCs components is a necessary task. Very recently, Yang et al. reviewed the progress of PSCs components recycling, including TCO substrates (FTO and ITO), TCO substrates with electron transport layer, lead compounds, metal electrodes and monolithic structure substrates with carrier transport layers [222]. The highest performance of recycled PSCs could sustain over 90% after twelfth-time recycling, demonstrating the feasibility of recycling, eco-friendly fabrication and harmless application [222].

7. Conclusion and future perspectives

The PSCs witnessed a remarkable enhancement of PCE from 3.8% to a certified value of 25.7% and the research efforts in this field increased in a tremendous way. Most of the research attempts have focused on improving performance, while deeper study about perovskite materials and their optical and electrical properties like tunable bandgaps, high absorption coefficients, and large carrier diffusion length has also been demonstrated. In addition, numerous scientific works on different

organic/inorganic charge transport layers, interfacial layers and deposition techniques of perovskite layers have been established. Moreover, efforts have been conducted to fabricate large-area SCs and modules that are of attraction in making this technology commercially viable.

However, PSCs have great barriers to further improvements as well as commercialization. Various life cycle assessments of PSCs confirmed that the lifetime of devices is a key issue. In addition, other drawbacks like hysteresis and toxicity of different elements of PSCs hinder further improvements. Hence, it is necessary to improve the stability of PSCs substantially to make them commercially competitive. Several strategies such as perovskite material engineering, interface engineering, the choice of CTls and electrodes, and encapsulation techniques have been established to achieve improvements in device stability. Furthermore, considerable research efforts have been made on non-toxic perovskite materials. Another significant issue of PSCs is the upgrading and repeatability of the film deposition process from laboratories to industry. With a small change in the preparation methods, there are considerable variations in the film properties as the films are highly sensitive to processing conditions. However, despite the problems in reproducibility of perovskite preparation, a number of research groups have achieved high-performing cells by carefully optimizing material properties and film preparation environments. For the potential production of PSCs, more research attempts should be made to scalable fabrication and to eliminate toxic materials. Compared to other photovoltaic technologies (thin film, organic, dye-sensitized), perovskite PV technology may be the best option for future SC applications.

CRediT authorship contribution statement

Dibyajyoti Saikia: Conceptualization. **Atanu Betal:** Formal analysis. **Jayanta Bera:** Formal analysis. **Satyajit Sahu:** Writing – review & editing.

Declaration of competing interest

The authors declare that they have no known competing financial interests or personal relationships that could have appeared to influence the work reported in this paper.

Data availability

No data was used for the research described in the article.

References

- P. Roy, N. Kumar Sinha, S. Tiwari, A. Khare, A review on perovskite solar cells: evolution of architecture, fabrication techniques, commercialization issues and status, Sol. Energy 198 (2020) 665–688, <https://doi.org/10.1016/j.solener.2020.01.080>.
- Y. Chen, L. Zhang, Y. Zhang, H. Gao, H. Yan, Large-area perovskite solar cells—a review of recent progress and issues, RSC Adv. 8 (2018) 10489–10508, <https://doi.org/10.1039/c8ra00384j>.
- P. Tonui, S.O. Oseni, G. Sharma, Q. Yan, G. Tessema Mola, Perovskites photovoltaic solar cells: an overview of current status, Renew. Sustain. Energy Rev. 91 (2018) 1025–1044, <https://doi.org/10.1016/j.rser.2018.04.069>.
- L. Perovski, Perovskites-based solar cells : a review of recent progress , materials and processing methods. <https://doi.org/10.3390/ma11050729>, 2018.
- X.J. Gao, M.B. Elowitz, Twenty-five years of low-cost solar cells, Nature 538 (2016) 463–464.
- M.S. Dresselhaus, G.W. Crabtree, M.V. Buchanan, Addressing grand energy challenges through advanced materials, MRS Bull. 30 (2005) 518–523, <https://doi.org/10.1557/mrs2005.144>.
- A. Kojima, K. Teshima, Y. Shirai, T. Miyasaka, Organometal halide perovskites as visible-light sensitizers for photovoltaic cells, J. Am. Chem. Soc. 131 (2009) 6050–6051, <https://doi.org/10.1021/ja809598r>.
- Best-Research-Cell-Efficiencies-Rev210726.Pdf, (n.d.).
- J.H. Im, C.R. Lee, J.W. Lee, S.W. Park, N.G. Park, 6.5% efficient perovskite quantum-dot-sensitized solar cell, Nanoscale 3 (2011) 4088–4093, <https://doi.org/10.1039/c1nr10867k>.
- H.S. Kim, C.R. Lee, J.H. Im, K.B. Lee, T. Moehl, A. Marchioro, S.J. Moon, R. Humphry-Baker, J.H. Yum, J.E. Moser, M. Grätzel, N.G. Park, Lead iodide perovskite sensitized all-solid-state submicron thin film mesoscopic solar cell with

- efficiency exceeding 9, *Sci. Rep.* 2 (2012) 1–7, <https://doi.org/10.1038/srep00591>.
- [11] J.H. Heo, S.H. Im, J.H. Noh, T.N. Mandal, C.S. Lim, J.A. Chang, Y.H. Lee, H. J. Kim, A. Sarkar, M.K. Nazeeruddin, M. Grätzel, S. Il Seok, Efficient inorganic-organic hybrid heterojunction solar cells containing perovskite compound and polymeric hole conductors, *Nat. Photonics* 7 (2013) 486–491, <https://doi.org/10.1038/nphoton.2013.80>.
- [12] M. Liu, M.B. Johnston, H.J. Snaith, Efficient planar heterojunction perovskite solar cells by vapour deposition, *Nature* 501 (2013) 395.
- [13] H. Zhou, Q. Chen, G. Li, S. Luo, T.B. Song, H.S. Duan, Z. Hong, J. You, Y. Liu, Y. Yang, Interface engineering of highly efficient perovskite solar cells, *Science* 345 (2014) 542–546, <https://doi.org/10.1126/science.1254050>, 80..
- [14] M. Sciences, E. Division, R es e a r c h | r e p o r t s, (n.d.).
- [15] C. Tao, S. Neutzner, L. Colella, S. Marras, A.R. Srimath Kandada, M. Gandini, M. De Bastiani, G. Pace, L. Manna, M. Caironi, C. Bertarelli, A. Petruzza, 17.6% stabilized efficiency in low-temperature processed planar perovskite solar cells, *Energy Environ. Sci.* 8 (2015) 2365–2370, <https://doi.org/10.1039/c5ee01720c>.
- [16] M. Saliba, T. Matsui, J.Y. Seo, K. Domanski, J.P. Correa-Baena, M.K. Nazeeruddin, S.M. Zakeeruddin, W. Tress, A. Abate, A. Hagfeldt, M. Grätzel, Cesium-containing triple cation perovskite solar cells: improved stability, reproducibility and high efficiency, *Energy Environ. Sci.* 9 (2016) 1989–1997, <https://doi.org/10.1039/c5ee03874j>.
- [17] L. Liu, A. Mei, X. Li, H. Han, Y. Dkhissi, A.D. Scully, R.A. Caruso, Y.B. Cheng, I. Jeong, J. Lee, M.J. Ko, K. Yong, B.S. Richards, T.L. Kelly, N. Pellet, M. Levi, S. Turri, M. Levi, S. Turri, Incorporation of rubidium cations into perovskite solar cells improves photovoltaic performance, *Science* 354 (2016) 206–209, 80..
- [18] D. Bi, C. Yi, J. Luo, J.D. Décupet, F. Zhang, S.M. Zakeeruddin, X. Li, A. Hagfeldt, M. Grätzel, Polymer-templated nucleation and crystal growth of perovskite films for solar cells with efficiency greater than 21, *Nat. Energy* 1 (2016) 1–5, <https://doi.org/10.1038/nenergy.2016.142>.
- [19] O. Ergen, S.M. Gilbert, T. Pham, S.J. Turner, M.T.Z. Tan, M.A. Worsley, A. Zettl, Graded bandgap perovskite solar cells, *Nat. Mater.* 16 (2017) 522–525, <https://doi.org/10.1038/nmat4795>.
- [20] W.S. Yang, B.W. Park, E.H. Jung, N.J. Jeon, Y.C. Kim, D.U. Lee, S.S. Shin, J. Seo, E.K. Kim, J.H. Noh, S. Il Seok, Iodide management in formamidinium-lead-halide-based perovskite layers for efficient solar cells, *Science* 356 (2017) 1376–1379, <https://doi.org/10.1126/science.aan2301>, 80..
- [21] H. Tan, A. Jain, O. Voznyy, X. Lan, F.P.G. De Arquer, J.Z. Fan, R. Quintero-Bermudez, M. Yuan, B. Zhang, Y. Zhao, F. Fan, P. Li, L.N. Quan, Y. Zhao, Z.H. Lu, Z. Yang, S. Hoogland, E.H. Sargent, Efficient and stable solution-processed planar perovskite solar cells via contact passivation, *Science* 355 (2017) 722–726, <https://doi.org/10.1126/science.aai9081>, 80..
- [22] S.S. Shin, E.J. Yeom, W.S. Yang, S. Hur, M.G. Kim, J. Im, J. Seo, J.H. Noh, S. Il Seok, 胶体制备的La掺杂BaSnO 3电极, 用于高效、光稳定的钙钛矿太阳能电池, *Science* 356 (2017) 167–171, <https://doi.org/10.1126/science.aam6620>, 80..
- [23] D. Luo, W. Yang, Z. Wang, A. Sadhanala, Q. Hu, R. Su, R. Shivanna, G.F. Trindade, J.F. Watts, Z. Xu, T. Liu, K. Chen, F. Ye, P. Wu, L. Zhao, J. Wu, Y. Tu, Y. Zhang, X. Yang, W. Zhang, R.H. Friend, Q. Gong, H.J. Snaith, R. Zhu, Enhanced photovoltage for inverted planar heterojunction perovskite solar cells, *Science* 360 (2018) 1442–1446, <https://doi.org/10.1126/science.aap9282>, 80..
- [24] M. Stoltzfus, C.M. Wolff, J.A. Márquez, S. Zhang, C.J. Hages, D. Rothhardt, S. Albrecht, P.L. Burn, P. Meredith, T. Unold, D. Neher, Visualization and suppression of interfacial recombination for high-efficiency large-area pin perovskite solar cells, *Nat. Energy* 3 (2018) 847–854, <https://doi.org/10.1038/s41560-018-0219-8>.
- [25] M. Feng, S. You, N. Cheng, J. Du, High quality perovskite film solar cell using methanol as additive with 19.5% power conversion efficiency, *Electrochim. Acta* 293 (2019) 356–363, <https://doi.org/10.1016/j.electacta.2018.09.195>.
- [26] E.H. Jung, N.J. Jeon, E.Y. Park, C.S. Moon, T.J. Shin, T.Y. Yang, J.H. Noh, J. Seo, Efficient, stable and scalable perovskite solar cells using poly(3-hexylthiophene), *Nature* 567 (2019) 511–515, <https://doi.org/10.1038/s41586-019-1036-3>.
- [27] Q. Jiang, Y. Zhao, X. Zhang, X. Yang, Y. Chen, Z. Chu, Q. Ye, X. Li, Z. Yin, J. You, Surface passivation of perovskite film for efficient solar cells, *Nat. Photonics* 13 (2019) 460–466, <https://doi.org/10.1038/s41566-019-0398-2>.
- [28] Y. Zhao, J. Duan, Y. Wang, X. Yang, Q. Tang, Precise stress control of inorganic perovskite films for carbon-based solar cells with an ultrahigh voltage of 1.622 V, *Nano Energy* 67 (2020), 104286, <https://doi.org/10.1016/j.nanoen.2019.104286>.
- [29] H. Ren, S. Yu, L. Chao, Y. Xia, Y. Sun, S. Zuo, F. Li, T. Niu, Y. Yang, H. Ju, B. Li, H. Du, X. Gao, J. Zhang, J. Wang, L. Zhang, Y. Chen, W. Huang, Efficient and stable Ruddlesden-Popper perovskite solar cell with tailored interlayer molecular interaction, *Nat. Photonics* 14 (2020) 154–163, <https://doi.org/10.1038/s41566-019-0572-6>.
- [30] M. Jeong, I.W. Choi, E.M. Go, Y. Cho, M. Kim, B. Lee, S. Jeong, Y. Jo, H.W. Choi, J. Lee, J.H. Bae, S.K. Kwak, D.S. Kim, C. Yang, Stable perovskite solar cells with efficiency exceeding 24.8% and 0.3-V voltage loss, *Science* 369 (2020) 1615–1620, <https://doi.org/10.1126/science.abb7167>, 80..
- [31] H. Min, D.Y. Lee, J. Kim, G. Kim, K.S. Lee, J. Kim, et al., Perovskite solar cells with atomically coherent interlayers on SnO₂ electrodes, *Nature* 598 (2021) 444–450.
- [32] T.A. Berhe, W.N. Su, C.H. Chen, C.J. Pan, J.H. Cheng, H.M. Chen, M.C. Tsai, L. Y. Chen, A.A. Dubale, B.J. Hwang, Organometal halide perovskite solar cells: degradation and stability, *Energy Environ. Sci.* 9 (2016) 323–356, <https://doi.org/10.1039/c5ee0273k>.
- [33] H.J. Snaith, A. Abate, J.M. Ball, G.E. Eperon, T. Leijtens, N.K. Noel, S.D. Stranks, J.T.W. Wang, K. Wojciechowski, W. Zhang, Anomalous hysteresis in perovskite solar cells, *J. Phys. Chem. Lett.* 5 (2014) 1511–1515, <https://doi.org/10.1021/jz500113x>.
- [34] M. Chen, M.G. Ju, H.F. Garces, A.D. Carl, L.K. Ono, Z. Hawash, Y. Zhang, T. Shen, Y. Qi, R.L. Grimm, D. Pacifici, X.C. Zeng, Y. Zhou, N.P. Padture, Highly stable and efficient all-inorganic lead-free perovskite solar cells with native-oxide passivation, *Nat. Commun.* 10 (2019) 1–8, <https://doi.org/10.1038/s41467-018-07951-y>.
- [35] F. Giustino, H.J. Snaith, Toward lead-free perovskite solar cells, *ACS Energy Lett.* 1 (2016) 1233–1240.
- [36] P.V. Kamat, J. Bisquert, J. Buriak, Lead-free perovskite solar cells, *ACS Energy Lett.* 2 (2017) 904–905, <https://doi.org/10.1021/acsenergylett.7b00246>.
- [37] H. Tang, Open access A short progress report on high-efficiency perovskite solar cells, <https://doi.org/10.1186/s11671-017-2187-5>, 2017.
- [38] C. Li, X. Lu, W. Ding, L. Peng, Y. Gao, Z. Guo, Formability of ABX₃ (X = F, Cl, Br, I) halide perovskites, *Acta Crystallogr. Sect. B Struct. Sci.* 64 (2008) 702–707, <https://doi.org/10.1107/S0108768108032734>.
- [39] J.S. Manser, J.A. Christians, P.V. Kamat, Intriguing optoelectronic properties of metal halide perovskites, *Chem. Rev.* 116 (2016) 12956–13008, <https://doi.org/10.1021/cacs.chemrev.6b00136>.
- [40] N.G. Park, Perovskite solar cells: an emerging photovoltaic technology, *Mater. Today* 18 (2015) 65–72, <https://doi.org/10.1016/j.mattod.2014.07.007>.
- [41] M.A. Green, A. Ho-Baillie, H.J. Snaith, The emergence of perovskite solar cells, *Nat. Photonics* 8 (2014) 506.
- [42] Z. Cheng, J. Lin, Layered organic-inorganic hybrid perovskites: structure, optical properties, film preparation, patterning and templating engineering, *CrysEngComm* 12 (2010) 2646–2662, <https://doi.org/10.1039/c01929a>.
- [43] D.B. Mitzi, K. Chondroudis, C.R. Kagan, Design, structure, and optical properties of organic-inorganic perovskites containing an oligothiophene chromophore, *Inorg. Chem.* 38 (1999) 6246–6256, <https://doi.org/10.1021/ic991048k>.
- [44] P.P. Boix, S. Agarwala, T.M. Koh, N. Mathews, S.G. Mhaisalkar, Perovskite solar cells: beyond methylammonium lead iodide, *J. Phys. Chem. Lett.* 6 (2015) 898–907, <https://doi.org/10.1021/jz502547f>.
- [45] P.S. Whitfield, N. Herron, W.E. Guise, K. Page, Y.Q. Cheng, I. Milas, M. K. Crawford, Structures, phase transitions and tricritical behavior of the hybrid perovskite methyl ammonium lead iodide, *Sci. Rep.* 6 (2016) 1–16, <https://doi.org/10.1038/srep35685>.
- [46] E. Sandor, W.A. Wooster, moller MAPbX3.pdf 1 (1958) 1958.
- [47] C.G. Bischak, C.L. Hetherington, H. Wu, S. Aloni, D.F. Ogletree, D.T. Limmer, N. S. Ginsberg, Origin of reversible photoinduced phase separation in hybrid perovskites, *Nano Lett.* 17 (2017) 1028–1033, <https://doi.org/10.1021/acsnanolett.6b04453>.
- [48] K. Korshunova, L. Winterfeld, W.J.D. Beenken, E. Runge, Thermodynamic stability of mixed Pb:Sn methyl-ammonium halide perovskites, *Phys. Status Solidi Basic Res.* 253 (2016) 1907–1915, <https://doi.org/10.1002/pssb.201600136>.
- [49] Z. Xiao, Y. Yan, Progress in theoretical study of metal halide perovskite solar cell materials, *Adv. Energy Mater.* 7 (2017) 1–20, <https://doi.org/10.1002/aenm.201701136>.
- [50] M. Zhong, W. Zeng, H. Tang, L.X. Wang, F.S. Liu, B. Tang, Q.J. Liu, Band structures, effective masses and exciton binding energies of perovskite polymorphs of CH3NH3PbI₃, *Sol. Energy* 190 (2019) 617–621, <https://doi.org/10.1016/j.solener.2019.08.055>.
- [51] S. Tao, I. Schmidt, G. Brocks, J. Jiang, I. Tranca, K. Meerholz, S. Olthof, Absolute energy level positions in tin- and lead-based halide perovskites, *Nat. Commun.* 10 (2019) 1–10, <https://doi.org/10.1038/s41467-019-10468-7>.
- [52] W.J. Yin, T. Shi, Y. Yan, Unique properties of halide perovskites as possible origins of the superior solar cell performance, *Adv. Mater.* 26 (2014) 4653–4658, <https://doi.org/10.1002/adma.201306281>.
- [53] N.J. Jeon, H. Na, E.H. Jung, T.Y. Yang, Y.G. Lee, G. Kim, H.W. Shin, S. Il Seok, J. Lee, J. Seo, A fluorene-terminated hole-transporting material for highly efficient and stable perovskite solar cells, *Nat. Energy* 3 (2018) 682–689, <https://doi.org/10.1038/s41560-018-0200-6>.
- [54] J. Burschka, N. Pellet, S.-J. Moon, R. Humphry-Baker, P. Gao, M.K. Nazeeruddin, M. Grätzel, Sequential deposition as a route to high-performance perovskite-sensitized solar cells, *Nature* 499 (2013) 316.
- [55] D. Zhong, B. Cai, X. Wang, Z. Yang, Y. Xing, S. Miao, W.H. Zhang, C. Li, Synthesis of oriented TiO₂ nanocones with fast charge transfer for perovskite solar cells, *Nano Energy* 11 (2015) 409–418, <https://doi.org/10.1016/j.nanoen.2014.11.014>.
- [56] M.M. Lee, J. Teuscher, T. Miyasaka, T.N. Murakami, H.J. Snaith, Efficient hybrid solar cells based on meso-superstructured organometal halide perovskites, *Science* 80 (2012), 1228604.
- [57] J.M. Ball, M.M. Lee, A. Hey, H.J. Snaith, Low-temperature processed meso-superstructured to thin-film perovskite solar cells, *Energy Environ. Sci.* 6 (2013) 1739–1743, <https://doi.org/10.1039/c3ee40810h>.
- [58] V.A. Online, D. Bi, S. Moon, L. Ha, G. Boschloo, L. Yang, M. Erik, J. Johansson, M. K. Nazeeruddin, M. Gra, A. Hagfeldt, *RSC Adv.* (2013) 18762–18766, <https://doi.org/10.1039/c3ra43228a>.
- [59] A. Manuscript, Materials Chemistry A, (n.d.). <https://doi.org/10.1039/x0xx00000x>.
- [60] K.C. Wang, P.S. Shen, M.H. Li, S. Chen, M.W. Lin, P. Chen, T.F. Guo, Low-temperature sputtered nickel oxide compact thin film as effective electron blocking layer for mesoscopic NiO/CH3NH3PbI₃ perovskite heterojunction solar cells, *ACS Appl. Mater. Interfaces* 6 (2014) 11851–11858, <https://doi.org/10.1021/am503610u>.

- [61] D. Bi, B. Xu, P. Gao, L. Sun, M. Grätzel, A. Hagfeldt, Facile synthesized organic hole transporting material for perovskite solar cell with efficiency of 19.8, *Nano Energy* 23 (2016) 138–144, <https://doi.org/10.1016/j.nanoen.2016.03.020>.
- [62] D. Yang, X. Zhou, R. Yang, Z. Yang, W. Yu, X. Wang, C. Li, S. Liu, R.P.H. Chang, Surface optimization to eliminate hysteresis for record efficiency planar perovskite solar cells, *Energy Environ. Sci.* 9 (2016) 3071–3078, <https://doi.org/10.1039/c6ee02139e>.
- [63] F. Zhang, W. Shi, J. Luo, N. Pellet, C. Yi, X. Li, X. Zhao, T.J.S. Dennis, X. Li, S. Wang, Y. Xiao, S.M. Zakeeruddin, D. Bi, M. Grätzel, Isomer-pure bis-PCBM-assisted crystal engineering of perovskite solar cells showing excellent efficiency and stability, *Adv. Mater.* 29 (2017) 1–7, <https://doi.org/10.1002/adma.201606806>.
- [64] J.J. Yoo, S. Wieghold, M.C. Sponseller, M.R. Chua, S.N. Bertram, N.T.P. Hartono, J.S. Tresback, E.C. Hansen, J.P. Correa-Baena, V. Bulović, T. Buonassisi, S.S. Shin, M.G. Bawendi, An interface stabilized perovskite solar cell with high stabilized efficiency and low voltage loss, *Energy Environ. Sci.* 12 (2019) 2192–2199, <https://doi.org/10.1039/c9ee00751b>.
- [65] K. Wojciechowski, M. Saliba, T. Leijtens, A. Abate, H.J. Snaith, Sub-150 °C processed meso-superstructured perovskite solar cells with enhanced efficiency, *Energy Environ. Sci.* 7 (2014) 1142–1147, <https://doi.org/10.1039/c3ee43707h>.
- [66] G.E. Eperon, V.M. Burlakov, P. Docampo, A. Goriely, H.J. Snaith, Morphological control for high performance, solution-processed planar heterojunction perovskite solar cells, *Adv. Funct. Mater.* 24 (2014) 151–157, <https://doi.org/10.1002/adfm.201302090>.
- [67] D. Liu, T.L. Kelly, Perovskite solar cells with a planar heterojunction structure prepared using room-temperature solution processing techniques, *Nat. Photonics* 8 (2014) 133–138, <https://doi.org/10.1038/nphoton.2013.342>.
- [68] Z. Yuan, Z. Wu, S. Bai, Z. Xia, W. Xu, T. Song, H. Wu, L. Xu, J. Si, Y. Jin, B. Sun, Hot-electron injection in a sandwiched TiO_x-Au-TiO_x structure for high-performance planar perovskite solar cells, *Adv. Energy Mater.* 5 (2015) 1–7, <https://doi.org/10.1002/aenm.201500038>.
- [69] E.H. Arakaki, A. Kermanpur, L. Steier, K. Domanski, T. Matsui, W. Tress, M. Saliba, A. Abate, M. Grätzel, A. Hagfeldt, J.P. Correa-Baena, Highly efficient and stable planar perovskite solar cells by solution-processed tin oxide, *Energy Environ. Sci.* 9 (2016) 3128–3134, <https://doi.org/10.1039/c6ee02390h>.
- [70] Y. Liu, Q. Chen, H.S. Duan, H. Zhou, Y. Yang, H. Chen, S. Luo, T. Bin Song, L. Dou, Z. Hong, Y. Yang, A dopant-free organic hole transport material for efficient planar heterojunction perovskite solar cells, *J. Mater. Chem. A* 3 (2015) 11940–11947, <https://doi.org/10.1039/c5ta02502h>.
- [71] H. Yoon, S.M. Kang, J.K. Lee, M. Choi, Hysteresis-free low-temperature-processed planar perovskite solar cells with 19.1% efficiency, *Energy Environ. Sci.* 9 (2016) 2262–2266, <https://doi.org/10.1039/c6ee01037g>.
- [72] N. Ahn, K. Kwak, M.S. Jang, H. Yoon, B.Y. Lee, J.K. Lee, P.V. Pikhitsa, J. Byun, M. Choi, Trapped charge-driven degradation of perovskite solar cells, *Nat. Commun.* 7 (2016) 1–9, <https://doi.org/10.1038/ncomms13422>.
- [73] Q. Jiang, Z. Chu, P. Wang, X. Yang, H. Liu, Y. Wang, Z. Yin, J. Wu, X. Zhang, J. You, Planar-structure perovskite solar cells with efficiency beyond 21, *Adv. Mater.* 29 (2017) 1–7, <https://doi.org/10.1002/adma.201703852>.
- [74] Z. Li, C. Xiao, Y. Yang, S.P. Harvey, D.H. Kim, J.A. Christians, M. Yang, P. Schulz, S.U. Nanayakkara, C.S. Jiang, J.M. Luther, J.J. Berry, M.C. Beard, M.M. Al-Jassim, K. Zhu, Extrinsic ion migration in perovskite solar cells, *Energy Environ. Sci.* 10 (2017) 1234–1242, <https://doi.org/10.1039/c7ee00358g>.
- [75] J.A. Dawson, A.J. Naylor, C. Eames, M. Roberts, W. Zhang, H.J. Snaith, P. G. Bruce, M. Saiful Islam, Mechanisms of lithium intercalation and conversion processes in organic-inorganic halide perovskites, *ACS Energy Lett.* 2 (2017) 1818–1824, <https://doi.org/10.1021/acsenergylett.7b00437>.
- [76] T. Leijtens, T. Giovenzana, S.N. Habisreutinger, J.S. Tinkham, N.K. Noel, B. A. Kamino, G. Sadoughi, A. Sellinger, H.J. Snaith, Hydrophobic organic hole transporters for improved moisture resistance in metal halide perovskite solar cells, *ACS Appl. Mater. Interfaces* 8 (2016) 5981–5989, <https://doi.org/10.1021/acsmami.5b10093>.
- [77] J.A. Christians, P. Schulz, J.S. Tinkham, T.H. Schloemer, S.P. Harvey, B. J. Tremolo De Villers, A. Sellinger, J.J. Berry, J.M. Luther, Tailored interfaces of unencapsulated perovskite solar cells for >1,000 hour operational stability, *Nat. Energy* 3 (2018) 68–74, <https://doi.org/10.1038/s41560-017-0067-y>.
- [78] P. Wang, X. Zhang, Y. Zhou, Q. Jiang, Q. Ye, Z. Chu, X. Li, X. Yang, Z. Yin, J. You, Solvent-controlled growth of inorganic perovskite films in dry environment for efficient and stable solar cells, *Nat. Commun.* 9 (2018) 1–7, <https://doi.org/10.1038/s41467-018-04636-4>.
- [79] C. Zuo, H.J. Bolink, H. Han, J. Huang, D. Cahen, L. Ding, Advances in perovskite solar cells, *Adv. Sci.* 3 (2016) 1–16, <https://doi.org/10.1002/advs.201500324>.
- [80] J.Y. Jeng, Y.F. Chiang, M.H. Lee, S.R. Peng, T.F. Guo, P. Chen, T.C. Wen, CH₃NH₃PbI₃ perovskite/fullerene planar-heterojunction hybrid solar cells, *Adv. Mater.* 25 (2013) 3727–3732, <https://doi.org/10.1002/adma.201301327>.
- [81] P. Docampo, J.M. Ball, M. Darwich, G.E. Eperon, H.J. Snaith, Efficient organometal trihalide perovskite planar-heterojunction solar cells on flexible polymer substrates, *Nat. Commun.* 4 (2013) 1–6, <https://doi.org/10.1038/ncomms3761>.
- [82] Q. Wang, Y. Shao, Q. Dong, Z. Xiao, Y. Yuan, J. Huang, Large fill-factor bilayer iodine perovskite solar cells fabricated by a low-temperature solution-process, *Energy Environ. Sci.* 7 (2014) 2359–2365, <https://doi.org/10.1039/c4ee00233d>.
- [83] L.M. Chen, Z. Hong, G. Li, Y. Yang, Recent progress in polymer solar cells: manipulation of polymer: fullerene morphology and the formation of efficient inverted polymer solar cells, *Adv. Mater.* 21 (2009) 1434–1449, <https://doi.org/10.1002/adma.200802854>.
- [84] W. Chen, Y. Wu, Y. Yue, J. Liu, W. Zhang, X. Yang, H. Chen, E. Bi, I. Ashraful, M. Grätzel, Efficient and stable large-area perovskite solar cells with inorganic charge extraction layers, *Science* 80 (2015) aad1015.
- [85] Y. Zhao, K. Zhu, CH₃NH₃Cl-assisted one-step solution growth of CH₃NH₃PbI₃: structure, charge-carrier dynamics, and photovoltaic properties of perovskite solar cells, *J. Phys. Chem. C* 118 (2014) 9412–9418, <https://doi.org/10.1021/jp502696w>.
- [86] P.W. Liang, C.Y. Liao, C.C. Chueh, F. Zuo, S.T. Williams, X.K. Xin, J. Lin, A.K. Y. Jen, Additive enhanced crystallization of solution-processed perovskite for highly efficient planar-heterojunction solar cells, *Adv. Mater.* 26 (2014) 3748–3754, <https://doi.org/10.1002/adma.201400231>.
- [87] K. Zhu, S. Cong, Z. Lu, Y. Lou, L. He, J. Li, J. Ding, N. Yuan, M.H. Rümmeli, G. Zou, Enhanced perovskite solar cell performance via defect passivation with ethylamine alcohol chlorides additive, *J. Power Sources* 428 (2019) 82–87, <https://doi.org/10.1016/j.jpowsour.2019.04.056>.
- [88] P.H. Lee, B.T. Li, C.F. Lee, Z.H. Huang, Y.C. Huang, W.F. Su, High-efficiency perovskite solar cell using cobalt doped nickel oxide hole transport layer fabricated by NIR process, *Sol. Energy Mater. Sol. Cells* 208 (2020), 110352, <https://doi.org/10.1016/j.solmat.2019.110352>.
- [89] D. Liu, J. Yang, T.L. Kelly, Compact layer free perovskite solar cells with 13.5% efficiency, *J. Am. Chem. Soc.* 136 (2014) 17116–17122, <https://doi.org/10.1021/ja508758k>.
- [90] E. Exceeding, Q. Hu, J. Wu, C. Jiang, T. Liu, X. Que, R. Zhu, Q. Gong, Engineering of Electron-Selective Contact for Perovskite Solar Cells with, 2014, pp. 10161–10167, <https://doi.org/10.1021/nn5029828>.
- [91] W. Ke, G. Fang, J. Wan, H. Tao, Q. Liu, L. Xiong, P. Qin, J. Wang, H. Lei, G. Yang, M. Qin, X. Zhao, Y. Yan, Efficient hole-blocking layer-free planar halide perovskite thin-film solar cells, *Nat. Commun.* 6 (2015) 1–7, <https://doi.org/10.1038/ncomms7700>.
- [92] T. Minemoto, M. Murata, Theoretical analysis on effect of band offsets in perovskite solar cells, *Sol. Energy Mater. Sol. Cells* 133 (2015) 8–14, <https://doi.org/10.1016/j.solmat.2014.10.036>.
- [93] L. Etgar, P. Gao, Z. Xue, Q. Peng, A.K. Chandiran, B. Liu, M.K. Nazeeruddin, M. Grätzel, Mesoscopic CH₃NH₃PbI₃/TiO₂ heterojunction solar cells, *J. Am. Chem. Soc.* 134 (2012) 17396–17399, <https://doi.org/10.1021/ja307789s>.
- [94] J. Shi, J. Dong, S. Lv, Y. Xu, L. Zhu, J. Xiao, X. Xu, H. Wu, D. Li, Y. Luo, Q. Meng, Hole-conductor-free perovskite organic lead iodide heterojunction thin-film solar cells: high efficiency and junction property, *Appl. Phys. Lett.* 104 (2014), <https://doi.org/10.1063/1.4864638>.
- [95] T. Wang, J. Chen, G. Wu, M. Li, Optimal design of efficient hole transporting layer free planar perovskite solar cell高效无空穴传输层平板钙钛矿太阳能电池的优化设计, *Sci. China Mater.* 59 (2016) 703–709, <https://doi.org/10.1007/s40843-016-5108-4>.
- [96] C.H. Nh, P. Heterojunction, S. Cells, J. Shi, Y. Luo, H. Wei, J. Luo, J. Dong, S. Lv, J. Xiao, Y. Xu, L. Zhu, X. Xu, H. Wu, D. Li, Q. Meng, Modified two-step deposition method for high-Efficiency TiO₂/CH₃NH₃PbI₃, 2014.
- [97] H. Wei, J. Shi, X. Xu, J. Xiao, J. Luo, J. Dong, S. Lv, L. Zhu, H. Wu, D. Li, Y. Luo, Q. Meng, Q. Chen, Electron blocking layer for hole-transporting, 2015, pp. 4937–4944, <https://doi.org/10.1039/c4cp04902k>.
- [98] M. Hu, L. Liu, A. Mei, Y. Yang, T. Liu, H. Han, Efficient hole-conductor-free, fully printable mesoscopic perovskite solar cells with a broad light harvester NH₂CH=NH₂PbI₃, *J. Mater. Chem. A* 2 (2014) 17115–17121, <https://doi.org/10.1039/c4ta03741c>.
- [99] A.B. Djurišić, F.Z. Liu, H.W. Tam, M.K. Wong, A. Ng, C. Surya, W. Chen, Z.B. He, Perovskite solar cells - an overview of critical issues, *Prog. Quant. Electron.* 53 (2017) 1–37, <https://doi.org/10.1016/j.pquantelec.2017.05.002>.
- [100] M. Kim, G.H. Kim, K.S. Oh, Y. Jo, H. Yoon, K.H. Kim, H. Lee, J.Y. Kim, D.S. Kim, High-temperature-short-time annealing process for high-performance large-area perovskite solar cells, *ACS Nano* 11 (2017) 6057–6064, <https://doi.org/10.1021/acsnano.7b02015>.
- [101] J. Shi, Y. Luo, H. Wei, J. Luo, J. Dong, S. Lv, J. Xiao, Y. Xu, L. Zhu, X. Xu, H. Wu, D. Li, Q. Meng, Modified two-step deposition method for high-efficiency TiO₂/CH₃NH₃PbI₃ heterojunction solar cells, *ACS Appl. Mater. Interfaces* 6 (2014) 9711–9718, <https://doi.org/10.1021/am502131t>.
- [102] S. Shahbazi, M.Y. Li, A. Fathi, E.W.G. Diau, Realizing a cosolvent system for stable tin-based perovskite solar cells using a two-step deposition approach, *ACS Energy Lett.* 5 (2020) 2508–2511, <https://doi.org/10.1021/acsenergylett.0c01190>.
- [103] K. Liang, D.B. Mitzi, M.T. Prikas, Cm970568F.Pdf, 2013, pp. 403–411, 4756.
- [104] C.-W. Chen, H.-W. Kang, S.-Y. Hsiao, P.-F. Yang, K.-M. Chiang, H.-W. Lin, Efficient and uniform planar-type perovskite solar cells by simple sequential vacuum deposition, *Adv. Mater.* 26 (2014) 6647–6652, <https://doi.org/10.1002/adma.201402461>.
- [105] Q. Ma, S. Huang, X. Wen, M.A. Green, A.W.Y. Ho-Baillie, Hole transport layer free inorganic CsPb₂Br₃ perovskite solar cell by dual source thermal evaporation, *Adv. Energy Mater.* 6 (2016) 2–6, <https://doi.org/10.1002/aenm.201502202>.
- [106] X. Chen, H. Cao, H. Yu, H. Zhu, H. Zhou, L. Yang, S. Yin, Large-area, high-quality organic-inorganic hybrid perovskite thin films: via a controlled vapor-solid reaction, *J. Mater. Chem. A* 4 (2016) 9124–9132, <https://doi.org/10.1039/c6ta03180c>.
- [107] J. Yin, H. Qu, J. Cao, H. Tai, J. Li, N. Zheng, Vapor-assisted crystallization control toward high performance perovskite photovoltaics with over 18% efficiency in the ambient atmosphere, *J. Mater. Chem. A* 4 (2016) 13203–13210, <https://doi.org/10.1039/c6ta04465d>.
- [108] H. Liu, Y. Liu, P. Ahlawat, A. Mishra, W.R. Tress, F.T. Eickemeyer, Y. Yang, F. Fu, Z. Wang, C.E. Avalos, B.I. Carlsen, A. Agarwalla, X. Zhang, X. Li, Y. Zhan, S. M. Zakeeruddin, L. Emsley, U. Rothlisberger, L. Zheng, A. Hagfeldt, M. Grätzel,

- Vapor-assisted deposition of highly efficient, stable black-phase FAPbI₃ perovskite solar cells, *Science* 80 (2020) 370, <https://doi.org/10.1126/science.abb8985>.
- [109] A. Ng, Z. Ren, Q. Shen, S.H. Cheung, H.C. Gokkaya, G. Bai, J. Wang, L. Yang, S. K. So, A.B. Djurišić, W.W.F. Leung, J. Hao, W.K. Chan, C. Surya, Efficiency enhancement by defect engineering in perovskite photovoltaic cells prepared using evaporated PbI₂/CH₃NH₃I multilayers, *J. Mater. Chem. A* 3 (2015) 9223–9231, <https://doi.org/10.1039/c4ta05070c>.
- [110] H. Hu, D. Wang, Y. Zhou, J. Zhang, S. Lv, S. Pang, X. Chen, Z. Liu, N.P. Padture, G. Cui, Vapour-based processing of hole-conductor-free CH₃NH₃PbI₃ perovskite/C₆₀ fullerene planar solar cells, *RSC Adv.* 4 (2014) 28964–28967, <https://doi.org/10.1039/c4ra03820g>.
- [111] W.-G. Choi, C.-G. Park, Y. Kim, T. Moon, Sn perovskite solar cells via 2D/3D bilayer formation through a sequential vapor process, *ACS Energy Lett.* (2020) 3461–3467, <https://doi.org/10.1021/acsenergylett.0c01887>.
- [112] Q. Chen, H. Zhou, Z. Hong, S. Luo, H.S. Duan, H.H. Wang, Y. Liu, G. Li, Y. Yang, Planar heterojunction perovskite solar cells via vapor-assisted solution process, *J. Am. Chem. Soc.* 136 (2014) 622–625, <https://doi.org/10.1021/ja411509g>.
- [113] T. Gotanda, S. Mori, A. Matsui, H. Oooka, Effects of gas blowing condition on formation of perovskite layer on organic scaffolds, *Chem. Lett.* 45 (2016) 822–824, <https://doi.org/10.1246/cl.160298>.
- [114] F. Huang, Y. Dkhissi, W. Huang, M. Xiao, I. Benesperi, S. Rubanov, Y. Zhu, X. Lin, L. Jiang, Y. Zhou, A. Gray-Weale, J. Etheridge, C.R. McNeill, R.A. Caruso, U. Bach, L. Spiccia, Y.B. Cheng, Gas-assisted preparation of lead iodide perovskite films consisting of a monolayer of single crystalline grains for high efficiency planar solar cells, *Nano Energy* 10 (2014) 10–18, <https://doi.org/10.1016/j.nanoen.2014.08.015>.
- [115] F. Paquin, J. Rivnay, A. Salleo, N. Stelingin, C. Silva, Multi-phase semicrystalline microstructures drive exciton dissociation in neat plastic semiconductors, *J. Mater. Chem. C* 3 (2015) 10715–10722, <https://doi.org/10.1039/b000000x>.
- [116] H. Wu, C. Zhang, K. Ding, L. Wang, Y. Gao, J. Yang, Efficient planar heterojunction perovskite solar cells fabricated by in-situ thermal-annealing doctor blading in ambient condition, *Org. Electron.* 45 (2017) 302–307, <https://doi.org/10.1016/j.orgel.2017.03.017>.
- [117] S. Tong, H. Wu, C. Zhang, S. Li, C. Wang, J. Shen, S. Xiao, J. He, J. Yang, J. Sun, Y. Gao, Large-area and high-performance CH₃NH₃PbI₃ perovskite photodetectors fabricated via doctor blading in ambient condition, *Org. Electron.* 49 (2017) 347–354, <https://doi.org/10.1016/j.orgel.2017.07.011>.
- [118] S. Razza, F. Di Giacomo, F. Matteocci, L. Cinà, A.L. Palma, S. Casaluci, P. Cameron, A. D'Epifanio, S. Licoccia, A. Reale, T.M. Brown, A. Di Carlo, Perovskite solar cells and large area modules (100 cm²) based on an air flow-assisted PbI₂ blade coating deposition process, *J. Power Sources* 277 (2015) 286–291, <https://doi.org/10.1016/j.jpowsour.2014.12.008>.
- [119] H. Ying, Y. Liu, Y. Dou, J. Zhang, Z. Wu, Q. Zhang, Y.B. Cheng, J. Zhong, Surfactant-assisted doctor-blading-printed FAPbBr₃ films for efficient semitransparent perovskite solar cells, *Front. Optoelectron.* 13 (2020) 272–281, <https://doi.org/10.1007/s12200-020-1031-1>.
- [120] Z. Yang, B. Cai, B. Zhou, T. Yao, W. Yu, S. Liu, W.H. Zhang, C. Li, An up-scalable approach to CH₃NH₃PbI₃ compact films for high-performance perovskite solar cells, *Nano Energy* 15 (2015) 670–678, <https://doi.org/10.1016/j.nanoen.2015.05.027>.
- [121] Z. Liang, S. Zhang, X. Xu, N. Wang, J. Wang, X. Wang, Z. Bi, G. Xu, N. Yuan, J. Ding, A large grain size perovskite thin film with a dense structure for planar heterojunction solar cells via spray deposition under ambient conditions, *RSC Adv.* 5 (2015) 60562–60569, <https://doi.org/10.1039/c5ra09110a>.
- [122] M. Adnan, J.K. Lee, Highly efficient planar heterojunction perovskite solar cells with sequentially dip-coated deposited perovskite layers from a non-halide aqueous lead precursor, *RSC Adv.* 10 (2020) 5454–5461, <https://doi.org/10.1039/c9ra09607h>.
- [123] S. Wang, L.K. Ono, M.R. Leyden, Y. Kato, S.R. Raga, M.V. Lee, Y. Qi, Smooth perovskite thin films and efficient perovskite solar cells prepared by the hybrid deposition method, *J. Mater. Chem. A* 3 (2015) 14631–14641, <https://doi.org/10.1039/c5ta03593g>.
- [124] M.R. Leyden, L.K. Ono, S.R. Raga, Y. Kato, S. Wang, Y. Qi, High performance perovskite solar cells by hybrid chemical vapor deposition, *J. Mater. Chem. A* 2 (2014) 18742–18745, <https://doi.org/10.1039/c4ta04385e>.
- [125] L. Qiu, S. He, Z. Liu, L.K. Ono, D.Y. Son, Y. Liu, G. Tong, Y. Qi, Rapid hybrid chemical vapor deposition for efficient and hysteresis-free perovskite solar modules with an operation lifetime exceeding 800 hours, *J. Mater. Chem. A* 8 (2020) 23404–23412, <https://doi.org/10.1039/d0ta09007g>.
- [126] X. Zhang, X. Ren, B. Liu, R. Munir, X. Zhu, D. Yang, J. Li, Y. Liu, D.M. Smilgies, R. Li, Z. Yang, T. Niu, X. Wang, A. Amassian, K. Zhao, S. Liu, Stable high efficiency two-dimensional perovskite solar cells via cesium doping, *Energy Environ. Sci.* 10 (2017) 2095–2102, <https://doi.org/10.1039/c7ee01145h>.
- [127] N. Li, Z. Zhu, C.C. Chueh, H. Liu, B. Peng, A. Petrone, X. Li, L. Wang, A.K.Y. Jen, Mixed cation FAxPEA1-xPbI₃ with enhanced phase and ambient stability toward high-performance perovskite solar cells, *Adv. Energy Mater.* 7 (2017) 1–9, <https://doi.org/10.1002/aenm.201601307>.
- [128] D.Y. Son, J.W. Lee, Y.J. Choi, I.H. Jang, S. Lee, P.J. Yoo, H. Shin, N. Ahn, M. Choi, D. Kim, N.G. Park, Self-formed grain boundary healing layer for highly efficient CH₃NH₃PbI₃ perovskite solar cells, *Nat. Energy* 1 (2016) 1–8, <https://doi.org/10.1038/nenergy.2016.81>.
- [129] G. Wang, W. Dong, A. Gurung, K. Chen, F. Wu, Q. He, R. Pathak, Q. Qiao, Improving photovoltaic performance of carbon-based CsPbBr₃ perovskite solar cells by interfacial engineering using P3HT interlayer, *J. Power Sources* 432 (2019) 48–54, <https://doi.org/10.1016/j.jpowsour.2019.05.075>.
- [130] Y. Hou, Y. Hou, X. Du, S. Scheiner, D.P. Mcmeekin, Z. Wang, N. Li, M.S. Killian, H. Chen, M. Richter, I. Levchuk, N. Schrenker, E. Specker, T. Stubhan, N. A. Luechingher, A. Hirsch, P. Schmuki, H. Steinrück, R.H. Fink, H.J. Snaith, C. J. Brabec, A generic interface to reduce the efficiency-stability-cost gap of perovskite solar, *Cells* 5561 (2017) 1–10.
- [131] J.W. Lee, D.H. Kim, H.S. Kim, S.W. Seo, S.M. Cho, N.G. Park, Formamidinium and cesium hybridization for photo- and moisture-stable perovskite solar cell, *Adv. Energy Mater.* 5 (2015), <https://doi.org/10.1002/aenm.201501310>.
- [132] J.S. Yun, A. Ho-Baillie, S. Huang, S.H. Woo, Y. Heo, J. Seidel, F. Huang, Y. B. Cheng, M.A. Green, Benefit of grain boundaries in organic-inorganic halide planar perovskite solar cells, *J. Phys. Chem. Lett.* 6 (2015) 875–880, <https://doi.org/10.1021/acs.jpclett.5b00182>.
- [133] Z. Xiao, Q. Dong, C. Bi, Y. Shao, Y. Yuan, Solvent annealing of perovskite-induced crystal growth for photovoltaic-device efficiency enhancement, 2014, pp. 1–7, <https://doi.org/10.1002/adma.201401685>.
- [134] N.J. Jeon, J.H. Noh, Y.C. Kim, W.S. Yang, S. Ryu, S. Il Seok, Solvent engineering for high-performance inorganic-organic hybrid perovskite solar cells, *Nat. Mater.* 13 (2014) 897–903, <https://doi.org/10.1038/nmat4014>.
- [135] W. Nie, H. Tsai, R. Asadpour, J.-C. Blancan, A.J. Neukirch, G. Gupta, J.J. Crochet, M. Chhowalla, S. Tretiak, M.A. Alam, High-efficiency solution-processed perovskite solar cells with millimeter-scale grains, *Science* 347 (2015) 522–525, 80.
- [136] X. Li, D. Bi, C. Yi, J.D. Décuppet, J. Luo, S.M. Zakeeruddin, A. Hagfeldt, M. Grätzel, A vacuum flash-assisted solution process for high-efficiency large-area perovskite solar cells, *Science* 353 (2016) 58–62, <https://doi.org/10.1126/science.aaf8060>, 80.
- [137] H. Chen, F. Ye, W. Tang, J. He, M. Yin, Y. Wang, F. Xie, E. Bi, X. Yang, M. Grätzel, L. Han, Perovskite films for efficient solar modules, *Nat. Publ. Gr.* 550 (2017) 92–95, <https://doi.org/10.1038/nature23877>.
- [138] W. Deng, X. Liang, P.S. Kubiak, P.J. Cameron, Molecular interlayers in hybrid perovskite solar cells, *Adv. Energy Mater.* 8 (2018) 1–20, <https://doi.org/10.1002/aenm.201701544>.
- [139] M. Ye, X. Hong, F. Zhang, X. Liu, Recent advancements in perovskite solar cells: flexibility, stability and large scale, *J. Mater. Chem. A* 4 (2016) 6755–6771, <https://doi.org/10.1039/c5ta09661h>.
- [140] N.G. Park, M. Grätzel, T. Miyasaka, K. Zhu, K. Emery, Towards stable and commercially available perovskite solar cells, *Nat. Energy* 1 (2016), <https://doi.org/10.1038/nenergy.2016.152>.
- [141] A. Urbina, The balance between efficiency, stability and environmental impacts in perovskite solar cells: a review, *J. Phys. Energy* 2 (2020), 022001, <https://doi.org/10.1088/2515-7655/ab5eee>.
- [142] R. Wang, M. Mujahid, Y. Duan, Z.K. Wang, J. Xue, Y. Yang, A review of perovskites solar cell stability, *Adv. Funct. Mater.* 29 (2019) 1–25, <https://doi.org/10.1002/adfm.201808843>.
- [143] A. Wakamiya, M. Endo, T. Sasamori, N. Tokitoh, Y. Ogomi, S. Hayase, Y. Murata, Reproducible fabrication of efficient perovskite-based solar cells: X-ray crystallographic studies on the formation of CH₃NH₃PbI₃ layers, *Chem. Lett.* 43 (2014) 711–713, <https://doi.org/10.1246/cl.140074>.
- [144] A.M.A. Leguy, Y. Hu, M. Campoy-Quiles, M.I. Alonso, O.J. Weber, P. Azarhoosh, M. Van Schilfgaarde, M.T. Weller, T. Bein, J. Nelson, P. Docampo, P.R.F. Barnes, Reversible hydration of CH₃NH₃PbI₃ in films, single crystals, and solar cells, *Chem. Mater.* 27 (2015) 3397–3407, <https://doi.org/10.1021/acs.chemmater.5b00660>.
- [145] J. Yang, B.D. Siempelkamp, D. Liu, T.L. Kelly, Investigation of CH₃NH₃PbI₃ degradation rates and mechanisms in controlled humidity environments using in situ techniques, *ACS Nano* 9 (2015) 1955–1963, <https://doi.org/10.1021/nn50684k>.
- [146] H.S. Kim, J.Y. Seo, N.G. Park, Material and device stability in perovskite solar cells, *ChemSusChem* 9 (2016) 2528–2540, <https://doi.org/10.1002/cssc.201600915>.
- [147] C.C. Stoumpos, C.D. Malliakas, M.G. Kanatzidis, Semiconducting tin and lead iodide perovskites with organic cations: phase transitions, high mobilities, and near-infrared photoluminescent properties, *Inorg. Chem.* 52 (2013) 9019–9038, <https://doi.org/10.1021/ic401215x>.
- [148] J. You, Z. Hong, T. Bin Song, L. Meng, Y. Liu, C. Jiang, H. Zhou, W.H. Chang, G. Li, Y. Yang, Moisture assisted perovskite film growth for high performance solar cells, *Appl. Phys. Lett.* 105 (2014), <https://doi.org/10.1063/1.4901510>.
- [149] K.J. Xu, R.T. Wang, A.F. Xu, J.Y. Chen, G. Xu, Hysteresis and instability predicted in moisture degradation of perovskite solar cells. <https://doi.org/10.1021/acsami.0c17323>, 2020.
- [150] R.K. Misra, S. Aharon, B. Li, D. Mogilyansky, I. Visoly-Fisher, L. Etgar, E.A. Katz, Temperature- and component-dependent degradation of perovskite photovoltaic materials under concentrated sunlight, *J. Phys. Chem. Lett.* 6 (2015) 326–330, <https://doi.org/10.1021/acs.jpclett.5b02642b>.
- [151] T. Leijtens, G.E. Eperon, S. Pathak, A. Abate, M.M. Lee, H.J. Snaith, Overcoming ultraviolet light instability of sensitized TiO₂ with meso-superstructured organometal tri-halide perovskite solar cells, *Nat. Commun.* 4 (2013) 1–8, <https://doi.org/10.1038/ncomms3885>.
- [152] N. Aristidou, I. Sanchez-Molina, T. Chotchuangchutchaval, M. Brown, L. Martinez, T. Rath, S.A. Haque, The role of oxygen in the degradation of methylammonium lead trihalide perovskite photoactive layers, *Angew. Chem.* 127 (2015) 8326–8330, <https://doi.org/10.1002/ange.201503153>.
- [153] D. Bryant, N. Aristidou, S. Pont, I. Sanchez-Molina, T. Chotchuangchutchaval, S. Wheeler, J.R. Durrant, S.A. Haque, Light and oxygen induced degradation limits the operational stability of methylammonium lead triiodide perovskite

- solar cells, *Energy Environ. Sci.* 9 (2016) 1655–1660, <https://doi.org/10.1039/c6ee00409a>.
- [154] B. Chen, J. Song, X. Dai, Y. Liu, P.N. Rudd, X. Hong, J. Huang, Synergistic effect of elevated device temperature and excess charge carriers on the rapid light-induced degradation of perovskite solar cells, *Adv. Mater.* 31 (2019) 1–8, <https://doi.org/10.1002/adma.201902413>.
- [155] A.F. Akbulatov, L.A. Frolova, N.N. Dremova, I. Zhdikov, V.M. Martynenko, S. A. Tsarev, S.Y. Luchkin, E.Z. Kurmaev, S.M. Aldoshin, K.J. Stevenson, P. A. Troshin, Light or heat: what is killing lead halide perovskites under solar cell operation conditions? *J. Phys. Chem. Lett.* 11 (2020) 333–339, <https://doi.org/10.1021/jpclett.9b03308>.
- [156] A. Dualeh, P. Gao, S. Il Seok, M.K. Nazeeruddin, M. Grätzel, Thermal behavior of methylammonium lead-trihalide perovskite photovoltaic light harvesters, *Chem. Mater.* 26 (2014) 6160–6164, <https://doi.org/10.1021/cm502468k>.
- [157] A. Poglitsch, D. Weber, Dynamic disorder in methylammonium trihalogenoplumbates (II) observed by millimeter-wave spectroscopy, *J. Chem. Phys.* 87 (1987) 6373–6378, <https://doi.org/10.1063/1.453467>.
- [158] S. Aharon, A. Dymshits, A. Rotem, L. Etgar, Temperature dependence of hole conductor free formamidinium lead iodide perovskite based solar cells, *J. Mater. Chem. A*, 3 (2015) 9171–9178, <https://doi.org/10.1039/c4ta05149a>.
- [159] B. Philippe, B.W. Park, R. Lindblad, J. Oscarsson, S. Ahmadi, E.M.J. Johansson, H. Rensmo, Chemical and electronic structure characterization of lead halide perovskites and stability behavior under different exposures-A photoelectron spectroscopy investigation, *Chem. Mater.* 27 (2015) 1720–1731, <https://doi.org/10.1021/acs.chemmater.5b00348>.
- [160] T.J. Jacobsson, W. Tress, J.P. Correa-Baena, T. Edvinsson, A. Hagfeldt, Room temperature as a goldilocks environment for CH₃NH₃PbI₃ perovskite solar cells: the importance of temperature on device performance, *J. Phys. Chem. C* 120 (2016) 11382–11393, <https://doi.org/10.1021/acs.jpcc.6b02858>.
- [161] M. Wang, V. Vasudevan, S. Lin, J. Jasieniak, S.P. Russo, N. Birbilis, N. V. Medekar, Molecular mechanisms of thermal instability in hybrid perovskite light absorbers for photovoltaic solar cells, *J. Mater. Chem. A*, 8 (2020) 17765–17779, <https://doi.org/10.1039/d0ta05356b>.
- [162] R. Heiderhoff, T. Haeger, N. Pourdavoud, T. Hu, M. Al-Khafaji, A. Mayer, Y. Chen, H.C. Scheer, T. Riedl, Thermal conductivity of methylammonium lead halide perovskite single crystals and thin films: a comparative study, *J. Phys. Chem. C* 121 (2017) 28306–28311, <https://doi.org/10.1021/acs.jpcc.7b11495>.
- [163] S. Ito, S. Tanaka, K. Manabe, H. Nishino, Effects of surface blocking layer of Sb₂S₃ on nanocrystalline TiO₂ for CH₃NH₃PbI₃ perovskite solar cells, *J. Phys. Chem. C* 118 (2014) 16995–17000, <https://doi.org/10.1021/jp500449z>.
- [164] A.F. Akbulatov, L.A. Frolova, M.P. Griffin, I.R. Gearba, A. Dolocan, D.A. Vanden Bout, S. Tsarev, E.A. Katz, A.F. Shestakov, K.J. Stevenson, P.A. Troshin, Effect of electron-transport material on light-induced degradation of inverted planar junction perovskite solar cells, *Adv. Energy Mater.* 7 (2017) 1–7, <https://doi.org/10.1002/aenm.201700476>.
- [165] R.S. Sanchez, E. Mas-Marza, Light-induced effects on Spiro-OMeTAD films and hybrid lead halide perovskite solar cells, *Sol. Energy Mater. Sol. Cells* 158 (2016) 189–194, <https://doi.org/10.1016/j.solmat.2016.03.024>.
- [166] J. Carrillo, A. Guerrero, S. Rahimnejad, O. Almora, I. Zarazua, E. Mas-Marza, J. Bisquert, G. Garcia-Belmonte, Ionic reactivity at contacts and aging of methylammonium lead triiodide perovskite solar cells, *Adv. Energy Mater.* 6 (2016) 1–7, <https://doi.org/10.1002/aenm.201502246>.
- [167] K. Norrman, M.V. Madsen, S.A. Gevorgyan, F.C. Krebs, Degradation patterns in water and oxygen of an inverted polymer solar cell, *J. Am. Chem. Soc.* 132 (2010) 16883–16892, <https://doi.org/10.1021/ja106299g>.
- [168] T. Sekimoto, T. Matsui, T. Nishihiara, R. Uchida, T. Sekiguchi, T. Negami, Influence of a hole-transport layer on light-induced degradation of mixed organic-inorganic halide perovskite solar cells, *ACS Appl. Energy Mater.* 2 (2019) 5039–5049, <https://doi.org/10.1021/acsaem.9b00709>.
- [169] A.G. Boldyreva, A.F. Akbulatov, M. Elnaggar, S.Y. Luchkin, A.V. Danilov, I. S. Zhdikov, O.R. Yamilova, Y.S. Fedotov, S.I. Bredikhin, E.Z. Kurmaev, K. J. Stevenson, P.A. Troshin, Impact of charge transport layers on the photochemical stability of MAPbI₃ in thin films and perovskite solar cells, *Sustain. Energy Fuels* 3 (2019) 2705–2716, <https://doi.org/10.1039/c9se00493a>.
- [170] A. Guerrero, R. You, C. Aranda, Y.S. Kang, G. Garcia-Belmonte, H. Zhou, J. Bisquert, Y. Yang, Interfacial degradation of planar lead halide perovskite solar cells, *ACS Nano* 10 (2016) 218–224, <https://doi.org/10.1021/acsnano.5b03687>.
- [171] Y. Kato, L.K. Ono, M.V. Lee, S. Wang, S.R. Raga, Y. Qi, Silver iodide formation in methyl ammonium lead iodide perovskite solar cells with silver top electrodes, *Adv. Mater. Interfac.* 2 (2015) 2–7, <https://doi.org/10.1002/admi.201500195>.
- [172] C. Li, A. Guerrero, Y. Zhong, A. Gräser, C.A.M. Luna, J. Köhler, J. Bisquert, R. Hildner, S. Huettner, Real-time observation of iodide ion migration in methylammonium lead halide perovskites, *Small* 13 (2017) 1–10, <https://doi.org/10.1002/smll.201701711>.
- [173] B. Rivkin, P. Fassl, Q. Sun, A.D. Taylor, Z. Chen, Y. Vaynzof, Effect of ion migration-induced electrode degradation on the operational stability of perovskite solar cells, *ACS Omega* 3 (2018) 10042–10047, <https://doi.org/10.1021/acsomega.8b01626>.
- [174] M.V. Khenkin, K.M. Anoop, E.A. Katz, I. Visoly-Fisher, Bias-dependent degradation of various solar cells: lessons for stability of perovskite photovoltaics, *Energy Environ. Sci.* 12 (2019) 550–558, <https://doi.org/10.1039/c8ee03475c>.
- [175] K. Domanski, E.A. Alharbi, A. Hagfeldt, M. Grätzel, W. Tress, Systematic investigation of the impact of operation conditions on the degradation behaviour of perovskite solar cells, *Nat. Energy* 3 (2018) 61–67, <https://doi.org/10.1038/s41560-017-0060-5>.
- [176] I.S. Kim, D.H. Cao, D.B. Buchholz, J.D. Emery, O.K. Farha, J.T. Hupp, M. G. Kanatzidis, A.B.F. Martinson, Liquid water- and heat-resistant hybrid perovskite photovoltaics via an inverted ALD oxide electron extraction layer design, *Nano Lett.* 16 (2016) 7786–7790, <https://doi.org/10.1021/acs.nanolett.6b03989>.
- [177] P. Holzhey, M. Saliba, A full overview of international standards assessing the long-term stability of perovskite solar cells, *J. Mater. Chem. A*, 6 (2018) 21794–21808, <https://doi.org/10.1039/C8TA06950F>.
- [178] J.H. Noh, S.H. Im, J.H. Heo, T.N. Mandal, S. Il Seok, Chemical management for colorful, efficient, and stable inorganic-organic hybrid nanostructured solar cells, *Nano Lett.* 13 (2013) 1764–1769, <https://doi.org/10.1021/nl400349b>.
- [179] R. Ruess, F. Benfer, F. Böcher, M. Stumpp, D. Schlettwein, Stabilization of organic-inorganic perovskite layers by partial substitution of iodide by bromide in methylammonium lead iodide, *ChemPhysChem* 17 (2016) 1505–1511, <https://doi.org/10.1002/cphc.201501168>.
- [180] T. Singh, T. Miyasaka, Stabilizing the efficiency beyond 20% with a mixed cation perovskite solar cell fabricated in ambient air under controlled humidity, *Adv. Energy Mater.* 8 (2018) 1–9, <https://doi.org/10.1002/aenm.201700677>.
- [181] L. Xie, P. Song, L. Shen, J. Lu, K. Liu, K. Lin, W. Feng, C. Tian, Z. Wei, Revealing the compositional effect on the intrinsic long-term stability of perovskite solar cells, *J. Mater. Chem. A*, 8 (2020) 7653–7658, <https://doi.org/10.1039/d0ta01668c>.
- [182] J. Cao, J. Jiang, N. Li, Y. Dong, Y. Jia, S. Tao, N. Zhao, Alkali-cation-enhanced benzylammonium passivation for efficient and stable perovskite solar cells fabricated through sequential deposition, *J. Mater. Chem. A*, 8 (2020) 19357–19366, <https://doi.org/10.1039/d0ta04680a>.
- [183] S. Ahmad, P. Fu, S. Yu, Q. Yang, X. Liu, X. Wang, X. Wang, X. Guo, C. Li, Dion-jacobson phase 2D layered perovskites for solar cells with ultrahigh stability, *Joule* 3 (2019) 794–806, <https://doi.org/10.1016/j.joule.2018.11.026>.
- [184] C. Liang, H. Gu, Y. Xia, Z. Wang, X. Liu, J. Xia, S. Zuo, Y. Hu, X. Gao, W. Hui, L. Chao, T. Niu, M. Fang, H. Lu, H. Dong, H. Yu, S. Chen, X. Ran, L. Song, B. Li, J. Zhang, Y. Peng, G. Shao, J. Wang, Y. Chen, G. Xing, W. Huang, Two-dimensional Ruddlesden-Popper layered perovskite solar cells based on phase-pure thin films, *Nat. Energy* 6 (2021) 38–45, <https://doi.org/10.1038/s41560-020-00721-5>.
- [185] J.H. Kim, S.T. Williams, N. Cho, C.C. Chueh, A.K.Y. Jen, Enhanced environmental stability of planar heterojunction perovskite solar cells based on blade-coating, *Adv. Energy Mater.* 5 (2015) 2–7, <https://doi.org/10.1002/aenm.201401229>.
- [186] C.H. Chiang, C.G. Wu, Film grain-size related long-term stability of inverted perovskite solar cells, *ChemSusChem* 9 (2016) 2666–2672, <https://doi.org/10.1002/cssc.201600887>.
- [187] W. Li, J. Fan, J. Li, G. Niu, Y. Mai, L. Wang, High performance of perovskite solar cells via catalytic treatment in two-step process: the case of solvent engineering, *ACS Appl. Mater. Interfaces* 8 (2016) 30107–30115, <https://doi.org/10.1021/acsami.6b09532>.
- [188] J. Luo, J. Xia, H. Yang, C. Sun, N. Li, H.A. Malik, H. Shu, Z. Wan, H. Zhang, C. J. Brabec, C. Jia, A pressure process for efficient and stable perovskite solar cells, *Nano Energy* 77 (2020), 105063, <https://doi.org/10.1016/j.nanoen.2020.105063>.
- [189] Y. Sun, Y. Wu, X. Fang, L. Xu, Z. Ma, Y. Lu, W.H. Zhang, Q. Yu, N. Yuan, J. Ding, Long-term stability of organic-inorganic hybrid perovskite solar cells with high efficiency under high humidity conditions, *J. Mater. Chem. A*, 5 (2017) 1374–1379, <https://doi.org/10.1039/c6ta08117g>.
- [190] J. Jin, H. Li, C. Chen, B. Zhang, L. Xu, B. Dong, H. Song, Q. Dai, Enhanced performance of perovskite solar cells with zinc chloride additives, *ACS Appl. Mater. Interfaces* 9 (2017) 42875–42882, <https://doi.org/10.1021/acsami.7b15310>.
- [191] X. Liu, J. Wu, Y. Yang, D. Wang, G. Li, X. Wang, W. Sun, Y. Wei, Y. Huang, M. Huang, L. Fan, Z. Lan, J. Lin, K.C. Ho, Additive engineering by bifunctional guanidine sulfamate for highly efficient and stable perovskites solar cells, *Small* 16 (2020) 1–9, <https://doi.org/10.1002/smll.202004877>.
- [192] S. Castro-Hermosa, S.K. Yadav, L. Vesce, A. Guidobaldi, A. Reale, A. Di Carlo, T. M. Brown, Stability issues pertaining large area perovskite and dye-sensitized solar cells and modules, *J. Phys. D Appl. Phys.* 50 (2017), 33001, <https://doi.org/10.1088/1361-6463/50/3/033001>.
- [193] S. Akin, Y. Altintas, E. Mutlugun, S. Sonmezoglu, Cesium-lead based inorganic perovskite quantum-dots as interfacial layer for highly stable perovskite solar cells with exceeding 21% efficiency, *Nano Energy* 60 (2019) 557–566, <https://doi.org/10.1016/j.nanoen.2019.03.091>.
- [194] Y. Dou, D. Wang, G. Li, Y. Liao, W. Sun, J. Wu, Z. Lan, Toward highly reproducible, efficient, and stable perovskite solar cells via interface engineering with CoO nanoplates, *ACS Appl. Mater. Interfaces* 11 (2019) 32159–32168, <https://doi.org/10.1021/acsami.9b11039>.
- [195] S.S. Mali, C.K. Hong, P-i/n-i-p type planar hybrid structure of highly efficient perovskite solar cells towards improved air stability: synthetic strategies and the role of p-type hole transport layer (HTL) and n-type electron transport layer (ETL) metal oxides, *Nanoscale* 8 (2016) 10528–10540, <https://doi.org/10.1039/c6nr02276f>.
- [196] Y. Dkhissi, S. Meyer, D. Chen, H.C. Weerasinghe, L. Spiccia, Y.B. Cheng, R. A. Caruso, Stability comparison of perovskite solar cells based on zinc oxide and titania on polymer substrates, *ChemSusChem* 9 (2016) 687–695, <https://doi.org/10.1002/cssc.201501659>.
- [197] J. Ma, Z. Lin, X. Guo, L. Zhou, J. Su, C. Zhang, Z. Yang, J. Chang, S. Liu, Y. Hao, Low-temperature solution-processed ZnO electron transport layer for highly efficient and stable planar perovskite solar cells with efficiency over 20%, *Sol. RRL*, 3 (2019) 1–10, <https://doi.org/10.1002/solr.201900096>.

- [198] M. Kim, J. Jeong, H. Lu, T.K. Lee, F.T. Eickemeyer, Y. Liu, I.W. Choi, S.J. Choi, Y. Jo, H.B. Kim, S.I. Mo, Y.K. Kim, H. Lee, N.G. An, S. Cho, W.R. Tress, S. M. Zakeeruddin, A. Hagfeldt, J.Y. Kim, M. Grätzel, D.S. Kim, Conformal quantum dot-SnO₂ layers as electron transporters for efficient perovskite solar cells, *Science* 375 (2022) 302–306, <https://doi.org/10.1126/science.abh1885>, 80–.
- [199] F. Hou, F. Jin, B. Chu, Z. Su, Y. Gao, H. Zhao, P. Cheng, J. Tang, W. Li, Hydrophobic hole-transporting layer induced porous PbI₂ film for stable and efficient perovskite solar cells in 50% humidity, *Sol. Energy Mater. Sol. Cells* 157 (2016) 989–995, <https://doi.org/10.1016/j.solmat.2016.08.024>.
- [200] B.X. Zhao, C. Yao, K. Gu, T. Liu, Y. Xia, Y.-L. Loo, A hole-transport material that also passivates perovskite surface defects for solar cells with improved efficiency and stability, *Energy Environ. Sci.* 13 (2020) 4334–4343, <https://doi.org/10.1039/d0ee01655a>.
- [201] Y. Deng, Q. Dong, C. Bi, Y. Yuan, J. Huang, Air-stable, efficient mixed-cation perovskite solar cells with Cu electrode by scalable fabrication of active layer, *Adv. Energy Mater.* 6 (2016) 1–6, <https://doi.org/10.1002/aenm.201600372>.
- [202] S. Wang, H. Liu, H. Bala, B. Zong, L. Huang, Z. an Guo, W. Fu, B. Zhang, G. Sun, J. Cao, Z. Zhang, A highly stable hole-conductor-free Cs_xMA_{1-x}PbI₃ perovskite solar cell based on carbon counter electrode, *Electrochim. Acta* 335 (2020), 135686, <https://doi.org/10.1016/j.electacta.2020.135686>.
- [203] A. Priyadarshi, L.J. Haur, P. Murray, D. Fu, S. Kulkarni, G. Xing, T.C. Sum, N. Mathews, S.G. Mhaisalkar, A large area (70 cm²) monolithic perovskite solar module with a high efficiency and stability, *Energy Environ. Sci.* 9 (2016) 3687–3692, <https://doi.org/10.1039/c6ee02693a>.
- [204] Z. Fu, M. Xu, Y. Sheng, Z. Yan, J. Meng, C. Tong, D. Li, Z. Wan, Y. Ming, A. Mei, Y. Hu, Y. Rong, H. Han, Encapsulation of printable mesoscopic perovskite solar cells enables high temperature and long-term outdoor stability, *Adv. Funct. Mater.* 29 (2019) 1–7, <https://doi.org/10.1002/adfm.201809129>.
- [205] S. Emami, J. Martins, D. Ivanou, A. Mendes, Advanced hermetic encapsulation of perovskite solar cells: the route to commercialization, *J. Mater. Chem. A* 8 (2020) 2654–2662, <https://doi.org/10.1039/c9ta11907h>.
- [206] F. Matteocci, L. Cinà, E. Lamanna, S. Cacovich, G. Divitini, P.A. Midgley, C. Ducati, A. Di Carlo, Encapsulation for long-term stability enhancement of perovskite solar cells, *Nano Energy* 30 (2016) 162–172, <https://doi.org/10.1016/j.nanoen.2016.09.041>.
- [207] E.L. Unger, E.T. Hoke, C.D. Baillie, W.H. Nguyen, A.R. Bowring, T. Heumüller, M. G. Christoforo, M.D. McGehee, Hysteresis and transient behavior in current-voltage measurements of hybrid-perovskite absorber solar cells, *Energy Environ. Sci.* 7 (2014) 3690–3698, <https://doi.org/10.1039/c4ee02465f>.
- [208] W. Tress, N. Marinova, T. Moehl, S.M. Zakeeruddin, M.K. Nazeeruddin, M. Grätzel, Understanding the rate-dependent J-V hysteresis, slow time component, and aging in CH₃NH₃PbI₃ perovskite solar cells: the role of a compensated electric field, *Energy Environ. Sci.* 8 (2015) 995–1004, <https://doi.org/10.1039/c4ee03664f>.
- [209] G.A. Nemnes, C. Besleaga, V. Stancu, D.E. Dogaru, L.N. Leonat, L. Pintilie, K. Torfason, M. Ilkov, A. Manolescu, I. Pintilie, Normal and inverted hysteresis in perovskite solar cells, *J. Phys. Chem. C* 121 (2017) 11207–11214, <https://doi.org/10.1021/acs.jpcc.7b04248>.
- [210] L. Meng, J. You, T.F. Guo, Y. Yang, Recent advances in the inverted planar structure of perovskite solar cells, *Acc. Chem. Res.* 49 (2016) 155–165, <https://doi.org/10.1021/acs.accounts.5b00404>.
- [211] Y. Shao, Z. Xiao, C. Bi, Y. Yuan, J. Huang, Origin and elimination of photocurrent hysteresis by fullerene passivation in CH₃NH₃PbI₃ planar heterojunction solar cells, *Nat. Commun.* 5 (2014) 1–7, <https://doi.org/10.1038/ncomms6784>.
- [212] Y. Zhong, M. Hufnagel, M. Thelakkat, C. Li, S. Huettner, Role of PCBM in the suppression of hysteresis in perovskite solar cells, *Adv. Funct. Mater.* 30 (2020), <https://doi.org/10.1002/adfm.201908920>.
- [213] D.Y. Son, S.G. Kim, J.Y. Seo, S.H. Lee, H. Shin, D. Lee, N.G. Park, Universal approach toward hysteresis-free perovskite solar cell via defect engineering, *J. Am. Chem. Soc.* 140 (2018) 1358–1364, <https://doi.org/10.1021/jacs.7b10430>.
- [214] S.G. Kim, C. Li, A. Guerrero, J.M. Yang, Y. Zhong, J. Bisquert, S. Huettner, N. G. Park, Potassium ions as a kinetic controller in ionic double layers for hysteresis-free perovskite solar cells, *J. Mater. Chem. A* 7 (2019) 18807–18815, <https://doi.org/10.1039/c9ta07595j>.
- [215] A. Babayigit, A. Ethirajan, M. Muller, B. Conings, Toxicity of organometal halide perovskite solar cells, *Nat. Mater.* 15 (2016) 247–251, <https://doi.org/10.1038/nmat4572>.
- [216] M.G. Ju, M. Chen, Y. Zhou, J. Dai, L. Ma, N.P. Padture, X.C. Zeng, Toward eco-friendly and stable perovskite materials for photovoltaics, *Joule* 2 (2018) 1231–1241, <https://doi.org/10.1016/j.joule.2018.04.026>.
- [217] P. Su, Y. Liu, J. Zhang, C. Chen, B. Yang, C. Zhang, X. Zhao, Pb-based perovskite solar cells and the underlying pollution behind clean energy: dynamic leaching of toxic substances from discarded perovskite solar cells, *J. Phys. Chem. Lett.* 11 (2020) 2812–2817, <https://doi.org/10.1021/acs.jpclett.0c00503>.
- [218] N.K. Noel, S.D. Stranks, A. Abate, C. Wehrenfennig, S. Guarnera, A. A. Haghhighirad, A. Sadhanala, G.E. Eperon, S.K. Pathak, M.B. Johnston, A. Petrozza, L.M. Herz, H.J. Snaith, Lead-free organic-inorganic tin halide perovskites for photovoltaic applications, *Energy Environ. Sci.* 7 (2014) 3061–3068, <https://doi.org/10.1039/c4ee01076k>.
- [219] T. Krishnamoorthy, H. Ding, C. Yan, W.L. Leong, T. Baikie, Z. Zhang, M. Sherburne, S. Li, M. Asta, N. Mathews, S.G. Mhaisalkar, Lead-free germanium iodide perovskite materials for photovoltaic applications, *J. Mater. Chem. A* 3 (2015) 23829–23832, <https://doi.org/10.1039/c5ta05741h>.
- [220] B.W. Park, B. Philippe, X. Zhang, H. Rensmo, G. Boschloo, E.M.J. Johansson, Bismuth based hybrid perovskites A₃Bi₂I₉ (A: methylammonium or cesium) for solar cell application, *Adv. Mater.* 27 (2015) 6806–6813, <https://doi.org/10.1002/adma.201501978>.
- [221] M. Zhang, D. Xin, X. Zheng, Q. Chen, W.H. Zhang, Toward greener solution processing of perovskite solar cells, *ACS Sustain. Chem. Eng.* 8 (2020) 13126–13138, <https://doi.org/10.1021/acssuschemeng.0c04289>.
- [222] W.T. Mujeeb Khan¹, Muhammed Nawaz Tahir^{*2}, Syed Farooq Adil¹, Hadayat Ullah Khan³⁴, M.Rafiq H. Siddiqui¹, Abdulrahman A. Al-warthan^{*1}, 美国科学院学报 materials chemistry A 材料化学 a, *J. Mater. Chem.* 121 (2015), <https://doi.org/10.1039/c7ta07529d>.